AC LOSSES AND MECHANICAL PROPERTIES OF MULTIFILAMENTARY HIGH TEMPERATURE SUPERCONDUCTOR TAPES AND WIRES

A Dissertation

Presented to

the Faculty of the Department of Mechanical Engineering

University of Houston

In Partial Fulfillment

of the Requirements for the Degree

Doctor of Philosophy

in Mechanical Engineering

by

Anis Ben Yahia

May 2019

AC LOSSES AND MECHANICAL PROPERTIES OF MULTIFILAMENTARY HIGH TEMPERATURE SUPERCONDUCTOR TAPES AND WIRES

Anis Ben Yahia

Approved:

Chair of the Committee
Venkat Selvamanickam, Professor,
Mechanical Engineering

Committee Members:

Jae-Hyun Ryou, Associate Professor,
Mechanical Engineering

John C. Wolfe, Professor,
Electrical and Computer Engineering

Yashashree Kulkarni, Associate Professor,
Mechanical Engineering

Haleh Ardebili, Associate Professor,
Mechanical Engineering

Suresh K. Khator, Associate Dean,
Cullen College of Engineering

Pradeep Sharma, Professor and Chair,
Mechanical Engineering

ACKNOWLEDGMENTS

I would like to express my sincere gratitude to my advisor Professor Venkat Selvamanickam for his continuous encouragement and guidance during this PhD. It is been a long journey and I am deeply grateful for the opportunity and the strong support throughout all these years. His knowledge, vision, suggestions and criticism allowed me to carry this work and complete this dissertation. Thank you.

I would also like to thank my committee members, Dr. Jae-Hyun Ryou, Dr. John C. Wolfe, Dr. Yashashree Kulkarni and Dr. Haleh Ardebili, for their valuable evaluations and insightful comments on this dissertation.

This work could not have been achieved without the help of several members of our research group. Beyond the research itself, it is the company, friendship and all fun moments that made this experience truly special. I would like to thank you all, especially George Pope, Lazaro Saldana, Joanna Taormina, Meysam H. Gharahcheshmeh, Rudra Pratap, Vasish Mohan, Yuan Zhang, Mehdi Kochat, Siwei Chen, Wenbo Luo, Sicong Sun, Khatiwada Devendra, and Jithin Sai Sandra. Special thanks to Dr. Xiao-fen Li, Dr. Soumen Kar, Dr. Goran Majkic and Dr. Eduard Galstyan for the invaluable help during the research.

I also want to thank the US Department of Energy (DOE-SBIR program awards DE-SC0015983 and DE-SC0018850) and Army Research Laboratory (award W911NF-12-2-044) for providing the funding that allowed this work.

Last but not least, I would like to express my deepest gratitude and love to my parents and to my brother for their endless love and support. Without your help and encouragement, it would have been impossible for me to complete this PhD. This work is dedicated to you. I hope it makes you proud.

AC LOSSES AND MECHANICAL PROPERTIES OF MULTIFILAMENTARY HIGH TEMPERATURE SUPERCONDUCTOR TAPES AND WIRES

An Abstract

Of a

Dissertation

Presented to

the Faculty of the Department of Mechanical Engineering

University of Houston

In Partial Fulfillment

of the Requirements for the Degree

Doctor of Philosophy

in Mechanical Engineering

by

Anis Ben Yahia

May 2019

ABSTRACT

With the ability to operate at high magnetic fields and high temperatures, and with significant progress in critical current density, RE-Ba-Cu-O (REBCO, RE = rare earth) coated conductors (CC) have an immense potential for use in various coil and cable applications. However, the tape form of these CC creates additional problems. The excessively high AC losses and the limited flexibility are major challenges impeding the development and commercialization of these tapes.

Recently, there have been efforts to convert flat REBCO tapes into a round wire. The diameter of these wires has been reduced using thinner substrate tapes and by positioning the copper stabilizer mainly on the REBCO film side. In this dissertation, using a combination of experimental and analytical results, the copper thickness on the REBCO side has been optimized to maximize the critical current retention of tapes with various substrate thicknesses at small bend diameters. The presented analytical method accounts for the neutral axis shift caused by the progressive plastic deformations. Using these results, an optimal design for ultra-small diameter symmetric tape round (STAR) wires is also proposed.

In addition, an alternate approach to enhance REBCO CC bending properties by using two tapes joined face-to-face is presented. In this structure, the two REBCO layers are positioned closer to the neutral axis. Two methods to fabricate such structures were implemented and their bending performance characterized.

To reduce the AC losses in REBCO tapes, a fully-scaled reel-to-reel filamentization process allowing the production of long length multifilamentary tapes has been developed. The process uses laser ablation followed by oxygenation and selective electroplating. The

AC losses of reel-to-reel produced multifilamentary tapes was significantly reduced by preventing copper growth on their back side. To address the coupling losses over long length, a new transposition pattern was also proposed and implemented.

Finally, the striation process was modified to allow the integration of the multifilamentary tapes into the STAR wires. STAR wires with various number of filaments per tape were fabricated and their AC losses characterized. Results showed exceptional AC losses reduction over a broad range of frequencies and fields compared to a normal REBCO tape.

TABLE OF CONTENTS

LIST OF FIGURES

LIST OF TABLES

CHAPTER 1. Introduction and Technical Background

1.1. Brief history of superconductivity

Superconductivity was first discovered in 1911 by Heike Kamerlingh Onnes [1]. While he was investigating the electrical resistance of various metals at liquid helium temperatures, he observed a sudden loss of resistance in mercury from 0.12 Ω at 4.3 K to less than 10^{-6} Ω below 4.2 K (Figure 1-1(a)). The resistivity of the superconducting state was later confirmed to be less than $3.6*10^{-23}$ Ω.cm by measurement of the persistent current decay as a function of time [2]. Below a certain critical temperature T_c, the resistance of the superconducting state is effectively zero. The second fundamental characteristic of a superconducting material is the perfect diamagnetism discovered by Walter Meissner and Robert Ochsenfeld in 1933 [3]. Figure 1-1(b) illustrates the so-called Meissner effect where superconductors cooled below their T_c in the presence of an external field, tend to expel nearly all the magnetic field from their interior.

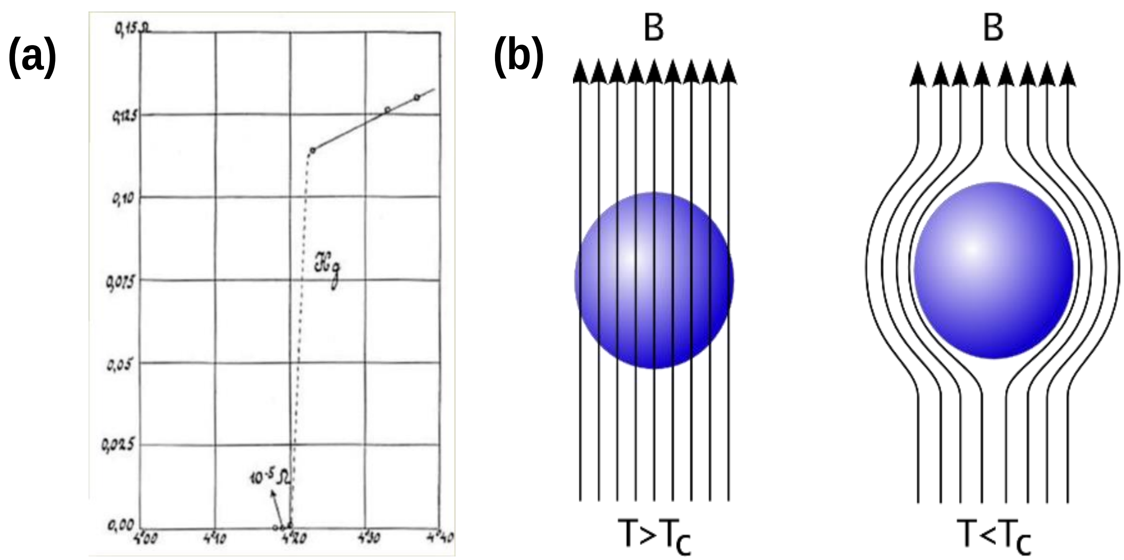

Figure 1-1 (a) Plot of resistance versus temperature from Onnes experiment in 1911 [1] (b) The Meissner effect.

Following the discovery of Onnes, superconductivity was observed in various metals, alloys and compounds such as NbTi, Nb_3Sn, and Nb_3Ge, with T_c values reaching 23.2 K for Nb_3Ge in the mid-seventies [4]. In all these materials, superconductivity at the microscopic level is successfully described by the BCS (Bardeen, Cooper, and Schrieffer) theory [5] based on electron-phonon coupling mechanisms. Based on the BCS theory, the highest possible T_c for a superconductor was predicted not to exceed the 30~40 K range.

However in 1986, a new type of "high"-temperature superconductivity was discovered by Müller and Bednorz in oxygen-deficient Ba-La-Cu-O compounds with a T_c of 35 K [6]. The discovery was quickly followed by the discovery of superconductivity at 93 K in Y-Ba-Cu-O (YBCO) compounds [7], pushing the T_c well above the temperature of liquid nitrogen and significantly increasing the number of possible applications for superconducting materials. Several other copper oxide compounds were also discovered in the pursuit of a higher T_c with Hg-Ba-Ca-Cu-O having the highest transition temperature of 133 K at ambient pressure [8] which could be increased up to 164 K by applying high hydrostatic pressure [9]. The second landmark in the development of high-temperature superconductors (HTS) was with the discovery of iron-based superconductors in 2006 [10, 11]. This new family of HTS compounds triggered a lot of interest in the scientific community since it is very different than cuprates and could help in developing the theory behind the non-BCS-type superconductivity. Another superconductor of the BCS family, Magnesium diboride (MgB_2), was discovered in 2001 [12]. Figure 1-2 summarizes some of the important historic milestones in the discovery of superconducting materials: the BCS-type superconductors are shown in green circles, the cuprates in blue diamonds, and the iron-based superconductors using yellow squares.

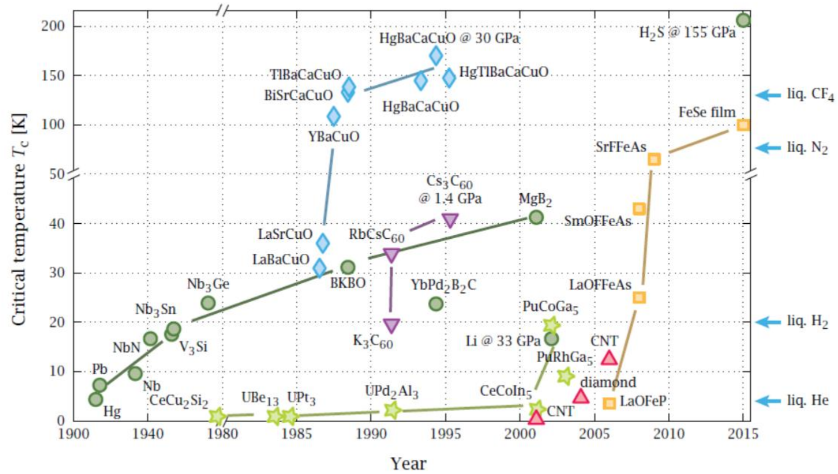

Figure 1-2 The history of some of the discovered superconducting compounds [13].

In addition to all the potential applications brought up by the possibility to operate above the temperature of liquid nitrogen, the high critical temperature of HTS comes with another advantage. They have a very high upper critical field $H_{c2}(T)$, which can exceed 100 T for $Bi_2Sr_2Ca_2Cu_3O_x$ (Bi-2223) and YBCO [14]. In fact, the real limit for applications is a lower characteristic field, the irreversibility field $H_{irr}(T)$ at which the critical current density goes to zero. Figure 1-3 shows the upper critical field $H_{c2}(T)$ (indicated in black) and irreversibility field $H_{irr}(T)$ (indicated in red) for some HTS (Bi-2223 and YBCO) and some low-temperature superconducting (LTS) materials.

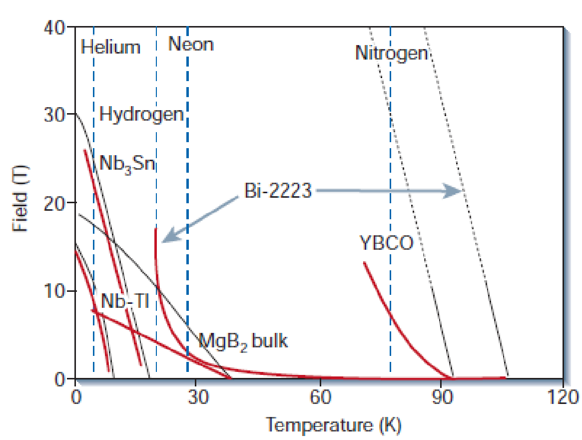

Figure 1-3 The upper critical field $H_{c2}(T)$ (black lines) and the irreversibility field $H_{irr}(T)$ (red lines) for NbTi, Nb_3Sn, MgB_2, Bi-2223 and YBCO. [14].

1.2. High temperature superconductors

1.2.1. BSCCO

While the high operational temperatures and high critical fields hold a lot of promises for HTS, the development of these materials into practical wires is more challenging than for LTS. The first commercially-developed HTS wire was Bismuth Strontium Calcium Copper Oxide (BSCCO). These superconducting wires, known now as the first-generation high temperature superconductor (1G HTS), were made in two different types: Bi-2212 and Bi-2223. The Bi-2223 was made using the powder-in-tube (PIT) process. The Bi-2223 powder is packed into Ag billets which are then drawn into a thin filament. The filaments are then packed and redrawn again until the desired structure is achieved. Finally, the wire is rolled into a tape to achieve the grain alignment and a high enough critical current density (J_e) for applications [15]. A cross-section of a multi-filament Bi-2223 tape is shown on the left of Figure 1-4.

The second type of BSCCO superconductor, the Bi-2212, can be made into round wires. In fact, to date, it is the only HTS material that can be made into a round form. While the first Bi-2212 wires were made in 1989 [16]. The low powder density was problematic in the as-drawn wire until 2014 when overpressure (OP) processing allowed to significantly increases J_e in long-length round Bi2212 wire and made it a potential candidate for high-field magnets operated at 4.2 K [17].

Figure 1-4 Cross-section of a Bi-2223 tape (left) and a Bi-2212 wire (right) [18].

1.2.2. REBCO

The second generation (2G) of HTS materials developed was the rare earth superconductors RE-Ba-Cu-O (REBCO, RE = rare earth) with the most famous compound being the Yttrium barium copper oxide (YBCO). However, the manufacturing of REBCO into wires was not very successful using conventional metallurgic processes, mainly because the REBCO performance is sensitive to the grain misalignment [19-21]. Thin film approaches were successful into depositing a high performance REBCO layer into a polycrystalline, flexible metallic substrates by using a template layer that has a biaxial texture which is then transferred to the superconductor by epitaxial growth. The three commonly-used processes to produce the textured substrate are the Rolling Assisted Biaxially Textured substrates (RABiTs) [22], the Ion Beam Assisted Deposition (IBAD) [23, 24] and the inclined-substrate deposition (ISD) method [25].

The structure of the buffer layers varies slightly depending on the manufacturer and methods used. Generally, it consists of a diffusion barrier, a nucleation layer and finally the biaxially textured template. Other layers could present to enhance the texture quality or absent depending on the technic employed. Examples of the materials used for the diffusion barrier are Al_2O_3 and YSZ. They prevent the diffusion of certain elements, like Ni, Cr, Mo and others, from the Hastelloy to the REBCO which could degrade the tape's performance or even destroy completely the superconductivity. For the IBAD process the texture is achieved either using yttria-stabilized-zirconium-oxide (YSZ) [26, 27] or MgO [28, 29]. The texture development in IBAD YSZ is an evolutionary process requiring about 1 μm to achieve the desired texture. While in IBAD MgO, the texture happens at the nucleation stages so only few nanometers are needed to achieve the texture. This allows for high deposition speeds for the IBAD MgO process.

An example of the configuration of a 2G HTS tape from Superpower Inc [30] is shown on the left side of Figure 1-5, the right side shows the structure of a similar tape made by Fuijikura [31]. The conductor from Superpower consists of a buffer stack made of Al_2O_3, Y_2O_3, MgO, and $LaMnO_3$ layers, deposited over an electro-polished Hastelloy substrate. The REBCO layer is ~ 1.6 μm thick produced by metal organic chemical vapor deposition (MOCVD). The tape is then coated with a 2 μm silver layer on the REBCO side and a 1.8 μm layer on the substrate side. Finally, the conductor is made available with or without a surrounding layer of copper stabilizer. Today, long lengths of these 2G-HTS coated conductors (CC) are commercially available from several companies such as American Superconductor, Superpower, Sunam, SuperOx, Fujikura and Bruker to name a few.

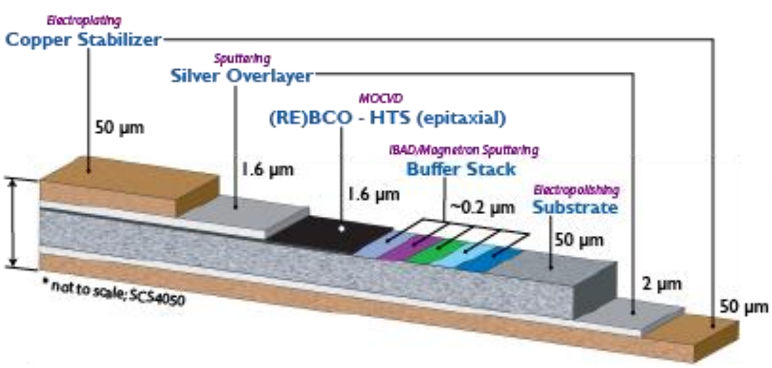

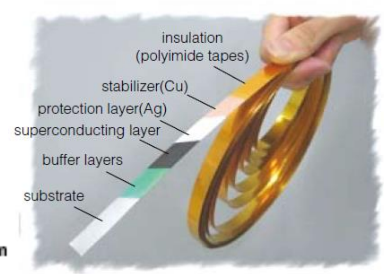

Figure 1-5 Configuration of SuperPower® 2G HTS Wire [30] (left) and a photograph of a 2G HTS wire from Fujikura [31] (right)

1.2.3. HTS: promises versus challenges

The continuous improvement of the performance of HTS coated conductors by the addition of artificial pinning centers [32-34] makes them the most promising candidate for a wide range of applications. Figure 1-6 some of the possible applications for superconducting materials classified and their corresponding operating field and temperature range. HTS materials are not just limited to high temperature applications such power cables, Fault current limiter (FCL), transformers and motors. They extend also to low temperature where LTS are eventually limited by their upper critical field. HTS still have substantial critical current density in magnetic field in excess of 25 T, as shown in Figure 1-7. Possible low temperature applications include compact fusion reactors, high field magnets for future particle accelerator and GHz-class NMR magnets.

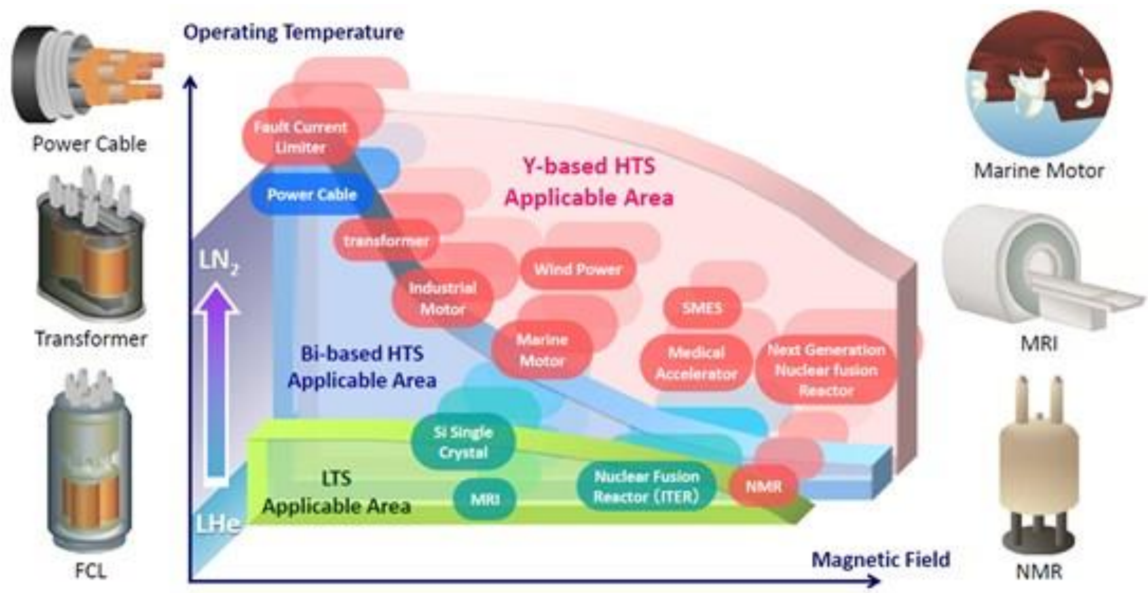

Figure 1-6 Various superconductor applications and most suitable superconducting material based on operating field and temperature [35]

Figure 1-7 also shows a comparison of the in-field performance of the various superconductors at 4.2 K and up to 31.2 T. It is clear that REBCO CC come with the highest promise in term of in-field critical current density. However, they also come with significant challenges that have to be addressed before all these promises could be translated into practical applications.

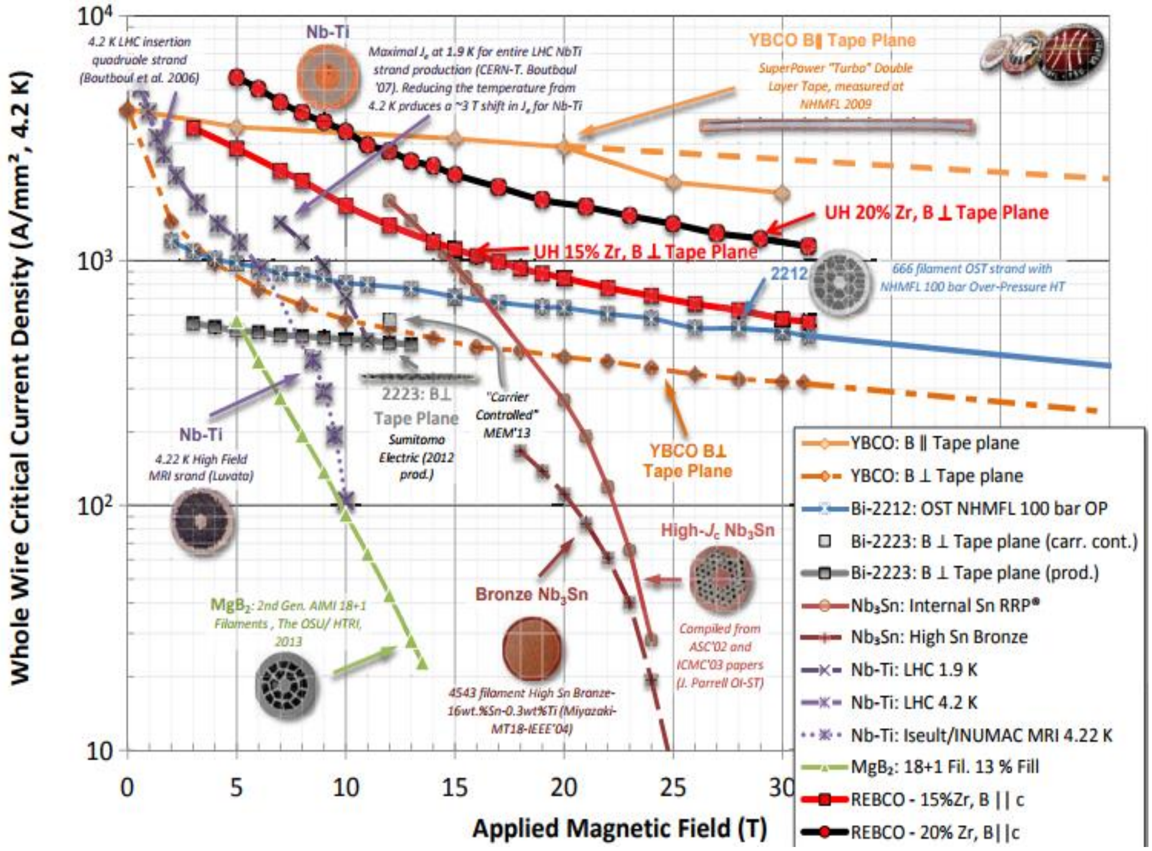

Figure 1-7 In-field critical current density for various type of commercial and experimental superconducting wires measured at the NHMFL [36].

First, the cost of these REBCO CC is still extremely high in comparison to LTS, restricting significantly their potential use. Significant amount of effort is invested into reducing the cost of these CC whether it is by improving the yield of current manufacturing processes [37, 38] or by the development of newer advanced deposition techniques allowing a more efficient deposition of thicker films with higher performance [34]. A record critical current density of 15 MA/cm^2 at 30 K 3 T was achieved recently with 4.8 μm thick films [39]. Such wire performance, when scaled for long length production, could enable the use of REBCO tapes in further applications.

The second challenge that still sets REBCO CC apart from most other commercially available superconductors is the lack of an easily reproducible process allowing the fabrication of REBCO-to-REBCO superconducting joints. There have been some reports of successful REBCO superconducting joints [40-43], but so far none of these techniques have been deployed on a large scale.

Another challenge lies in the mechanical performance of these HTS coated conductors (which this dissertation tries to address long with the AC losses issue). REBCO is a brittle ceramic material and its performance is sensitive to strain. The flexibility of the tape will be major constraint in a variety of applications and for some others, a round conductor with isotropic properties is necessary. Besides, the aforementioned high-field applications will result in large stresses which the conductors have to withstand, without degradation, during operations. To achieve any of the promises carried by REBCO CC, there is a need for highly flexible and robust REBCO tapes and wires.

Finally, there is the question of AC losses in HTS coated conductors. In AC applications, the tape geometry of the REBCO CC with a very thin superconducting layer and a high aspect ratio makes AC losses a significant problem in practical applications. The extraction of heat due to these losses represent not only an additional operational cost but depending on the operating conditions, they could be so high so that they would render the use of a REBCO tape practically impossible. There is a need for low magnetization, low AC losses REBCO tapes and wires.

1.3. Mechanical properties of REBCO conductors

1.3.1. The REBCO strain limits

The current carrying capabilities of REBCO coated conductors are sensitive to the applied strain on the conductor. Early studies [44, 45] showed that the effect of strain on the critical current density is reversible up to a certain strain irreversibility limit ε_{irr}. For strains in excess of ε_{irr}, the REBCO starts degrading due to crack propagation in an irreversible manner. The strain dependence of the critical current density is an intrinsic property of the REBCO which strongly depends on the magnetic field and temperature. Besides, the strain tolerance of commercially-available REBCO tapes has been studied and the critical current (I_c) dependence on the strain within the superconducting layer was found to be a characteristic of the manufacturing process [46]. Each type of tape exhibits specific compressive and tensile strain limits and a different reversible and irreversible behavior that are due to reasons beyond the simple difference in substrate thicknesses. Figure 1-8 shows an example for the critical current dependence on the axial bending strain for tapes from two different manufacturers. The tape from SuperOx can withstand more compressive strain before the onset of critical current decay while the tape from Bruker starts degrading with very little compressive strain. That degradation is reversible up to ~1% strain. It should be noted that these differences cannot explained simply by the residual strain in the film and need further investigation [46].

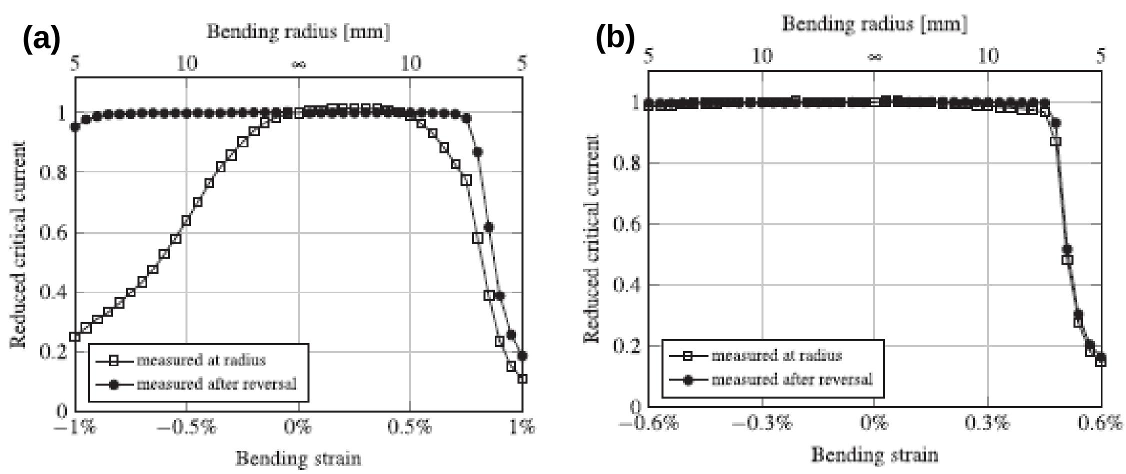

Figure 1-8 Reduced critical current as a function of the bending strain for (a) a Bruker tape with 97µm substrate and 20µm Cu stabilizer and (b) a SuperOx tape with 60µm substrate and 20µm Cu stabilizer [46].

Another interesting behavior observed for both RABiTS and IBAD CCs is the extension of the irreversibility strain limit by the addition of a copper layer. In addition to improving the thermal and electrical stability of the tape, the added copper layer, whether it is electroplated at room temperature for the IBAD conductor or laminated at 200ºC in the case of RABiTS tapes, enhanced the tolerance of the both coated conductors to axial strain. The irreversibility strain limit increased from ~0.4% to ~0.5%, as shown in Figure 1-9. This is due to a combination of a fracture toughness improvement of the REBCO tape with the Cu layer preventing or delaying the crack initiation, and the differential thermal contraction between the Cu layer and the substrate [45, 47].

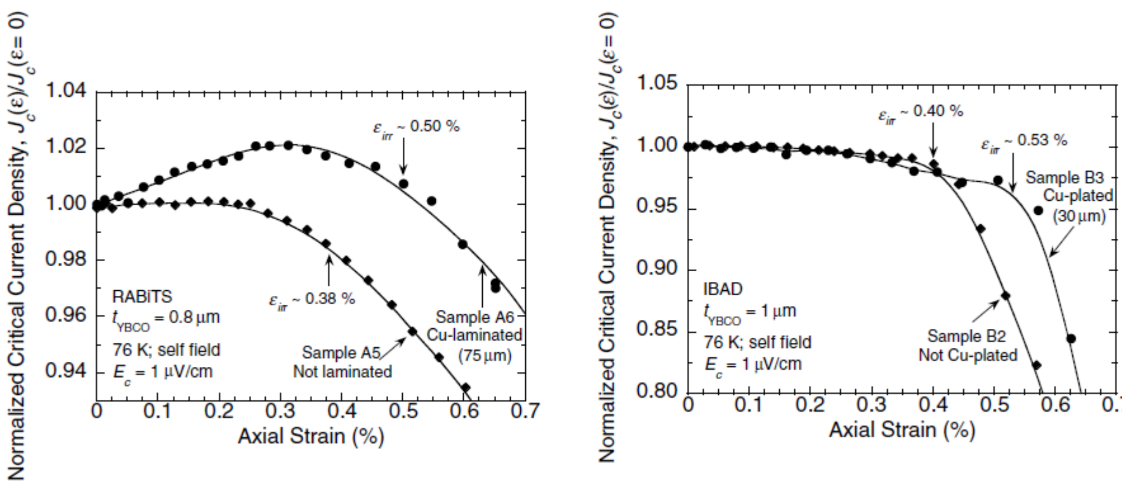

Figure 1-9 Normalized critical-current density as a function of axial tensile strain at 76 K for two REBCO CC with and without Cu stabilizer [45].

1.3.2. Application requirements

There are challenges that come with the tape form of the REBCO CC even though REBCO tapes have better mechanical properties than BSCCO superconductors both in term of tensile strength and bending performance [48, 49]. This bending performance and the strain limits mentioned in the previous section are only valid in the longitudinal direction (the easy-way bending). When bent in the transverse direction, the hard-way bending, the performance of the tapes is not the same. Besides, multistrand round cables are desirable for high field, low inductance magnets and the design and performance of these cables are dictated mainly by the mechanical properties of the tape used [50]. There has been some clever magnet designs circumvent the hard-way bending of tape and avoid the degradation of the tape's critical current [51, 52]. For example, if REBCO tapes are used in a conventional accelerator dipole magnet layout they would be subject to transverse bending at the coil ends [53]. Figure 1-10 shows the design proposed for the REBCO 20T+ magnet under development at CERN which uses cloverleaf coil-ends to avoid hard-way bending of REBCO tapes. While the Cloverleaf coil-ends design has the benefit of avoiding the hard-way bending of the conductor or cable, it could complicate or prevent the usual dual aperture configuration of the beams. There is definitely a need for more flexible REBCO tapes, preferably with isotropic bending properties.

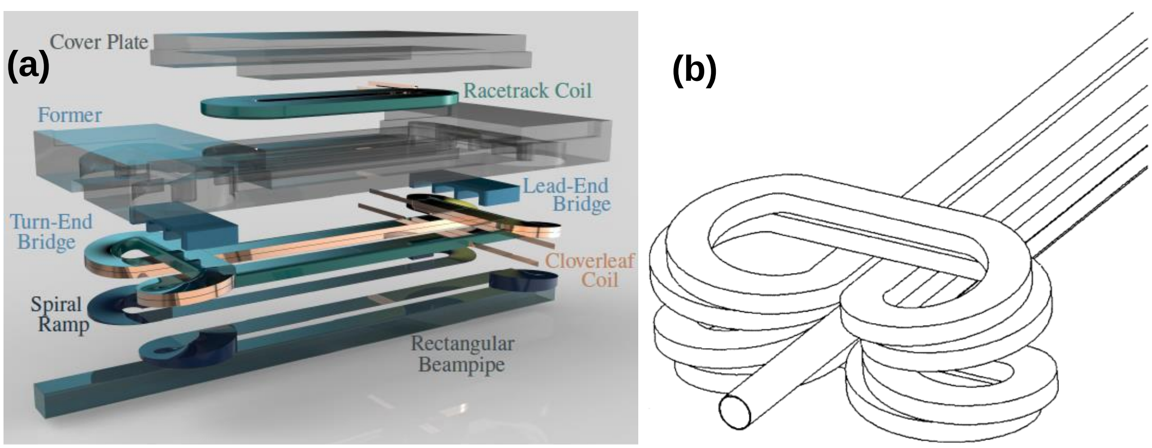

Figure 1-10 (a) Conceptual design of the REBCO 20T+ magnet under development at CERN [53] (b) Overpass/Underpass end design of the cloverleaf coil [54].

However, for certain magnet designs, a tape is not suitable and round conductor is needed. A perfect example is Canted Cosine Theta magnets, currently under development for potential use in the High-Luminosity upgrade of the LHC (HL-LHC) [55, 56] and for proton therapy at the Lawrence Berkeley National Laboratory (LBNL) [57]. In this type of magnet, shown schematically in Figure 1-11, the conductor is wound as two oppositely-tilted solenoids, requiring a round conductor with isotropic bending performance. Besides for this particular design, the conductor has to meet a certain minimum J_e requirement for each application.

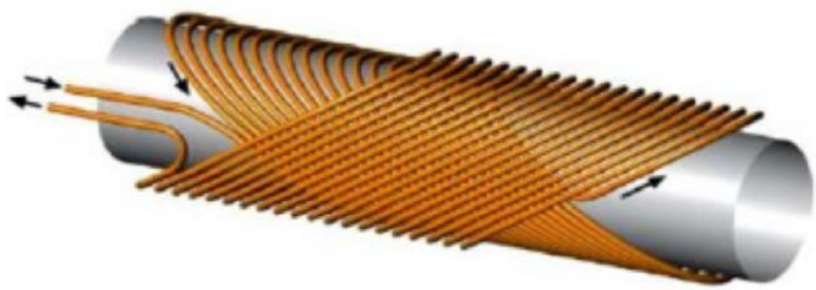

Figure 1-11 Canted Cosine Theta magnet scheme [58].

1.3.3. Technology status

1.3.3.1. Substrate thickness

The most intuitive and straightforward approach to increase the tape flexibility is to make it thinner. Over the last decade, there have been remarkable progress in the current carrying capabilities of 2G-HTS tapes. Most of that progress was made by improving artificial pinning and growing thicker films [32, 33, 39, 59]. Manufacturers offer REBCO films on substrate thicknesses ranging between 50 and 100 μm and there have been little effort to reduce the substrate thickness until recently. In 2014, Superpower Inc. reported the development of REBCO tapes on 38 μm substrates [60] and on 30 μm substrates in 2016 [61]. Parallel efforts to produce thinner substrate tape are being conducted at the University of Houston and REBCO tapes with ultra-thin substrates ranging from 18 to 24 μm have been successfully demonstrated [62-65].

1.3.3.2. Common cabling concepts:

There having been numerous designs for HTS cables aiming ultimately at achieving a multi-tape high current cable with low AC losses and good mechanical properties. These cabling concepts can be grouped into three different categories based the tape arrangement in the cable.

- **ROEBEL Assembled Coated Conductors (RACC)**

Ludwig ROEBEL proposed, in 1914, a new design to reduce AC losses in copper cables used in generators [66]. The ROEBEL cable design is based on separating the current in several strands and that are transposed along the cable direction over a short distance. This allows to reduce the eddy current and heat generated in the copper conductors of power generators. The first application of the ROEBEL concept to superconducting cables was with NbTi (shown in Figure 1-12) as part of the Large Coil Task (LCT) project [67], a fusion reactor program in the 80's.

Figure 1-12 NbTi ROEBEL cable used in the Large Coil Task project [67].

In order to use a ROEBEL structure with REBCO CC, the tapes have to be mechanically cut into a ROEBEL strand shape and assembled into a cable as shown in Figure 1-13. The final strand arrangement is electrically equivalent to the original

ROEBEL concept and the transposition length is not determined by the tape bending properties. While this type of cable does not provide any solution to the previously stated mechanical limitations of the REBCO tape, it has the advantage of offering lower AC losses thanks to the transposed strands and most importantly, it has a high tape filling factor making its engineering density high enough to meet the requirement for future accelerator magnets [53, 68].

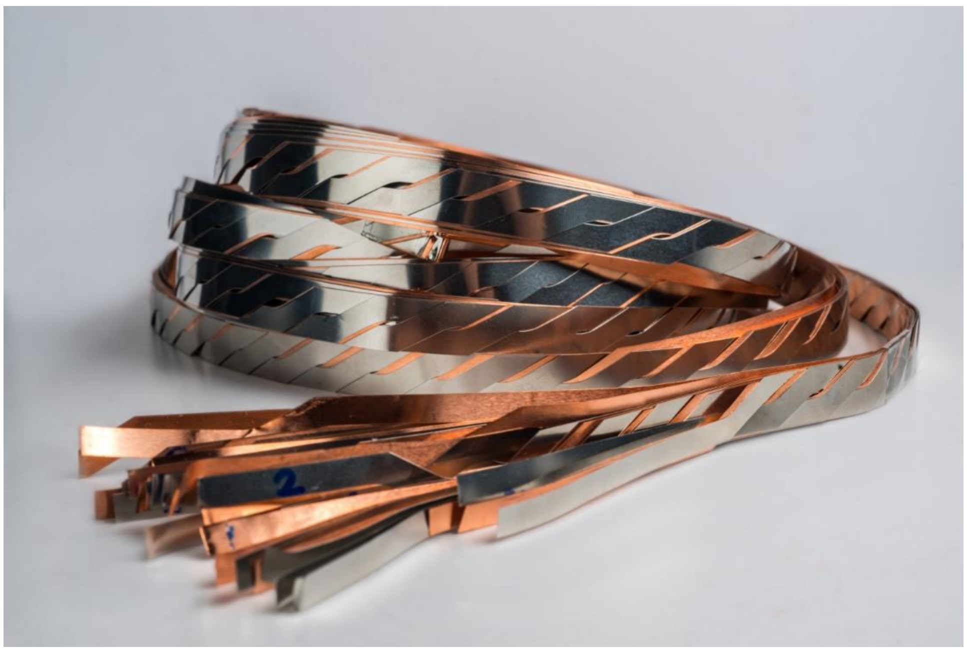

Figure 1-13 Prototype ROEBEL cable [69].

- **Twisted Stacked-Tape Cables (TSTC)**

The twisted stacked-tape, proposed at MIT [70], is a much simpler and economical design than that of the ROEBEL since no tape is lost in the process (Between half to two third of the original tape is lost in the cutting of the ROEBEL strands). However, the twisting has to be over relatively large distance (the twist pitch is around 20 cm for the example shown in Figure 1-14) to avoid excessive degradation of the tape critical current [71]. Besides, theses cables have limited flexibility and are more suitable for certain bent geometries that are accommodated to the cable twist pitch such us a pentagon coil shape instead of conventional solenoid winding [72].

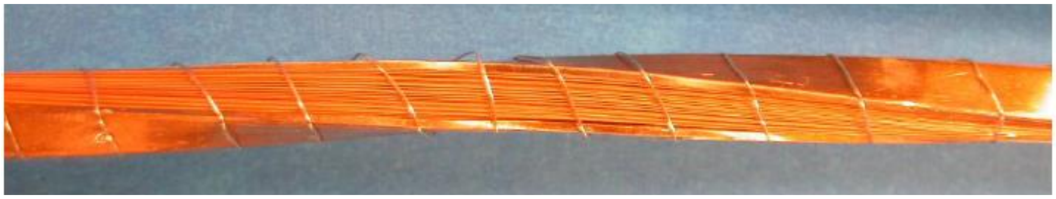

Figure 1-14 A 32 tapes REBCO Twisted Stacked Tape Cable (TSTC) with 200 mm twist pitch [73].

Circular strands were made by incorporating the tape stack between two pre-shaped copper pieces [50, 74]. The critical current of the obtained strand makes it suitable mainly for fusion magnets where the bending requirements are less stringent.

- **Helical wrapping around a central support**

In this layout, one or several REBCO tapes are helically wrapped around a round core. The concept was originally proposed in 2005 [75] as a mean to create a round conductor from a REBCO tape that could be incorporated in a variety of application such as power cables, power transformers and rotating machines. In 2009, helically wound CORC (Conductor on Round Core) cables were introduced [76], shown in Figure 1-15. They consist of multiple layers of commercial REBCO tapes, wound in alternating directions on a round former. The diameter of the former ranging from 2.2 mm to 4 mm and the final wire outer diameter from 3 to 5 mm [76, 77]. While this type of wires offers isotropic bending and more flexibility than the RACC and TSTC conductors, it is limited in term of engineering current density. The use of a large Cu core reduces the J_e significantly. So far, achieved current densities do not meet future particle accelerator magnets currently set at 700 A/mm^2 at 20 T overall engineering current density in the magnet. Besides, because of the large Cu core, to achieve a high enough critical current density, a significant number of layers is needed which not only increases the overall wire OD but also reduces its flexibility which results in excessive critical current degradation at small bend diameters [77, 78].

Figure 1-15 CORC wire and cable [77].

More recently, a dramatic improvement in bend tolerance as well as high engineering current density were achieved by the use of REBCO tapes with ultra-thin substrates (18-22 μm) combined with the copper stabilizer positioned predominantly on the REBCO layer side [64, 65]. In this tape architecture, shown in Figure 1-16, the REBCO layer is positioned near the geometric center, close to the neutral plane [79, 80]. REBCO tapes on ultrathin substrates with the superconductor film positioned near the geometric center exhibit exemplary bend tolerance. Critical current retention of nearly 100% has been demonstrated even when wound on formers as small as 0.51 mm [64].

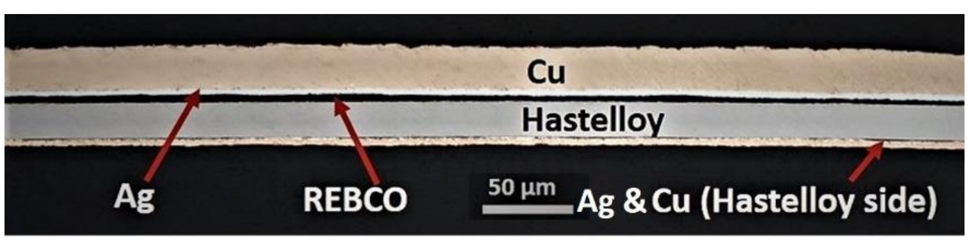

Figure 1-16 Cross-section of a tape used in the STAR wires where the REBCO film is near the center to minimize bend strain [81].

Such tapes have been used to fabricate Symmetric Tape Round (STAR) REBCO wires of just 1.6 – 1.9 mm in diameter that exhibit high J_e even when bent to a radius of 15 mm [81, 82]. In order to achieve the high critical current density and flexibility requirements, the copper thickness has to be carefully optimized. In this dissertation, a combination of experimental measurements and analytical results will used to determine the optimal Cu thickness needed in each layer in order to maximize the wire engineering current density and optimize the layout of the STAR wires.

Figure 1-17 (Left) Photograph of a 1.6 mm diameter REBCO STAR wire made of 6 layers wound on a 0.81 mm diameter former. (Right) The wire bent to 3 cm diameter [64].

1.4. HTS applications and AC losses

1.4.1. Origin of AC losses in superconductors

Superconductors can carry current without losses only in DC operations. When operated under time varying magnetic fields or with alternating currents, there is energy dissipation in type-II superconductors referred to as AC losses. These losses are heat generated at cryogenic temperature, which needs to be extracted creating an additional operational cost when a superconductor is used with AC currents or AC fields. In the case where a superconductor is carrying an AC transport current in an AC magnetic field, the total AC losses will be the sum of both contributions with each component depending on both the applied field and current [83, 84].

Magnetization losses are the more significant component of AC losses in superconductors and can be divided in three categories: hysteretic, coupling and eddy current losses. Hysteretic losses are due to the hysteretic nature of the magnetization in type II superconductors generated by the flux pinning. In the mixed state, the irreversible motion of the flux lines driven by the external field causes the energy dissipation. In a time-varying magnetic field, currents will flow to oppose the flux change inside the superconductor, starting from the outside. However, when J_c is reached, deeper regions will also attempt to exclude the field. And the flux passing over these currents still attempt to increase them further but is prevented by the resistance that appears which leads to the ohmic dissipation of heat [85]. The area enclosed by the magnetization curve, shown in Figure 1-18, through a field cycle represents the losses.

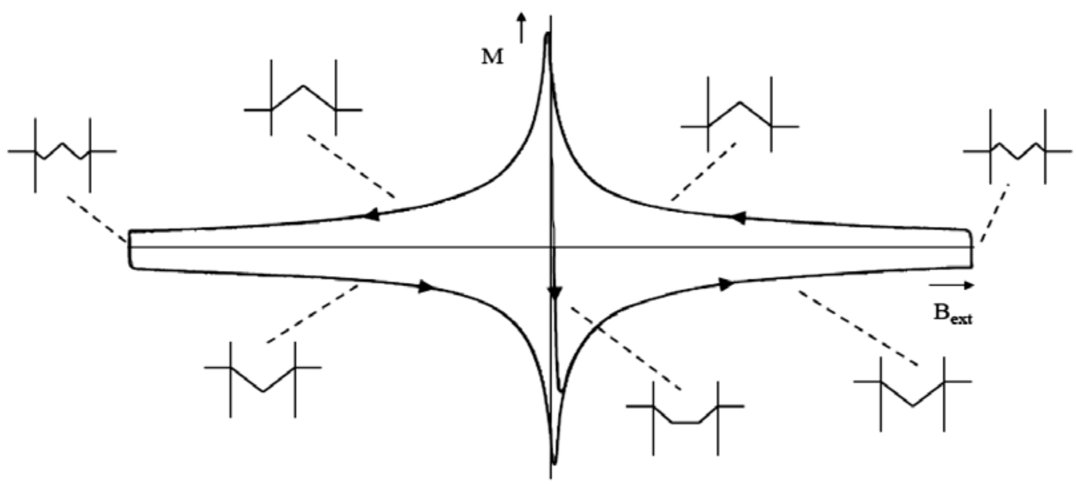

Figure 1-18 Magnetization loop for a type II superconductor [86]. The plots on the sides show the magnetic field profile across the tape's width at the various stages of the magnetization cycle.

When subject to a time varying magnetic field, the normal metal stabilizer and substrate will be subject to conventional eddy current losses which also need to be addressed. Finally, coupling losses occurs in the case of a composite superconducting material made of several superconducting filaments embedded in a normal-metal matrix. The changing magnetic field could cause the screening currents to flow through the normal metal matrix and the multifilamentary superconducting wire will behave as a monofilament in term of magnetization response as shown in Figure 1-19. In fact, such configuration provides higher screening, and from Lenz's law, this should take priority provided there is enough driving voltage to overcome the matrix resistance. When currents flow through the normal resistive matrix, this creates what is referred to as coupling losses [87].

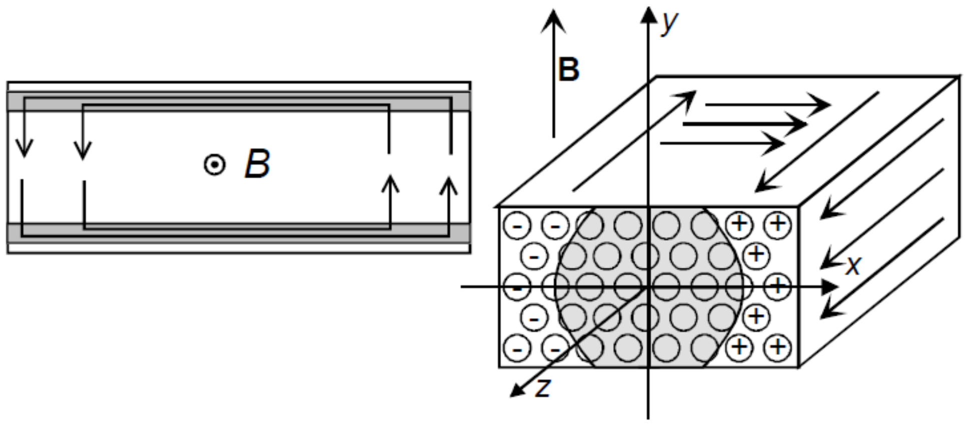

Figure 1-19 Coupling current in multifilamentary superconducting wire [88].

1.4.2. Application requirements

Several applications considered for superconductors involves AC fields and currents such as superconducting motors and generators, power transmission lines, transformers, fault current limiters and many others. For some of them like aircraft electric propulsion and power transmission lines, there have been an increasing interest since the discovery of HTS. One of the main challenges facing the achievement of these particular applications is AC losses.

Superconducting windings can allow the development of the high-power density motors and generators needed for future electric or hybrid-electric aircraft design (shown in Figure 1-20). Using normal conductors, the motor power density is estimated to reach at best 20 kW/kg, while with superconducting materials, it could attain 45 kW/kg [89-91]. Because of their high in-field current carrying capabilities, superconducting winding can operate at much higher fields thus increasing efficiency and reducing the size of the device. However, higher-field operations will result in higher AC losses which have to extracted at cryogenic temperatures. For aircraft propulsion, this would mean added weight to accommodate the additional cooling requirement. REBCO CC are among the potential candidates that could enable such machines. It has been estimated that in its current status, as a monofilament conductor, the AC losses generated by the REBCO is excessively high and they need to be reduced by a factor of 100 to meet the design requirements [89].

Figure 1-20 Schematic of a turboelectric propulsion system, highlighting required electrical machines [92].

Another application where HTS have been demonstrated is power transmission cables. Figure 1-21 shows an example such cables made by Sumitomo Electric [93]. Several demonstrations of in-grid cables have been made along with studies of the reliability and stability over long term operations [94-96]. AC losses reduction will be helpful to minimize cryogen consumption and operating cost [97-99].

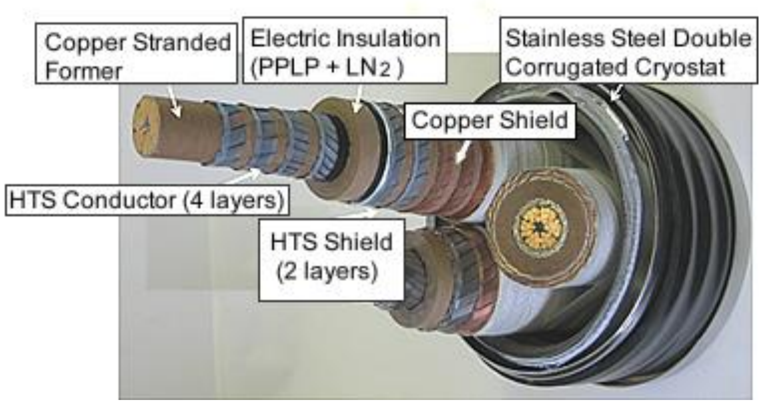

Figure 1-21 A three-core HTS power transmission cable from Sumitomo Electric [93]

1.4.3. AC loss reduction techniques

The high AC losses of REBCO coated conductors (compared to other superconductors) is due the tape layout where the superconducting layer is only 1~2 um thick and few millimeters wide. In 1999, Carr and Oberly [100] have proposed that in order to reduce AC losses in REBCO CC, the tape could be split into several strip-like narrower filaments. In addition, these filaments need to be twisted along the conductor length to minimize both coupling and eddy current losses [100-102], as shown in Figure 1-22. In addition, the striation will also reduce the eddy current losses in the stabilizer layer since these losses are proportional to the width squared [83].

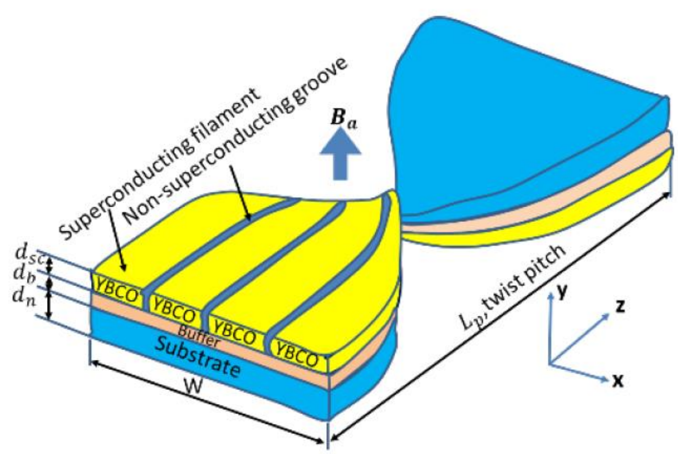

Figure 1-22 A schematic of the filamentization and twisting concept [86].

A variaty of techniques have been used to achieve the filamentization such as mechanical scribing [103], inkjet printing [104, 105], laser ablation [106, 107], substrate modfication [108] and laser lithography along with chemical etching [109]. Filamentization has been proven to be an effective method in reducing magnetization AC loss of RE-Ba-Cu-O (REBCO) coated conductors with the highest values of AC loss reduction in coated conductors fabricated with a thick copper stabilizer achieved using laser ablation and selective copper electroplating [110, 111]. However, reel-to-reel produced samples using this method showed lower reduction levels [112]. Other top-down approches, where the striation is performed on an already copper-stablized tape, were attempted but they resulted in excessive critical current reduction with a limited AC losses reduction [113]. Furukawa Electric [114] produced multifilamentary tapes using laser ablation, but the superconducting filaments are bridged by the silver overlayer and the surrounding copper stabilizer, as shown in Figure 1-23. This makes such tape not very effective for AC operations because of the coupling losses. Long length production of low AC losses REBCO tape is still an ongoing reseach venue.

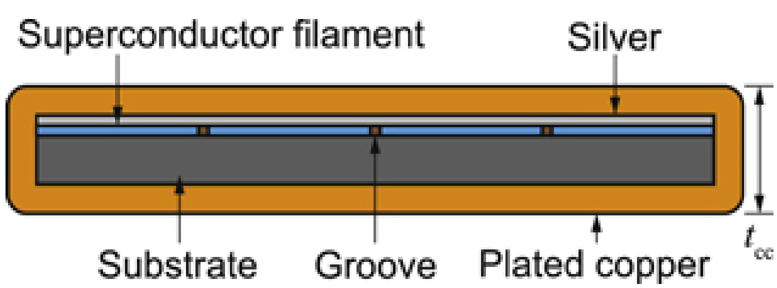

Figure 1-23 Schematic cross section of striated coated conductor [114].

1.5. Objective and outline of the dissertation

The first objective of this work is to develop an analytical model that describes REBCO CC bending behavior. This model will then be used to optimize the layout of helically-wound REBCO STAR wires. The second goal is to present alternative tape structures allowing for enhanced bending performance of REBCO CC.

The third goal is to develop a fully-scaled reel-to-reel filamentization process allowing the production of long length multifilamentary tapes with low AC losses along with a method to transpose the filaments without any mechanical twisting. The final goal is to integrate the multifilamentary tapes into the ultra-small diameter STAR wires to produce highly flexible multifilamentary STAR wires with extremely low AC losses.

This dissertation is structured as follows:

Chapter 1 provides an introduction to superconductivity, the application requirements and challenges related to HTS tapes and the goals of the dissertation.

Chapter 2 provides an analytical model that captures REBCO CC bending behavior by accounting for the progressive plastic deformation in the various layers during bending. The validity of model is examined using experimental measurement on tapes with various substrate thicknesses. Based on these results, an optimized structure for helically-wound ultra-small diameter REBCO STAR wires is proposed.

Chapter 3 presents an alternative new approach to enhance bending properties of REBCO coated conductors by using two tapes joined face-to-face. Two methods to fabricate such structures are presented: silver to silver diffusion bonding and soldering.

Chapter 4 provides the details on a reel-to-reel filamentization process. The various process parameters are presented and their effects on the microstructure and the AC losses performance of the tapes are discussed along with the design allowing the transposition of the filaments. Finally, the integration of the multifilamentary tapes into the ultra-small diameter, helically-wound, STAR wires is presented. The critical current retention and AC losses performance of several wire configurations are shown.

In the conclusion, a summary of the major results is provided along with recommendations for potential future work.

CHAPTER 2. REBCO Tapes Bending Modeling and Helically Wound Ultra-Small Diameter STAR Wires Optimal Design

2.1. Introduction

A dramatic improvement in bend tolerance as well as a high engineering current density (J_e) were achieved by the use of REBCO tapes with ultra-thin substrates (20-22 μm) combined with the copper stabilizer positioned predominantly on the REBCO layer side [64, 65]. In this tape architecture, the REBCO layer is positioned near the geometric center, close to the neutral plane [79, 80]. In order to achieve high critical current (I_c) retention at small bend diameter, the relative thickness of copper stabilizer on REBCO and substrate sides had to been carefully optimized based on the substrate thickness. In addition, at such diameters, the strains in the various layers exceed by far their elastic limits and plastic deformations have to be considered in order to properly assess the REBCO coated conductors' bending behavior.

In this chapter, an analytical model based on laminate beams bending is presented. The model accounts for the neutral axis shift caused by the progressive plastic deformation in the various layers. The results show that using a single-sided optimal stabilizer thickness, significant reduction in the strains in the REBCO layer could be achieved at small bend diameters. Samples with various substrate thicknesses were electroplated only on the REBCO side with various copper thicknesses and their bending performance tested. The scaling of the critical current retention as a function of the strain in the REBCO layer confirms that difference in bending performance is due to the differences in neutral axis location among the various configurations. Finally, based on these results, an optimized structure for helically wound ultra-small diameter REBCO STAR wires is discussed.

2.2. Bending strain derivation and model's assumptions

The tape is treated as an inextensible thin composite beam undergoing pure bending. The tape's thickness is small so that any shear is neglected and the Euler-Bernoulli hypotheses are used to derive the strain. The strains throughout the cross section are assumed to be continuous and are determined by the local curvature κ of the neutral axis ($\kappa = 1/\rho$, ρ being the bending radius, Figure 2-1) and the distance y_i between each element and the neutral axis [46, 115]

$$\varepsilon_i = -y_i \kappa = -\frac{y_i}{\rho}. \tag{2-1}$$

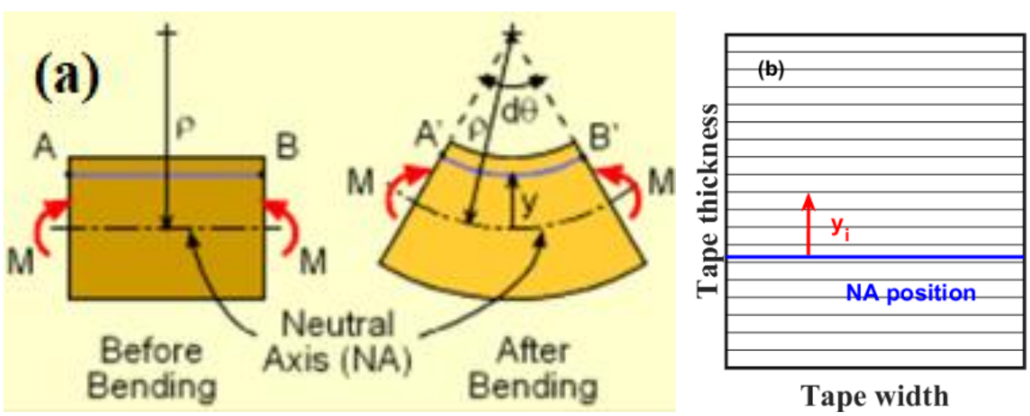

Figure 2-1 (a) Small beam element undergoing bending [116] (b) Configuration of the tape's cross-sectional elements

The tape's cross section is subdivided into 0.01 μm thick elements over which the strains are assumed to be constant. The stresses are then calculated in each element and summed over the cross-section by assuming a certain position for the neutral axis. The neutral axis during pure bending is defined by balancing the internal stresses, σ, generated by the external bending moment

$$\sum_i \int_{A_i} \sigma_i dA = \sum_i \int_{h_i} \sigma_i dy = 0, \tag{2-2}$$

where A_i and h_i refer respectively to the cross-sectional area and height of the i^{th} layer of the tape. The calculation is then repeated by changing the assumed position of the neutral axis by a step of 0.01 µm throughout the entire tape thickness until the position that satisfies the stress balance between the tensile and the compressive sides is determined.

2.3. Materials properties

The stress-strain curves of the Hastelloy, silver and copper are shown in Figure 2-2. Only the Hastelloy, silver, REBCO and copper layers are represented. The buffer stack is not considered due to its negligible thickness. This data used is relevant to tapes from Superpower Inc [117], since in this work their tapes were used to evaluate the validity of these calculations. In addition, the silver, REBCO and buffer layers were chemically etched and the Hastelloy stress-strain characteristic was also investigated by uniaxial tensile testing and was found to match the data from [117]. For both the Hastelloy and copper, the stress-strain curves were extrapolated outside of the measurement range using Ramberg–Osgood equation [118]. The silver was modeled as elastic perfectly plastic with a Young's modulus and a yield strength of 84 GPa and 54 MPa respectively [119]. Only elastic deformations were considered for the REBCO layer using a modulus of elasticity of 200 GPa [120]. Although, the presented results are specific to Superpower tapes, material properties relevant to other tapes could be used to derive similar results.

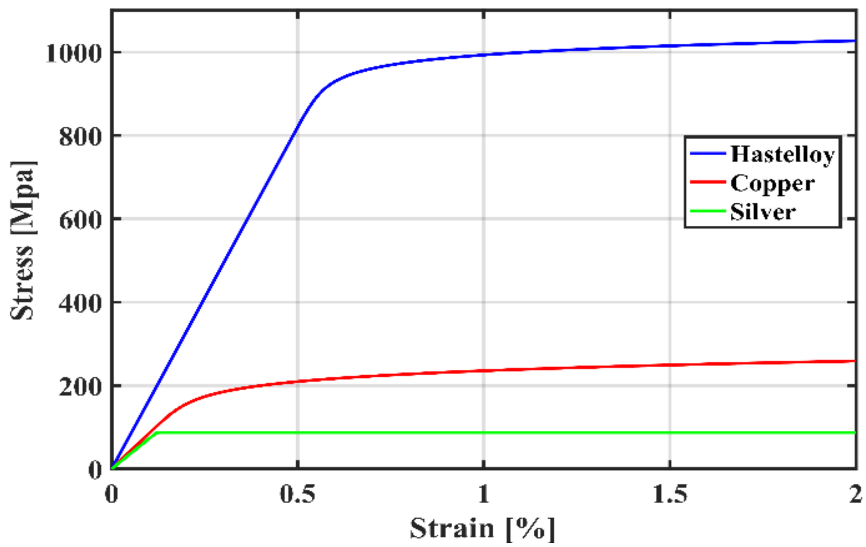

Figure 2-2 Stress-strain characteristic of the various layers at room temperature

2.4. Calculation results

2.4.1. Neutral axis shift

The first important result when working with tapes having such asymmetric structure is that the position of the neutral axis (NA) location is no longer fixed but is rather a function of the bend diameter. This shift is caused by the progressive plastic deformations throughout the various layers with decreasing bend diameter. Figure 2-3 shows an example of the neutral axis shift for a 20 µm substrate tape with 30 µm Cu on the REBCO side. The bending is such that the REBCO would be in compression at smaller diameters (equivalent to having the Cu layer facing the former). Initially, in the elastic regime, the NA location is fixed and for this example, it is at the Ag/REBCO interface. As the strains increase (i.e. the bend diameter is decreased), the Cu layer will exceed its elastic limits and can no longer carry the additional stresses so the neutral axis starts shifting toward the Hastelloy in order to satisfy the stress balance between the tensile and compressive sides. Eventually, at some smaller diameter the strains increase to the point the Hastelloy starts yielding in tension. Then the NA position starts moving back toward the REBCO layer to maintain the stress balance until the substrate reaches its yield point in compression as well. Figure 2-4 shows a configuration where such stress distribution would happen in the tape and the corresponding NA location. In this example, the strain in REBCO layer has reached ~1% in compression at 1mm bend diameter.

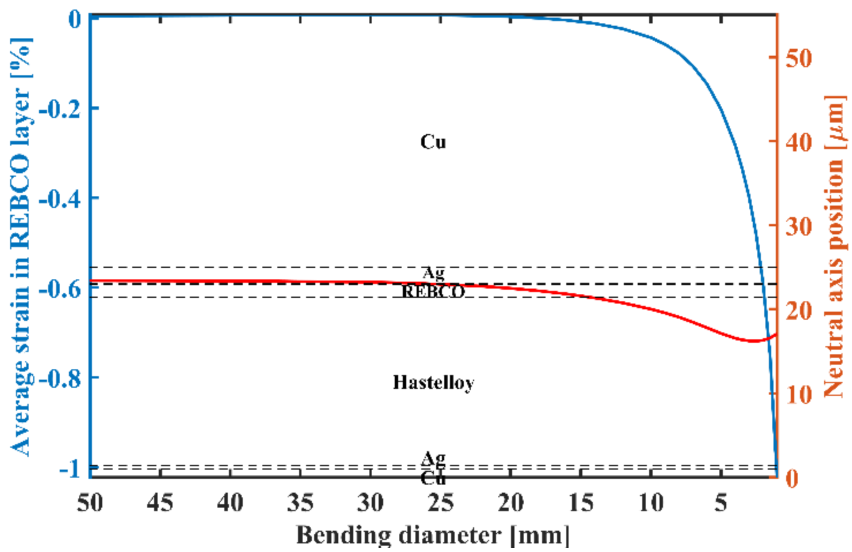

Figure 2-3 Neutral axis shift and average bending strain in the REBCO as a function of the bend diameter.

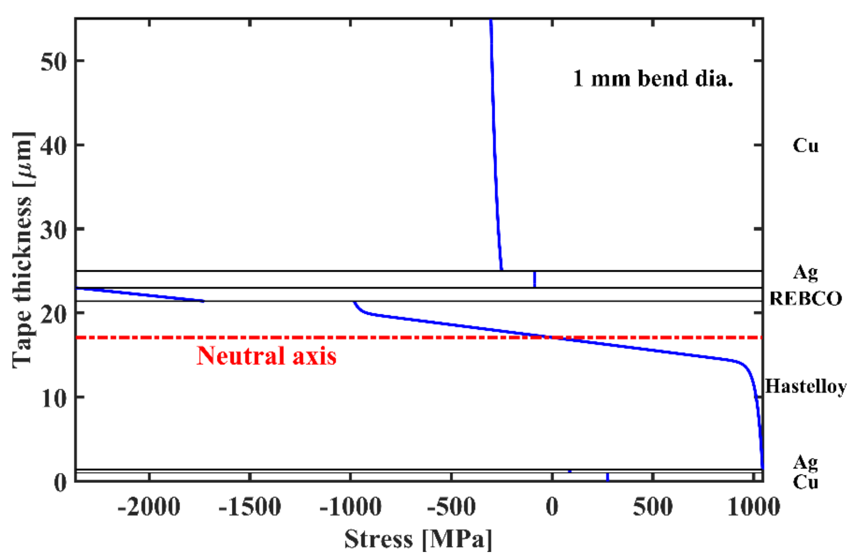

Figure 2-4 Stress distribution at 1 mm bend diameter for a 20 µm substrate tape with 30 µm Cu on the REBCO side.

2.4.2. Copper thickness optimization

These calculations show that at a given bend diameter, a certain copper thickness could be used to reduce the strain levels in the REBCO layer to a certain desired value (as shown in Figure 2-5); that value will depend on the targeted I_c retention based on a specific application. There will be limits as to the maximum copper thickness that can be used, mainly determined by the maximum elongation that the copper can sustain. This will be increasingly relevant with increasing substrate thickness as the required Cu thickness to bring the NA closer to REBCO layer will be become larger and larger (Although the strains in the REBCO layer will be small because of its proximity to the NA, the outermost fibers of the Cu layer would be subject to very large strains). There are also few practical considerations to account for when using this approach such as the increased tape stiffness and the compromise between the increase in I_c and the decrease in J_e due the increased tape cross-section (A discussion of this particular point is presented in section 2.6.2 for helically wound round REBCO wires).

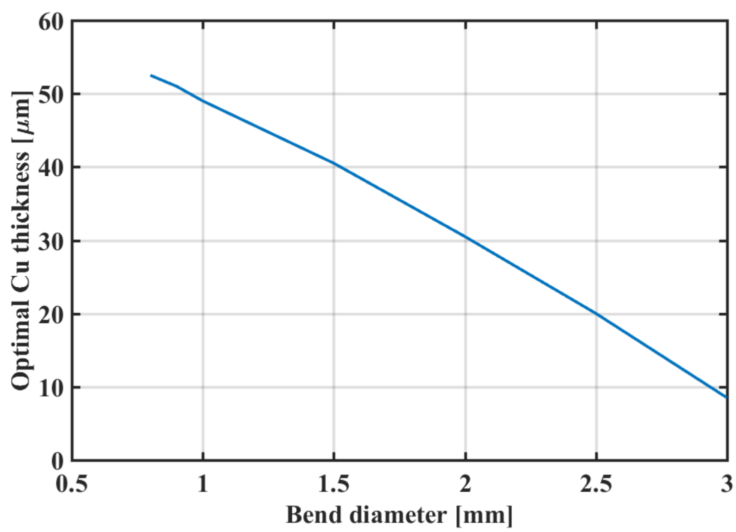

Figure 2-5 Optimal Cu thickness as a function of the bend diameter corresponding to an average strain of 0.6% in the REBCO layer. Optimal being the minimum Cu thickness needed to keep strain below the 0.6% threshold. This example is for a 20 μm substrate tape.

2.5. Experimental validation

To evaluate the validity of the calculations, the I_c dependence on the bend diameter was measured on tapes with different substrate thicknesses. The effect of the single-sided copper thickness for each substrate was also investigated. The measurements were carried on 2 mm wide tapes wound a full turn on cylindrical formers ranging from 12.5 to 0.81 mm in diameter. The REBCO layer was in compression for these tests. The tapes were fixed using Kapton tape, immersed in liquid nitrogen and their critical current measured by the four-probe method. A 1 μV/cm criterion was used to determine the I_c.

The REBCO CC used in this work were originally 12 mm wide tapes from Superpower Inc. The conductors were laser slit using a fiber laser with a wavelength of 1064 nm. The tapes were then re-sputtered with a thin (~0.5 μm) layer of silver, followed by annealing in oxygen flow for 2 h at 500 ºC. Finally, the copper stabilizer was electroplated using a water-based $CuSO_4$ solution. The thickness was controlled by adjusting the applied dc current and the Cu was deposited on the REBCO side only by shielding the back side of the tape from the solution flow. It should be noted that this does not prevent entirely the Cu deposition on the substrate side and there is always about 1~2 μm deposited on the Hastelloy side.

2.5.1. I_c retention of 50 μm substrate tapes

Figure 2-6 shows the experimentally-measured I_c retention (I_c at bend radius relative to the flat I_c) for a series of 50 μm substrate tapes with various Cu thicknesses, from no Cu to 90 μm deposited on the REBCO side only, measured from 12.5 to 1.1 mm diameter. As anticipated from the calculations, at each specific bend diameter, there is an increase in the I_c retention with increasing Cu thickness. For example, the tape with only

18 μm of Cu experiences about 20% I_c degradation at 5 mm bend diameter while the tape electroplated with 90 μm experiences the same level of degradation only below 3 mm bend diameter. The thicker Cu is capable of carrying more load and thus places the NA closer to the REBCO layer. Figure 2-7 shows the same results but converted into bending strains. The scaling of the critical current retention as a function of the strain in the REBCO layer confirms that difference in bending performance is due to the differences in NA location in the various configurations.

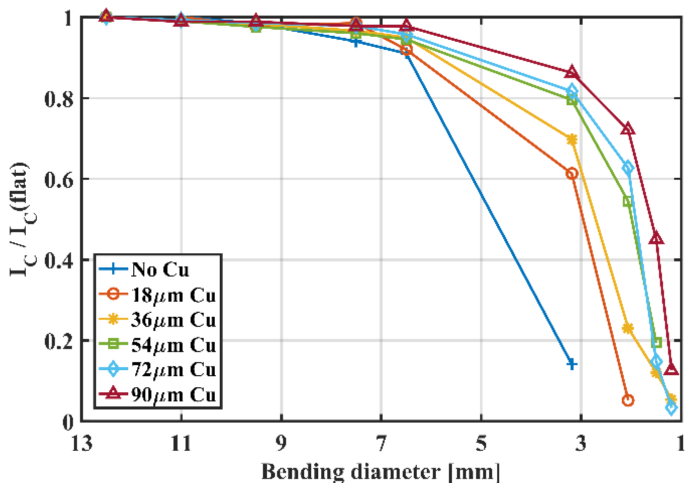

Figure 2-6 Measured I_c retention of 50 μm substrate tapes with various Cu thicknesses dependence on bend diameter.

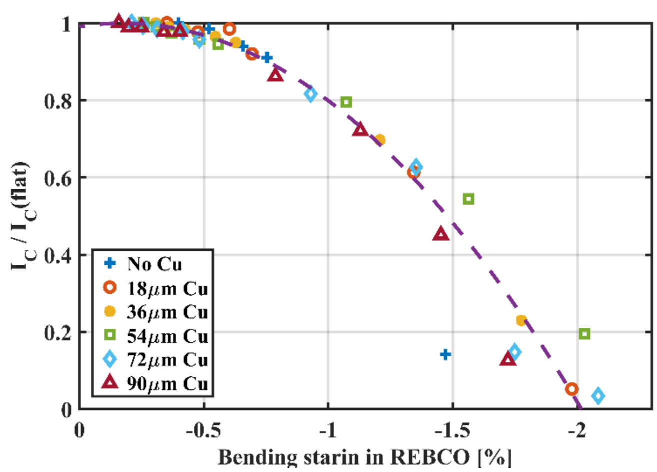

Figure 2-7 I_c retention of 50 μm substrate tapes with various Cu thicknesses dependence on the bending strain in the REBCO layer. Dashed line is a quadratic fitting to all the data to help guide the eye.

2.5.2. I_c retention of 30 µm substrate tapes

The same experiment was carried on 30 µm substrate tapes from Superpower. Figure 2-8 shows the results of the I_c retention at different bend diameter. And as in the 50 µm case, there is an increase in the I_c retention with increasing Cu thickness although this time, the thinner substrate allowed for higher retention at smaller diameter with less Cu thickness. In term of strains, the behavior is similar to that of 50 µm substrate tapes although there is slight difference due to some differences between the mechanical properties of the two substrates [61].

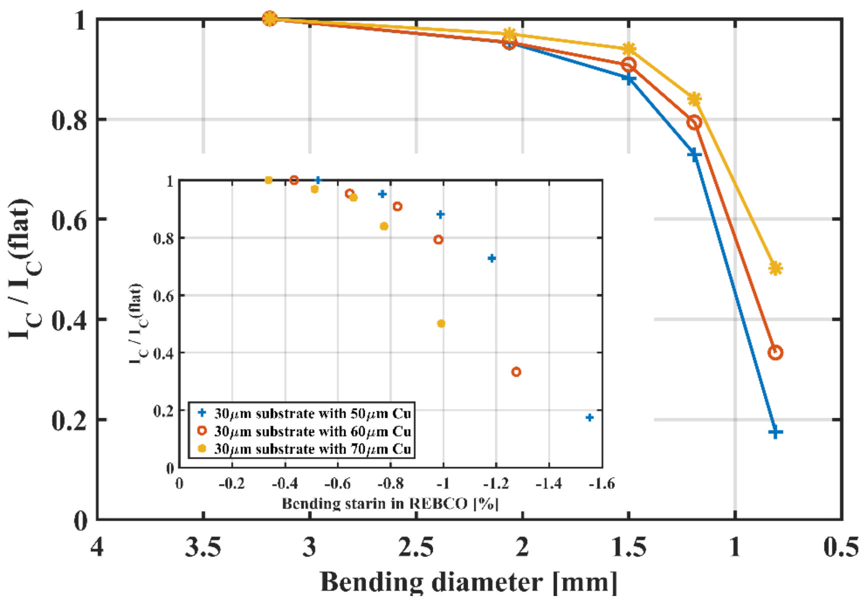

Figure 2-8 Measured I_c retention vs bend diameter of 30 µm substrate tapes with various Cu thicknesses. Inset shows the same values as a function of the strain.

2.5.3. I_c retention of thinner substrate tapes

Further verification was carried on thinner substrate tapes. These tapes are originally 50 µm substrate tapes from Superpower whose substrates were reduced by abrasive grinding [62]. This enables the production of tapes with substrates thicknesses ranging from 10 to 24 µm. The experimental values were determined by measuring several single-layer helically-wound round REBCO wires. Figure 2-9 shows a picture of such samples. They consist of 2.5 mm wide tapes wound onto a 1 mm copper core. For each substrate thickness, samples with different copper thicknesses were prepared [62, 63]. Their I_c was then measured and compared with the flat I_c of the tape before the winding in order to determine the I_c retention. The experimentally-determined optimal Cu thickness corresponding to ~75% I_c retention is shown in Figure 2-10, optimal being the minimum Cu thickness used to achieve 75% I_c retention. And since these thin tapes were originally 50 μm tapes whose substrate thickness was reduced by abrasive grinding, the mechanical properties (elastic modulus and yield strength) of the substrate remains unchanged. Based on the previously obtained scaling of the I_c retention as a function of the strain in 2.5.1, the 75% I_c retention rate would correspond to about 1.1% axial compressive strain in the REBCO layer. The solid line in Figure 2-10 shows the calculated optimal copper thickness based on a maximum of 1.1% axial compressive strain in the REBCO layer. The calculated values show a good agreement with those determined experimentally which confirms the validity of the proposed model in capturing the bending performance of REBCO coated conductors.

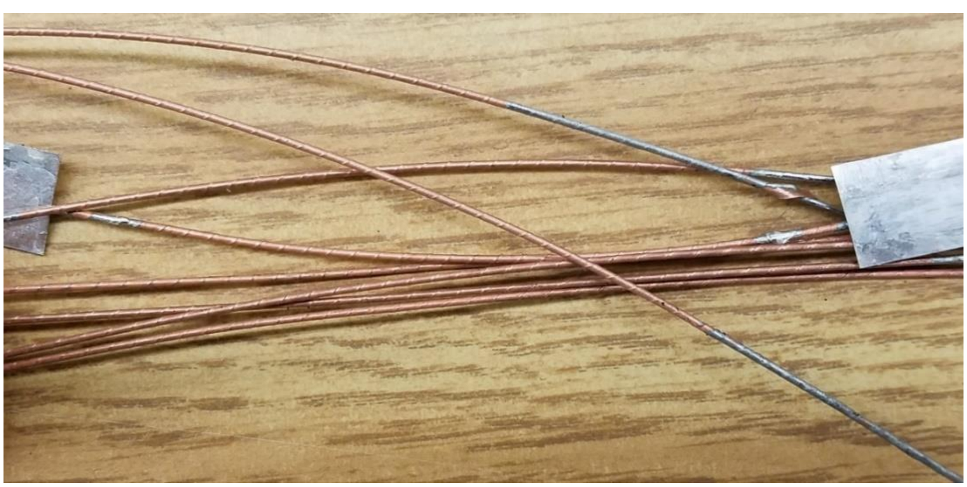

Figure 2-9 Picture of the single-layer round wires

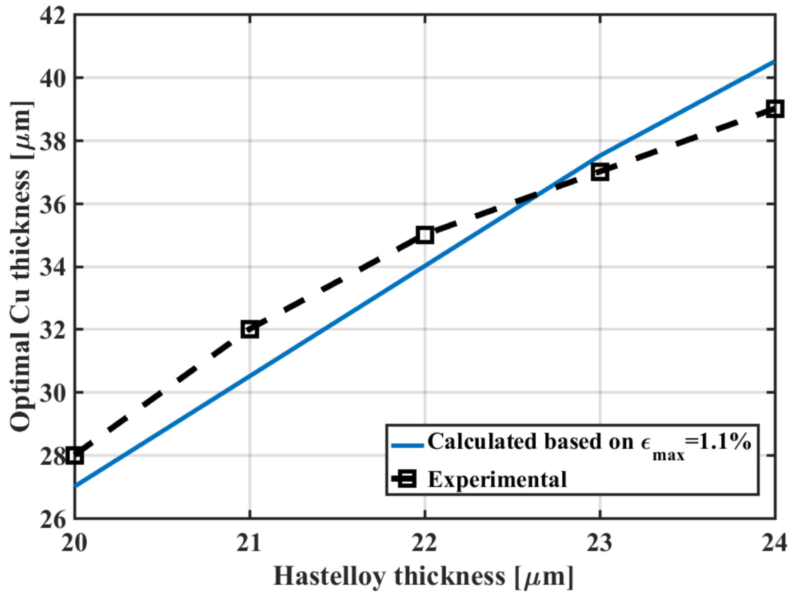

Figure 2-10 Optimal copper thickness corresponding to 75% Ic retention for tapes of various substrate thickness

2.5.4. The transverse bending component

In all the previously described measurements, the tapes are not subject to a pure longitudinal bending. There is a transverse (along the tape's width) bending component in each experiment by the nature of the helical geometry itself. In the comparison made between the calculated values (modeled as pure bending) and the measured ones (by helical winding), the effect of the transverse bending component is, in fact, negligible in comparison to that of the longitudinal bending. This does not mean the transverse strain does not affect the I_c retention in general, but under certain conditions, its effect can be actually neglected. Those conditions are determined by the tape's geometry, the bending radius and the twist pitch. Using the constant-perimeter method, which models the tape conductor as a developable surface that can be unfolded to a plane without stretching or tearing [121], the curvature of the bent tape in a helical winding, shown in Figure 2-11, can be expressed in term of axial and transverse curvatures [121-123] as follows

$$\kappa_{axial} = \frac{\sin^2 \alpha}{r} \text{ and} \tag{2-3}$$

$$\kappa_{transverse} = \frac{\cos^2 \alpha}{r}, \tag{2-4}$$

where α is the winding angle between the helix curve and axis of the Cu core.

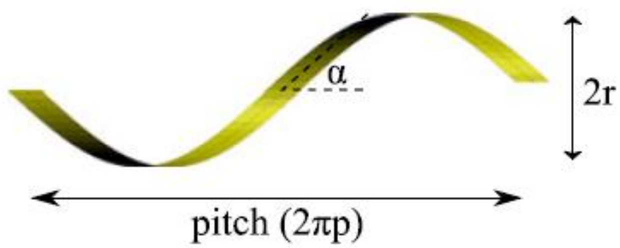

Figure 2-11 Tape bent in a helical form around a cylindrical former[122].

The strain in the REBCO layer is proportional to the local curvature of the neutral plane. The axial and transverse strain on the REBCO layer are then given by

$$\varepsilon_{axial} = -y\ \kappa_{axial} = -\frac{y\ \sin^2 \alpha}{r} \text{ and} \tag{2-5}$$

$$\varepsilon_{transverse} = -y\ \kappa_{transverse} = -\frac{y\ \cos^2 \alpha}{r}, \tag{2-6}$$

where y is the distance between the neutral plane and the REBCO layer.

The variation of the axial and transverse curvature as a function of the bend diameter for a 2 mm twist pitch is shown in Figure 2-12. This is the twist pitch of most of the samples measured in the previous sections and indeed for such small twist pitch, the strain is essentially in the axial direction. The transverse curvature increases as the diameter is reduced since

$$\alpha = \cot^{-1} \frac{p}{r}. \tag{2-7}$$

For a 2 mm twist pitch, the transverse strain would be equal to 10% of the axial strain at 1 mm bend diameter and 15% at 0.8 mm diameter.

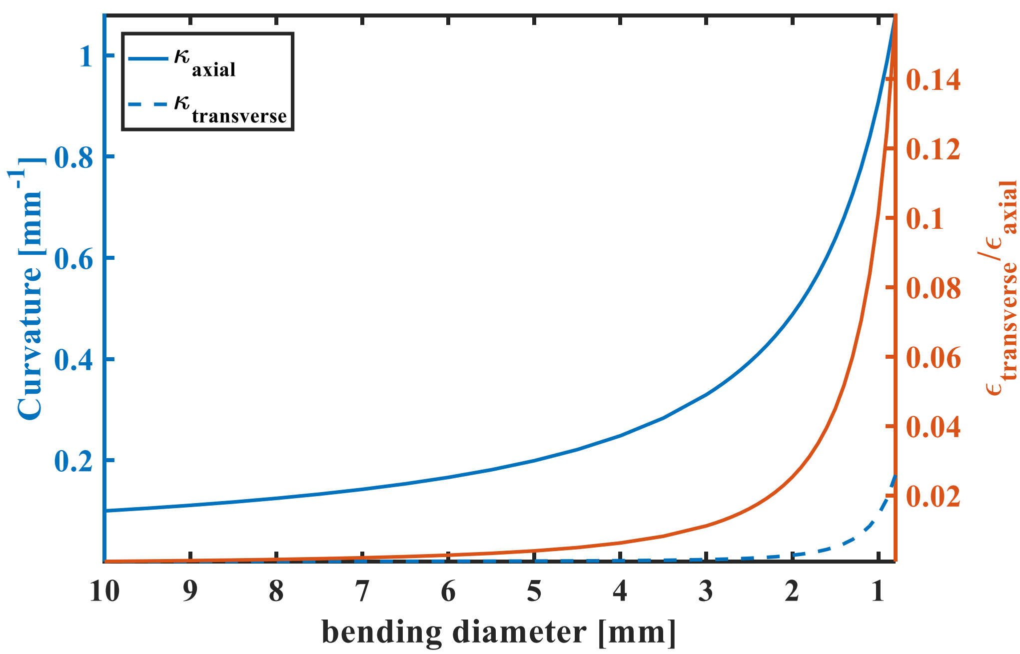

Figure 2-12 Axial and transverse curvature as a function of the bend diameter for a 2 mm twist pitch. The secondary y-axis shows the ratio of the transverse and axial strains in the REBCO layer.

The effect of the transverse curvature increases with increasing twist pitch as shown in Figure 2-13. For larger twist pitch, the effect of the transverse curvature on the REBCO bending performance has to be included in order for the model to remain valid, but within the range of this study (wires with very small twist pitches), this effect can be neglected.

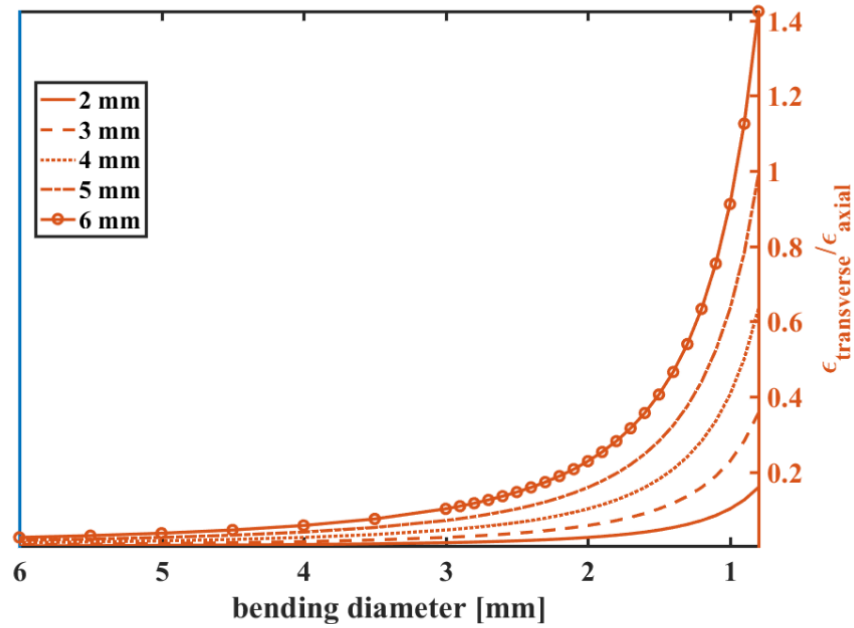

Figure 2-13 The ratio of the transverse to axial strains in the REBCO layer for various twist pitches as function of the bend diameter.

2.6. Ultra-small diameter REBCO round wires optimal design

The results of the previous section are of a particular interest for helically-wound REBCO wires like CORC [124] and STAR [64, 65, 81, 82] wires where the goal is to maximize the J_e within a certain wire outer diameter (OD) limit. For such wires, since the J_e is defined over the entire wire cross sectional area including the Cu former and since the I_c retention of the tape depends on Cu thickness which in turn increases the wire OD, the choice of the former diameter, I_c retention and necessary Cu thickness are no longer obvious. The presented analytical calculations allow us to explore and optimize these design parameters for such conductors.

2.6.1. The core diameter

First, regarding the choice of the former, Figure 2-14 shows the optimal Cu thickness as a function of the bend diameter for a 30 µm substrate tape at various strain values, optimal being defined as the minimum Cu thickness so that strain in the REBCO layer does not exceed a specified value. To maximize J_e, it is preferable to use the smallest possible former by adding more Cu on the REBCO side. By using about 30 μm of additional Cu, the former diameter could be reduced by a factor of two while maintaining the same stress levels in the superconducting layer. This would allow adding several layers of superconducting tape instead of what would have been simply Cu in the former, thus increasing significantly the J_e of the wire. The final choice would be determined by additional practical considerations such as the minimum tape width and the maximum tape stiffness during the winding process.

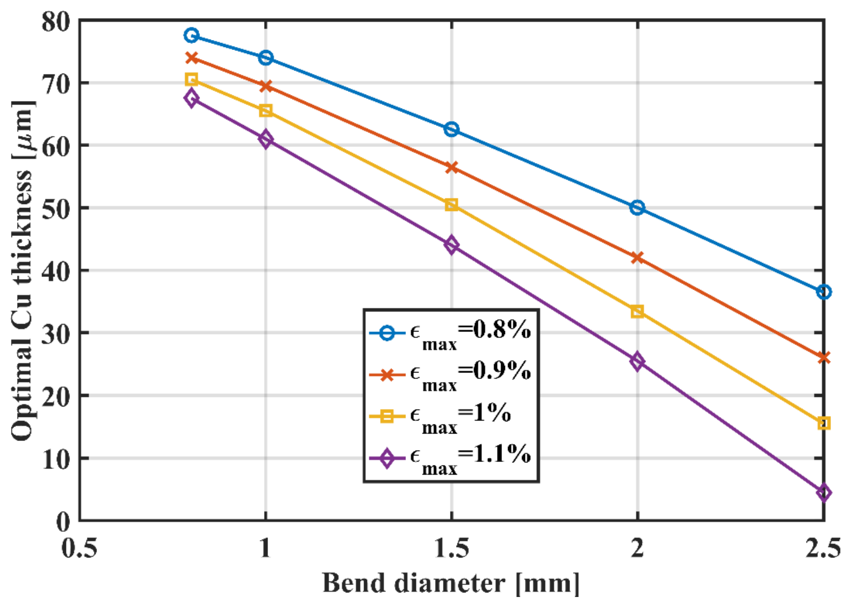

Figure 2-14 Optimal Cu thicknesses for a 30 μm substrate tape as a function of the bend diameter for various strain levels.

2.6.2. Optimal I_c retention

The second design parameter would be the choice of the optimal I_c retention per layer. Currently, that value is optimized only for the first layer. In these multi-layered conductors, since the actual bend diameter increases with additional layers, using the same Cu thickness for all the layer would results in under-stressed tapes in the outer layers compared to those in the inner ones. The cross-sectional image of a STAR wire in Figure 2-15 shows that between the first and the sixth layer there is a 65% increase in the bend diameter. A better layout could be achieved if the copper thickness is decreased gradually with increasing layer diameter thus maintaining the same constant strain level in all layers. Table 2-1 shows the potential gain in J_e such approach would provide. Although the wire with the optimized Cu thickness for each layer has a lower total I_c, there is about 9% increase in J_e thanks to the reduction in the wire diameter. Due to the Cu low yield point, the lower I_c retention would increase J_e until the point where the same J_e could be achieved using one less layer and having all the layers at high I_c retention. Practically, the exact value would be determined by economical consideration of what would be the acceptable added cost per increment in J_e.

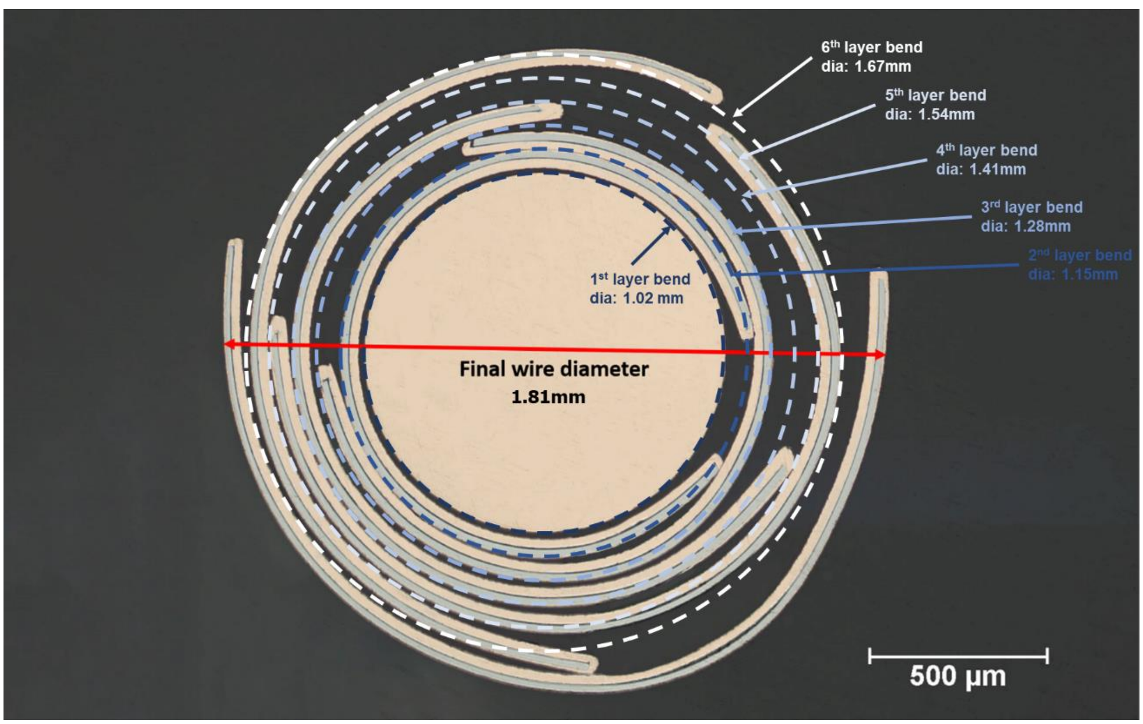

Figure 2-15 A cross-sectional image of a STAR wire showing the bend diameter increase with increasing layers (Adapted from [81])

Table 2-1 Comparison between the conventional and the optimized layouts.

Layer	Constant Cu thickness based on the I_c retention of the 1st layer				Optimal Cu thickness based on the actual layer bend dia.			
	Cu thickness (μm)	Bend dia. (mm)	Avg. strain in REBCO layer (%)	I_c retention (%)	Cu thickness (μm)	Bend dia. (mm)	Avg. strain in REBCO layer (%)	I_c retention (%)
1st	32	1.02	-1.14	76.9	32	1.02	-1.14	76.9
2nd	32	1.14	-1.04	80.5	27	1.14	-1.14	76.9
3rd	32	1.27	-0.96	83.4	23	1.25	-1.14	76.9
4th	32	1.39	-0.89	85.6	18	1.36	-1.14	76.9
5th	32	1.52	-0.83	87.5	14	1.45	-1.14	76.9
6th	32	1.64	-0.78	88.8	11	1.54	-1.14	76.9
	Total I_c		502.7 A		Total I_c		461.5 A	
	Wire OD		1.76 mm		Wire OD		1.62 mm	
	J_e		205.7 A/mm^2		J_e		223.9 A/mm^2	

Calculation based on a 22μm substrate tape and a 1.02mm Cu core. A 100A flat I_c for all layers is used to estimate the total wire I_c.

2.7. Conclusion

In this chapter, the presented analytical calculation showed that by using an optimized Cu thickness on the REBCO side only, significant reduction in the strains in the REBCO layer could be achieved at small bend diameter. Such reduction is due to the shift of the neutral axis position closer to the REBCO layer. The validity of the calculation results was evaluated against a variety of experimental measurements and was found to accurately describe the bending performance of REBCO CC over a broad range. Finally, based on these results, an optimized design aiming at maximizing the J_e of helically-wound ultra-small diameter REBCO STAR wires was presented.

CHAPTER 3. A Two-Tape Structure for Enhanced REBCO CC Bending Performance

3.1. Introduction

In the previous chapter, significant improvement of the tape bending performance and critical current retention has been achieved by placing the REBCO layer closer to the neutral axis/plane of the tape using an optimized copper thickness on the REBCO side only (in contrast with the standard surrounding stabilizer used with most tapes which results in the neutral axis being at the center of the substrate). As part of the on-going effort to further reduce the diameter of the STAR wires and explore alternative tape architecture allowing to build highly flexible REBCO wires with high J_e, in this chapter, the same principle of placing the REBCO layer in a more mechanically favorable location closer to the neutral axis is sought, but, instead of tuning the stabilizer thickness to achieve such result, two tapes could be joined face-to-face thus placing the two REBCO layers of the resulting structure closer to the neutral axis. Despite being widely used in various type of joints [125, 126], this particular tape structure has not been used as a means to enhance the single tape mechanical properties. The challenge for such use lies in the thickness of the filler material used to achieve the bond between the tapes. It has to be kept to a minimum; otherwise the bending properties could be worse than that of a single tape [127].

In this chapter, the potential advantages and drawbacks when REBCO tapes are used in such configuration will be first presented. Then, the strain values in such structures will be determined as a function of the filler material thickness. Potential improvement and how to address the asymmetric tensile/compressive strain limits in REBCO tapes are also discussed. Next, the two methods, diffusion bonding and soldering, used to implement this concept are presented. Finally, the bending performance of these two-tape structures have been measured and compared to the analytical predictions.

3.2. Basic concepts and potential advantages

The proposed structure is illustrated schematically in Figure 3-1. Two tapes with the same substrate thickness are oriented so that the two REBCO layers are facing each other. The joint structure could be obtained either by direct silver diffusion bonding between the top silver layer of each tape as shown in Figure 3-1(b) or by means of a solder layer, as shown in Figure 3-1(c), connecting the two tapes. This would place both REBCO layers, in the resulting structure, close enough to the neutral axis and would allow potentially the bending to smaller diameters without a significant critical current degradation compared to a single tape.

Another advantage of such structure is that it would have double the engineering current density than tapes with single-sided stabilizer on the REBCO side, where using the single sided stabilizer to balance the stresses reduces the tape J_e. On the other hand, such structure will lack the electrical and thermal benefit of a thick stabilizer layer that the regular tapes have [128]. Although there will be the possibility for strong current sharing between the two REBCO layers and a stabilizer layer could be surrounding the entire structure, this particular tape configuration would be more suitable for higher temperature operations where HTS tapes are very stable due to the significantly increased heat capacity at higher temperatures and the larger thermal margins [53].

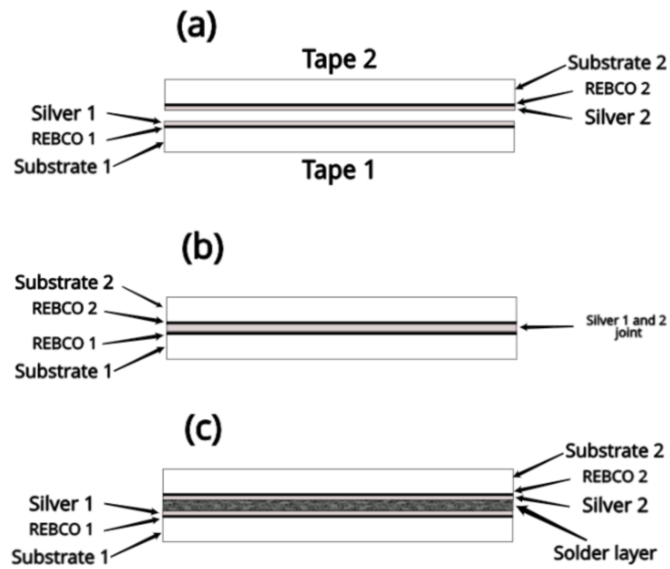

Figure 3-1 (a) Tapes orientation before joining. The two-tape structure (b) by diffusion bonding and (c) by soldering.

A second potential advantage of such structure is to have a lesser asymmetry in the angular dependence of the critical current compared to the single tape case. First, in tapes with various pinning structures, the intrinsic pinning peaks measured at the parallel (0°) and anti-parallel (180°) field direction can be significantly different [59, 129, 130]. This variation has been attributed to the difference in surface pinning barrier between the substrate-film interface and the film-silver interface [129]. The second case where a more symmetrical angular dependence of the critical current could be achieved is for tapes with tilted crystallographic axis with respected to the tape's geometric axis. Certain deposition processes like ion-beam assisted deposition (IBAD) produces buffer layers (and subsequent REBCO layer) that are tilted by a few degrees with respect to the tape normal [131], others like inclined-substrate deposition (ISD) produces tapes with c-axis tilts in the range of 25-30° [25]. A symmetrical arrangement could be achieved in the joint structure by rotating one of the tapes by 180° around the tape normal (in addition to the fact that the tapes are already facing each other). A schematic representing the two possible orientations for tilted-axis tapes is displayed in Figure 3-2. Figure 3-3 shows a calculated example of what would be the resulting angular dependence of critical current based on the chosen orientation. An angular dependence of the kind

$$J_c(\theta) \propto \frac{1}{\cos^2\theta + u^2 \sin^2\theta} \tag{3-1}$$

from [132] was used (a Lorentzian-induced angular dependence with a scale factor u), with a 30° tilt between the intrinsic pinning peak and the tape's surface. When the two tapes are used in the same orientation a stronger peak is observed at the location of the peak of one tape. The 180° rotated tapes show a more symmetric distribution of critical current and a higher critical current is obtained over a broader range of angles. The presented example represents only the sum of the critical current contribution from each tape based on the chosen orientation and does not take into account any potential interaction between the tapes to show the potential advantages of using tapes in this configuration but the exact angular dependence behavior remains to be fully studied.

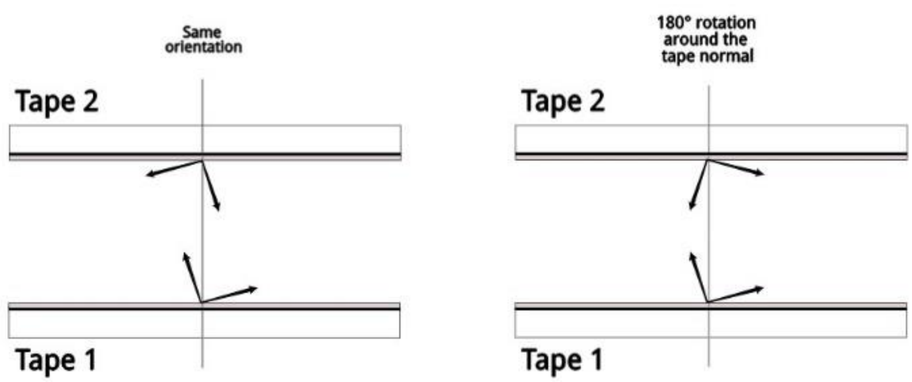

Figure 3-2 Possible tape orientations when the crystallographic directions are tilted with respect to the tape geometric axis.

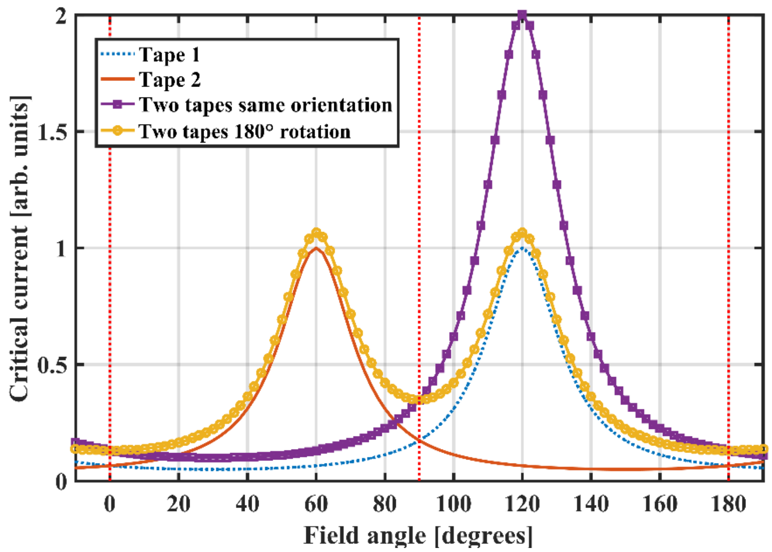

Figure 3-3 Angular dependence of in-field critical current of the structures made by joining two REBCO tapes where the REBCO layer has a 30° c-axis tilt with respect to the tape normal. The field angle is defined with respect to the tape normal.

3.3. Strain calculation

The major characteristic of such structure is the symmetry plane it possesses in the middle. This would place the neutral axis always within that plane. And since the strains throughout the cross section can be determined by the local curvature of the neutral axis ($\kappa = 1/\rho$, ρ being the bending radius) and the distance y between each layer and the neutral axis $\epsilon = -y/\rho$ [46, 115], the strains in the REBCO layers are only determined by the thickness of the interlayer separating them regardless of the substrate thickness of the initial tapes. Figure 3-4 shows the strains and stresses throughout the tape cross-section. The calculations are based on the model presented in the previous chapter and takes into account the plastic deformations and any potential shift of the neutral axis at smaller bend diameter. Even though, in this particular geometry, the neutral axis location is fixed, this will be of a particular importance later when we will discuss the case of an offset in thicknesses between the two substrates. The example in Figure 3-4 shows the case of two 30 µm substrate tapes joined by silver-to-silver diffusion bonding which would be the ideal case for such structure since it does not require any additional layer to bond the tapes; this arrangement minimizes the distance between the two REBCO layers and the neutral axis and thus the strains.

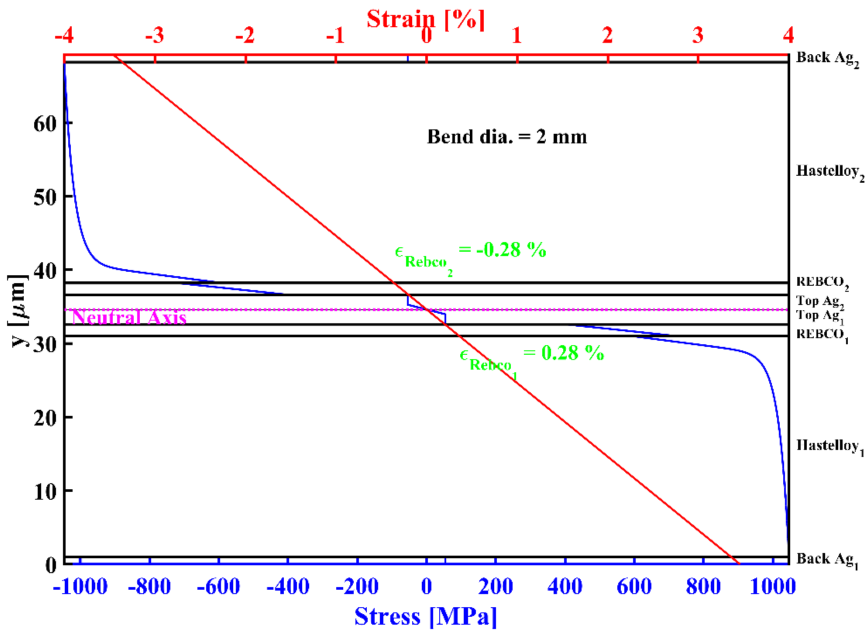

Figure 3-4 Strain and stress distributions throughout the cross-section of a two-tape structure made by diffusion bonding. The layers "Back Ag", Hastelloy, REBCO and "Top Ag" have a thickness of 1, 30, 1.6 and 2 µm respectively. The subscript 1 denotes the layer under tension and 2 the layer under compression during bending.

In the case where a solder layer is used to bond the two tapes, the solder thickness will add to the Ag layers thicknesses and the resulting structure will have higher strains in the REBCO layers than the diffusion bonding case. Figure 3-5 shows the average strain in the REBCO layer as a function of the bend diameter for various solder thicknesses from 0 to 16 µm, the 0 µm solder thickness being the diffusion bonding case. Only the strains of the layer undergoing tension are represented since the layer under compression experiences the same strains but of opposite sign. The strain values increase gradually with the increasing solder thickness and in order to determine the minimum bend diameter of such structure, we should consider the original (single) tape strain limits.

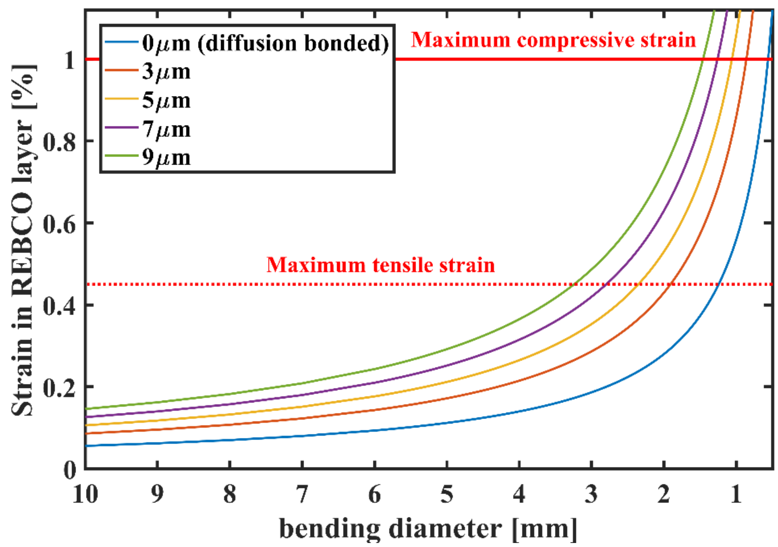

Figure 3-5 Average strain in the REBCO layer as function of the bend diameter for various solder thicknesses. The 0 μm case represent tapes joint by silver diffusion bonding. The red lines correspond to the axial strain limits of a commercial REBCO tape from Superpower Inc.

For REBCO coated conductors, the axial compressive and axial tensile limits are usually different. For recent commercial tapes made on Hastelloy substrates, these limits ranges from 0.4% to 0.7% for the axial tensile strain and from 0.5% to 1% for the axial compressive strain [46, 133, 134]. The strain limit corresponds to a maximum of 20% reduction in the critical current of the tapes. This particular property of REBCO coated conductors has a significant implication on the bending performance of the proposed two-tape structure. The lowest limit, usually the tensile one, will determine the minimum operable bend diameter. The red lines in Figure 4 shows the measured strain limits for the REBCO tape from Superpower used in making these symmetric two-tape structures. These tapes can sustain significantly higher strain in compression (up to 1% strain corresponding to about 20% I_c degradation) than in tension (only 0.45~0.5%). So, for a symmetric two-tape structure made by soldering, if the solder layer is 9 μm thick, the tape under compression could be bent up to 1.5 mm diameter while the tape under tension will exceed the tensile strain limit at 3.2 mm bend diameter, limiting the use of the entire structure to a minimum bend diameter of 3.2 mm.

While this represents a significant improvement compared to the single tape bending performance, this configuration is still far from optimal because one of the tapes reaches its strain limit while the other is still way below its maximum. Ideally, the two tapes should reach their respective limits at the same diameter both in compression and in tension. And since the tensile and compressive limits are different, the only way to achieve that would be if there is a slight difference between the two substrate thicknesses. If the tape with a higher strain limit had a thinner substrate, the neutral axis in the bent two-tape structure would have to shift toward the thicker substrate tape in order to maintain the stress balance throughout the cross section. This would make the strains lower in the side where the substrate is thicker. Figure 3-6 shows the shift in the neutral axis location in comparison to Figure 3-4 when $Hastelloy_2$ (in the compressive side) is 2 µm thinner than $Hastelloy_1$ (in the tensile side). At 2 mm bend diameter, a 2 µm offset between the two substrates will change the strain in the REBCO layers from being 0.28% both in tension and compression to 0.41% in compression and 0.15% in tension. This would allow to reach both strain limits for each tape at the same bend diameter, lowering further the minimum possible bend diameter compared to the case where both substrates have the same thickness. Figure 3-7 shows a comparison of the strain vs the bend diameter between the perfectly symmetric case and the 2 µm offset case (example for diffusion bonding). With a 2 µm offset, the two tapes reach their corresponding maximum strain at the same bend diameter (0.8 mm in this case), where for the perfectly symmetric structure, the tape under tension reaches its limit at 1.3 mm bend diameter.

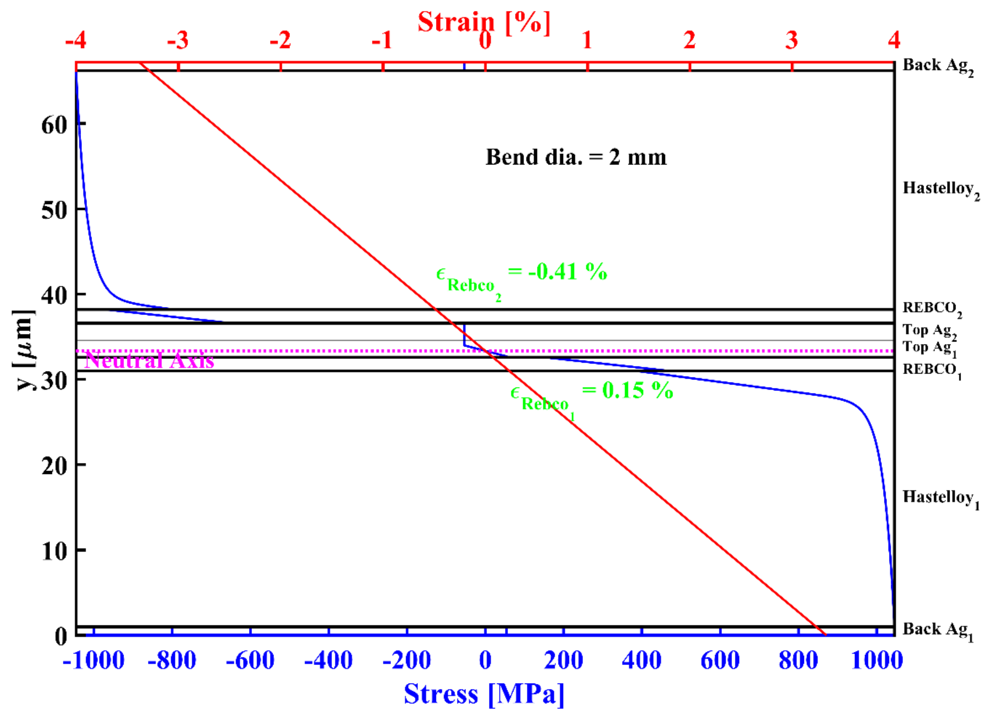

Figure 3-6 Strain and stress distributions throughout the cross-section of a two-tape structure with 2 µm offset

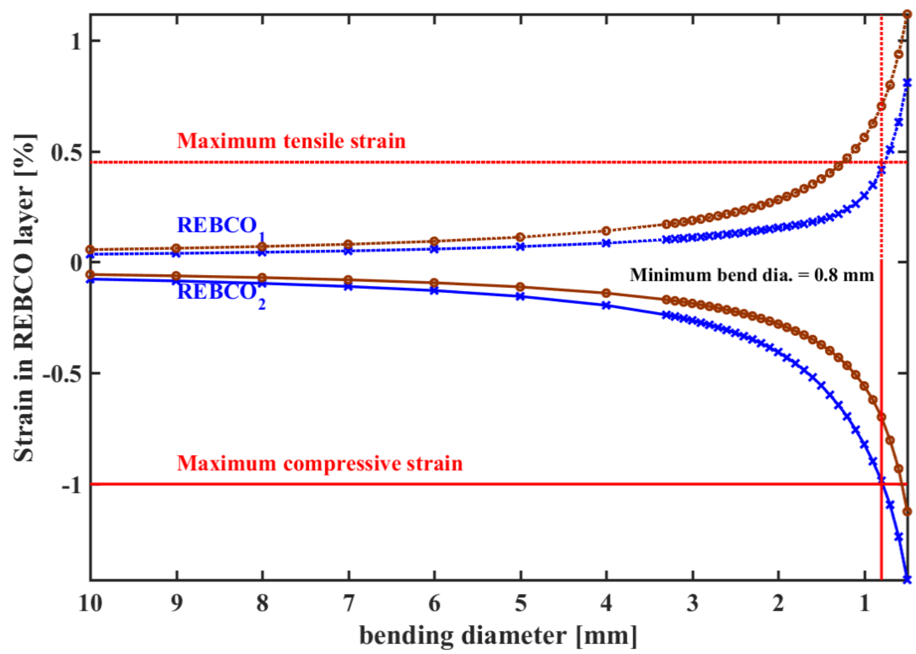

Figure 3-7 Bending strain variation as function of the bend diameter for the two cases: same substrate thickness (circles) and with 2 µm offset (crosses). $REBCO_1$ denotes the layer under tension and $REBCO_2$ the layer under compression

It should be noted that if the offset exceeds a certain optimal value, then the tape undergoing compression will reach its maximum before the tape undergoing tension. The optimal value being defined, as illustrated in Figure 3-7, as the value allowing both REBCO layers to reach their corresponding strain limits at the same bend diameter which would correspond to the smallest possible bend diameter. Table 3-1 summarize the potential improvement achieved with a 2 µm offset as function of the solder thickness. The 2 µm value is obtained for Superpower tapes based on their material properties and strain limits. The same approach could be applied to other tapes and an optimal value could be determined based on their specific material properties and strain limits.

Table 3-1 Minimum bend diameter as function of the solder thickness for the two-tapes structures

Solder thickness (µm)	Minimum bend dia. (mm)	
	Symmetric case	**With 2 µm offset**
0	1.3	0.8
3	1.9	1.2
5	2.4	1.5
7	2.8	1.8
9	3.2	2.2

3.4. Experimental methodology

Three types of these two-tape structures were prepared and tested: diffusion bonded samples with equal substrate thicknesses, soldered samples with the same substrate and soldered samples with 2~3 µm offset between the two substrates. Two types of tapes were used: for the equal substrate structures, 50 µm tapes from Superpower were used, and the offset samples consisted of 38 and 40 µm substrate tapes fabricated by abrasive grinding from the Superpower 50 µm tapes [62].

In all these types of structures, it is essential to control the thickness and uniformity of the interlayer separating the two REBCO tapes. A non-uniform interlayer can create higher strains locally which can not only degrade the bending performance but also cause the delamination of the tapes.

For the diffusion bonded samples, the method used is similar to that reported by Kato et al. [135]. The two 12 mm wide tapes were held face to face with a pressure of 15 ~ 20 MPa using a custom-made press, shown in Figure 3-8, made of Inconel 625. The pressure was controlled by adjusting the applied torque on the three bolts at the center. The press is then inserted inside a furnace, heated and held at 500 ºC for 2 h in O_2 flow. The resulting joint structure was then laser slit into 2 mm wide tapes using a fiber laser with a wavelength of 1064 nm for the subsequent bending test.

Figure 3-8 Inconel press used to hold the two tapes during the diffusion bonding and the soldering process

The soldered samples were first laser slit into 2 mm tapes, re-sputtered with a thin (~0.5 µm) layer of silver then annealed in oxygen flow for 2 h at 500 ºC. The soldered two-tape structure is achieved in a two-step process. The tapes are first pre-tinned and soldered together manually using a solder pen to ensure good contact between the tapes. Indium-tin eutectic (52:48 wt%) solder was used because of its low melting point to avoid any degradation of the superconducting layer during the process. In the second part of the process, the two soldered tapes are put inside the Inconel press and a pressure of ~20 MPa is applied. The entire block is then inserted inside a preheated furnace at 185 °C and held there for 30 minutes in air. During that time, the solder reflow combined with applied pressure ensures the uniformity of the thickness of the solder layer by pushing any excess solder through the edges of the tapes as shown in Figure 3-9. The temperature and duration chosen for this part of the process were mainly dictated by the large thermal mass of the press, which requires a certain time to reach the proper temperature allowing the solder reflow. This heat treatment causes ~5% degradation of the critical current of the tapes, most likely due the oxygen out-diffusion from the REBCO layer [136, 137]. Finally, the block is taken out and cooled down so that the remaining solder re-solidifies under the applied pressure. A picture of the final joint structure, after removing from the press, is shown in Figure 3-10.

Figure 3-9 The soldered samples after the heat treatment under pressure. Excess solder is squeezed out.

Figure 3-10 A picture of a soldered sample at the end of the process.

To evaluate the bending performance of these structures, the I_c dependence on the bend diameter was measured for several samples. The measurements were carried by helically winding a single turn on cylindrical formers ranging from 3.2 to 0.8 mm in diameter. The tapes were fixed using Kapton tape, immersed in liquid nitrogen and their critical current measured by the four-probe method. A 1 µV/cm criterion was used to determine the I_c.

3.5. Results and discussion

The first tests were carried on soldered samples without the additional pressing and heat treatment. The red circles in Figure 3-11 shows some of the results for such samples. As expected from the calculation shown in section 3.3, if the solder layer thickness exceeds 9 µm, the critical current of the two-tape structure degrades significantly below 3.2 mm bend diameter. The samples exhibited 60% I_c retention at 3.2 mm bend diameter and ~22% at 1.5 mm. Since these samples were simply hand soldered and not pressed, there was no control on the solder thickness nor on its uniformity along the joint area. This resulted in significant number of samples delaminating during or after the test due to much higher stresses on areas where the solder is thicker than the rest of the joint. Still, the I_c retention of the two-tape structure is already better than the performance of single 50 µm substrate tape which show zero critical current below 3 mm bend diameter.

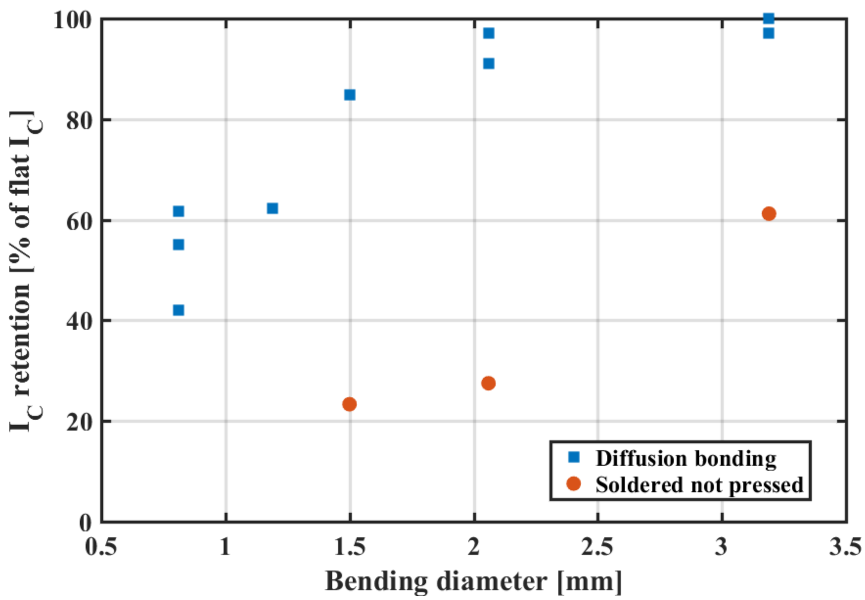

Figure 3-11 I_c retention as a function of the bending diameter for diffusion-bonded samples and soldered samples with thick solder layer (10~30 µm).

On the other end of the spectrum, the diffusion bonded samples constitute the ideal demonstration of the concept (short of making REBCO-to-REBCO joints). Without the use of any additional solder material, the REBCO layer is only 2 µm away from the neutral axis (2 µm being the thickness of the original Ag cap layer). Besides, diffusion bonding processes results, under the proper conditions, in homogeneous and uniform interfaces [135, 138]. Figure 3-12 shows an optical microscope image of the cross-section of a typical symmetric two-tape structure made by diffusion bonding two 50 µm substrate tapes. These samples showed remarkably high I_c retention during the bending test with almost no degradation up to 2 mm bend diameter and up to 60% I_c retention at 0.8 mm bend dia. However, the degradation started at 1.5 mm bend diameter which differs from the calculated values in section 3.3 (no I_c degradation up to 1.3 mm bend diameter for a symmetric diffusion bonded structure). Two possible reasons could explain this difference. First, there could be voids remaining at the interface creating locally higher stresses and causing the premature degradation. Second, the choice of the diffusion bonding process parameters (pressure, temperature and duration) was based only on the flat I_c. While higher pressure/temperature and longer time will create a more homogenous interface with less voids, it could also lead to the degradation of the REBCO layer [136, 138, 139]. The chosen parameters were a trade-off between interface quality and avoiding damage to the REBCO layers. That assessment was based solely on the flat I_c of the resulting structure and it is possible that this annealing under pressure has an effect on the bending properties that is not discernible during flat I_c measurement, for example by creating additional “micro”-cracks (compared to the freshly-deposited REBCO layer) which tend to propagate during the bending and cause the early failure.

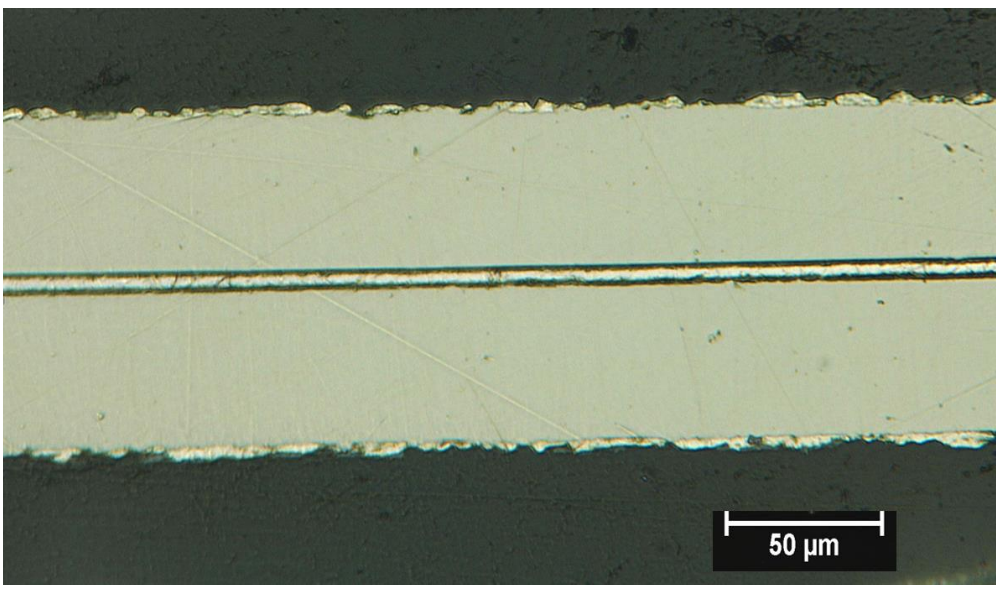

Figure 3-12 Cross-sectional view of a diffusion-bonded sample.

For the soldered and pressed samples, the final solder layer is thin (between 3 to 5 µm). The initial amount of applied solder does not affect the final solder thickness since the excess solder is squeezed out during the solder reflow under the applied pressure. Figure 3-13 represent an image of the cross-section of such sample made along the length of the joined tapes and it can be seen that the thickness of the solder layer is quite uniform over several millimeters' length.

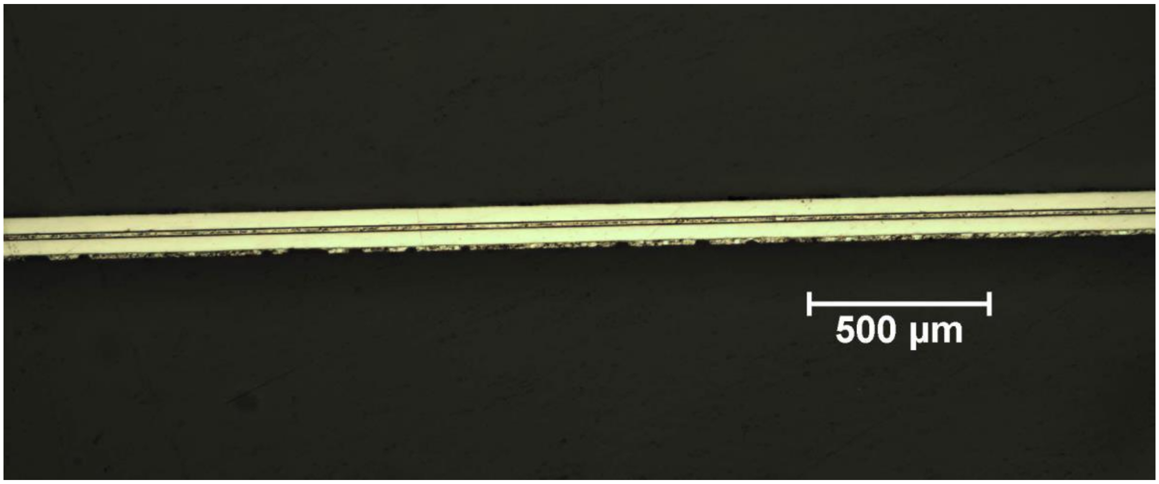

Figure 3-13 Longitudinal cross-sectional optical microscope image of a soldered sample.

Figure 3-14 summarizes the bending results for both the symmetric (same substrate thickness) soldered two-tape structures and those made with 2~3 µm offset in the substrate thickness. For the symmetric samples, the upper envelope of the results is not far from the theoretical predictions and the slight differences could be attributed to errors in thickness measurement (performed using a micrometer with +/-0.5 µm accuracy) at the various steps of the process but the large scatter of the results and the lower end of the results could not be explained but such errors. In addition, the offset samples, which are meant to compensate for the difference between the tensile and compressive limits of the REBCO layers, provided limited improvement: about 20% improvement on average at bend diameters smaller than 3 mm compared to the symmetric case. Besides, the persisting scatter in the bending results suggests that there is another underlying mechanism limiting the performance of both samples, symmetric and offset, aside from the originally considered parameters (solder thickness and strain limits).

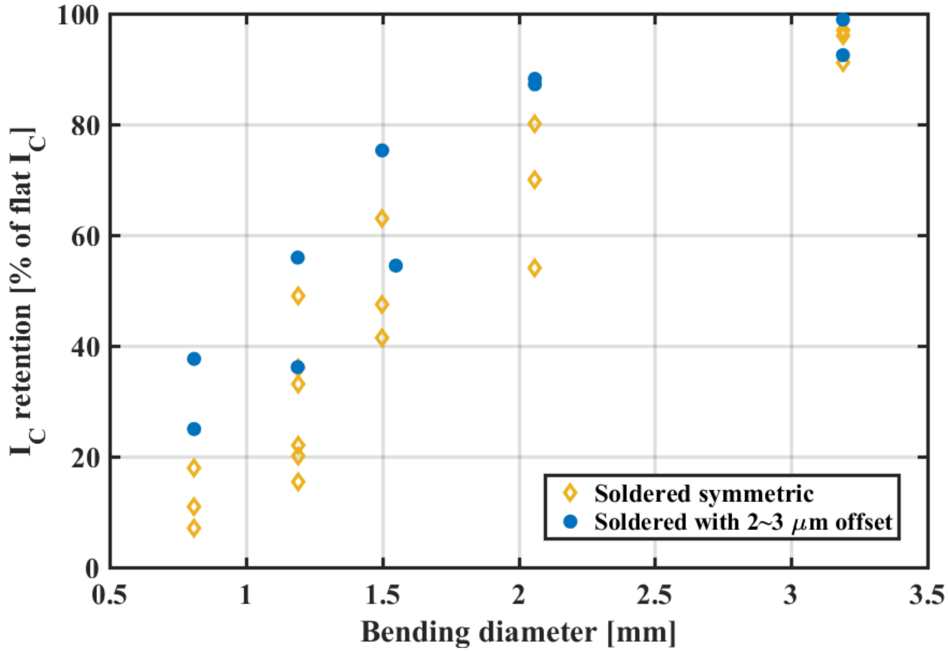

Figure 3-14 I_c retention as function of the bending diameter for soldered samples with thin solder layer (3~5 μm).

Figure 3-15 shows a higher magnification of the cross-section of these samples. The solder interlayer shows a significant number of voids formed between the two tapes. Void formation during soldering has been observed in various processes and it could be due to trapped gases from the interaction between the flux and Ag oxides and other contaminants at the interface [140, 141]. However, it is believed that it is not the main factor in the void formation in this case, but rather surface tension effects due to the very small thickness of the solder interlayer. During the solder reflow, the remaining solder at the interface will tend to coalesce in liquid form to reduce surface energy. Such voids were observed on all samples. Even though they were not severe enough to cause delamination during the measurement, these voids will cause stress concentration around them during the bending [142] and by their close proximity to the REBCO layers will affect the bending performance of the structure.

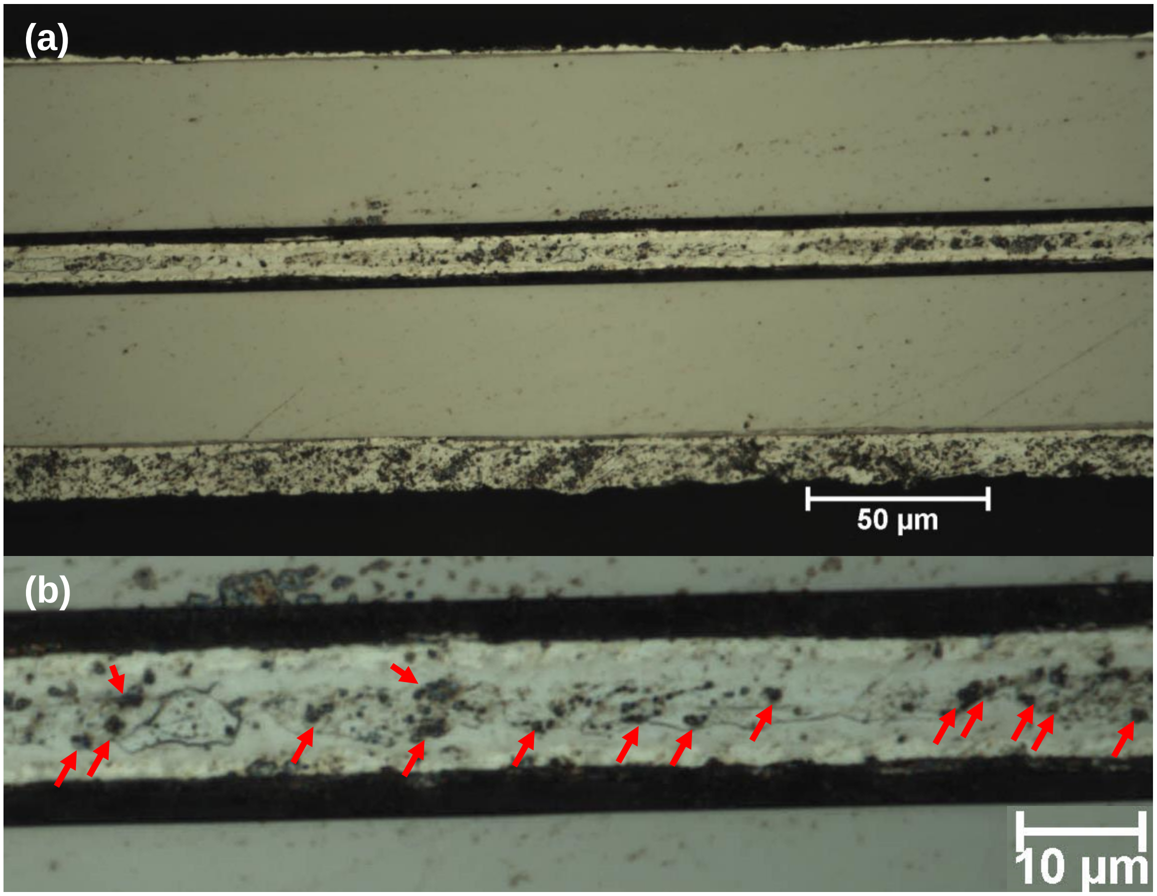

Figure 3-15 (a) Cross-sectional view of a soldered samples with ~2 μm offset in substrate thickness, (b) higher magnification of the solder interlayer, the red arrows point at some of the void formed at the interface.

3.6. Conclusion

In this chapter, two tapes assembled face-to-face were used as a mean to enhance the bending properties of REBCO coated conductors. Calculation results showed that in such symmetric structure, the improvement of bending properties is independent of the substrate thickness of the original tapes and only depends on the thickness of the interlayer separating the REBCO layers from the interface and on their strain limits. In the case where the REBCO layer has different tensile and compressive strain limits, an offset between the two substrate thicknesses allows the shift of the neutral axis of the structure toward the tape with the lower strain limit. During the bending, both layers will reach their maximum allowable strain at the same bend diameter, thus, maximizing the bending performance of these structures. Finally, two methods to make such structures were implemented and tested. The obtained results showed the potential of such tape structure in enhancing the mechanical properties of REBCO CC regardless of the substrate thickness, given enough control on the thickness and homogeneity of the interlayer between the two tapes.

CHAPTER 4. Reel-To-Reel Filamentization for AC Losses Reduction in REBCO Tapes and Wires

4.1. Introduction

The improvement of the performance of high temperature superconductor (HTS) coated conductors (CC) by the addition of artificial pinning centers [32, 33] makes them very attractive for use in DC applications. However, in AC applications, the tape geometry of the CC with a very thin superconducting layer and a high aspect ratio makes AC losses a significant problem in practical applications. There is a need for low magnetization, low AC loss REBCO tapes and wires. These AC losses are the highest when the AC magnetic field is perpendicular to the tape's surface and are the lowest when it is parallel to its edge. Since it is generally not possible to have the tape always parallel to the AC field, it is important to seek ways to reduces these losses. An effective way to achieve this is to subdivide the superconducting layer into several narrow filaments with lower aspect ratio [100, 143]. While filamentization reduces the hysteretic magnetization losses, it introduces, potentially, additional coupling losses. The level and magnitude of these losses will be determined by the quality of the filamentization process and the tape's orientation with respect to the applied field. To minimize coupling losses, a combination of a highly resistive barrier between the filaments and limiting the effective length over which these filaments are exposed to a certain field orientation is needed [100, 101].

A variety of techniques has been used to achieve the filamentization such as mechanical scribing [103], inkjet printing [104, 105], laser ablation [106, 107], substrate modfication [108] and laser lithography along with chemical etching [109]. Although expected AC losses reduction levels have been achieved over short segments of multifilamentary tapes using stationary processes, reel-to-reel produced samples still show lower reduction levels [112]. Besides, regardless of how effective the striation process is in reducing AC losses over short segments of tape, coupling losses will arise over long lengths and will need to be suppressed by transposing the filaments in order to maintain the desired levels of AC loss reduction.

4.2. Chapter organization

In this chapter, a laser striation technique followed by selective electroplating of copper used to fabricate long lengths of fully-stabilized multifilamentary REBCO tapes is presented as follows:

- In the first part, a description of the various steps (the laser ablation, the oxygenation and the selective electroplating) of the striation process using a femtosecond laser is provided. The effect of the most relevant parameters on the tape's critical current, microstructure and AC losses is presented.
- Then, the filament-to-filament resistance and its effect on the coupling losses is investigated. A new approach to reduce the coupling losses by limiting the copper growth on the substrate side of the tape is proposed.
- Also, a new patterning design was developed and implemented in order to transpose the filaments without any mechanical twisting.
- In the second part, the striation results using a nanosecond laser is presented. A comparison with the femtosecond laser striation process is provided and the approach used to achieve the desired loss reduction using this type of laser is also explained.

- Finally, the striation process is adapted to enable the production of multifilamentary STAR wires. Several wires with various number of filaments per tape were fabricated and their AC losses characterized.

4.3. The laser ablation

Laser ablation consists in removing material from a surface by irradiating it using a continuous wave (CW) or a pulsed laser beam. A continuous wave laser is characterized by a stable and continuous output power while pulsed lasers have short time output pulses with durations ranging from milliseconds to femtoseconds and peak output powers usually much higher than that of a CW laser beam having the same average output power, as illustrated in Figure 4-1. So, the laser ablation could be a thermal or non-thermal process depending on the type of laser used. For CW lasers, the laser beam energy is absorbed by the material, increasing its temperature until the material evaporates. For short laser pulses (e.g. femtosecond pulses) the electron-ion energy exchange and heat conduction time scales are much larger than the pulse duration, so the ions remain cold. Ionization occurs at the beginning of the pulse then the laser energy is absorbed by the free electrons. The electric field generated by the charge separation pulls the ions out of the target thus creating an efficient non-equilibrium mechanism of ablation [144]. For long-pulsed lasers (nanoseconds and longer), in addition to ionization, several other phenomena occur during the ablation such as vaporization, convection, melting and shockwaves [145-147].

In addition to the laser's pulse width, which determine the fundamental processes involved in the ablation, there are several other factors that need to be considered in the choice of the best laser for a specific process. A key parameter is the wavelength which determines the absorption depth. A small absorption depth results in a high energy deposition within a small volume which makes the laser ablation quicker and more efficient. Another important parameter is the energy fluence (the laser energy per unit area) defined by laser pulse energy (J) / focal spot size (cm^2). It has to exceed the material ablation threshold in order for the plasma to form and for the ablation to occur. Other parameters such as the repetition rate, beam quality and scanning speeds play also an important role in the ablation process.

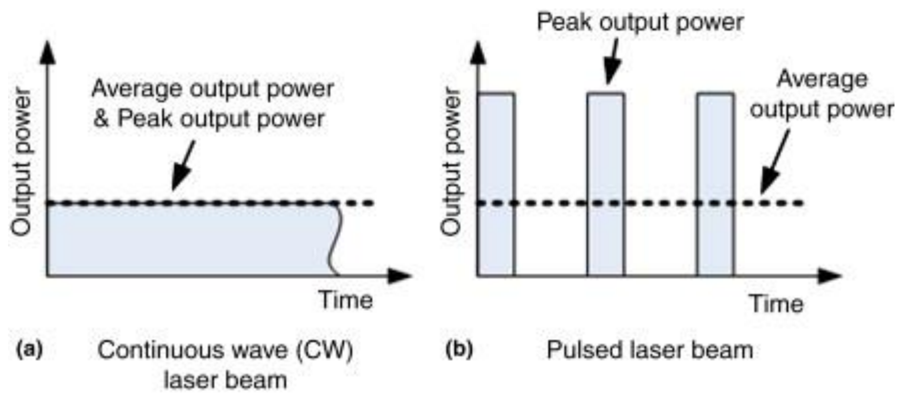

Figure 4-1 Illustration of the peak output power and the average output power of a CW laser beam and pulsed laser beam [148].

In this work, the parameters for REBCO CC striation are determined and optimized based on three essential considerations. First, the effect of ablation on the tape's critical current (I_c) should be minimal. Second, the quality of the produced groove should enable the subsequent selective electroplating. And finally, it should achieve the targeted AC losses reduction levels.

Two types of lasers, a femtosecond and a nanosecond laser, were used to make the striation in this dissertation. Since femtosecond laser ablation is a non-thermal process, it is especially suitable for REBCO CC striation since there is no possible degradation of the tape's critical current due to heating during the striation process. However, the cost of these laser remains significantly high compared to other types of lasers. At the end of the chapter, results, using a nanosecond laser, with equal striation quality and levels of AC losses reduction as in the femtosecond case will be presented. With a careful choice of the pulse energy, repetition rate, scanning speed and power, it is possible to mitigate the thermal effect on the REBCO layer and maintain the same level of AC losses reduction. However, with the nanosecond laser, that was achieved at the expense of the process speed.

Figure 4-2 shows a picture of the femtosecond laser used, along the reel-to-reel system built around it. It constist of a diode-pumped solid-state femtosecond laser from Jenoptik (JenLas® *D2.fs* Yb:KYW, ytterbium-doped potassium yttrium tungstate). The system produces laser pulses of less than 400 fs with a repetition rate ranging from 30 to 200 kHz. The laser energy per pulse is 40 μJ at 100 kHz and 20 μJ at 200 kHz. The laser's specifications are summarized in Table 4-1. The laser is also equipped with an optical scanner which consists of two scanning mirrors and an F-theta scanning lens allowing to control and maintain the focus of the laser beam over an area of about 6 by 6 cm.

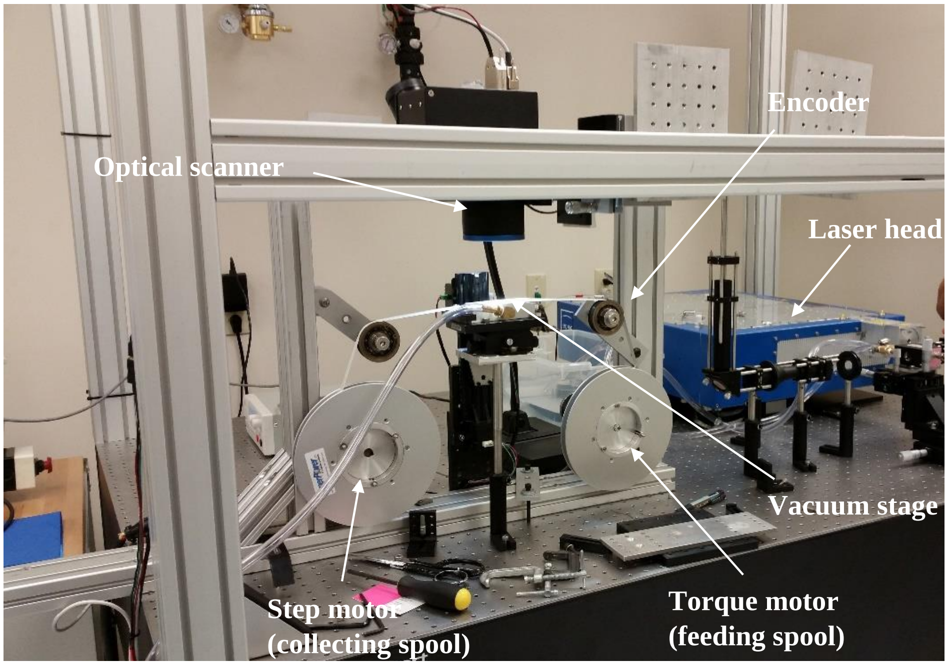

Figure 4-2 The reel-to-reel femtosecond laser striation system.

The reel-to-reel motion is achieved using two motors: a stepper motor drives the tape and controls its speed while the torque motor is used to maintain a constant tension during the tape motion. An encoder is used to determine the actual tape moving speed and adjust the stepper motor to maintain a constant speed during operations. During the striation, the tape was kept flat using a vacuum stage, shown in Figure 4-3(a), to maintain it within the laser depth of focus. Additionally, a laser fume extractor from Fumex [149], shown in Figure 4-3(b), was installed next to the vacuum stage to remove any unhealthy fumes and particles created by the ablation and prevent their redeposition inside the grooves. In the following subsections, the most relevant parameters in the reel-to-reel ablation process will be presented along with their effect on the tape's microstructure and the subsequent steps of the filamentization process.

Table 4-1 Characteristic of the JenLas® D2.fs laser.

Laser	Yb:KYW Thin-disk laser, diode-pumped
Wavelength	1025 nm
Output energy	40 μJ @ 100 kHz / 20 μJ @ 200 kHz
M^2	≤ 1.25
Pulse Repetition rate	30 – 200 kHz
Pulse width	< 400 fs

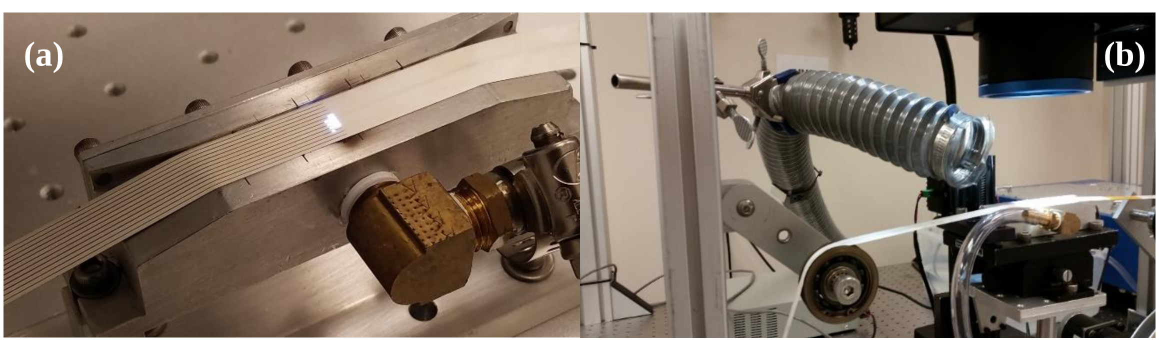

Figure 4-3 Pictures of (a) the vacuum stage and (b) the laser fume extractor.

4.3.1. The groove geometry

For AC losses reduction, the REBCO layer has to be subdivided into narrow filaments with aspect ratios lower than the original non-striated tape. So, the first step would to determine the process parameters that ensures a continuous and deep enough cut that completely separates the individual filaments. In addition, the groove has to be deep enough to reach the substrate to allow the oxide layer formation at the bottom of the groove later on. This would set a minimum depth of 5 µm for the groove. In addition, during the electroplating, there will be some lateral copper growth on the edge of the filament as illustrated in Figure 4-4. A certain minimum groove width is also needed, so that after the electroplating, the deposited copper does not create low resistance bridges between the filaments which in turn creates coupling losses and reduces the effectiveness of the filamentization. This minimum width value depends on the targeted thickness for the Cu layer. In this work, a groove width of 60 to 70 µm was found to be enough to deposit 20 to 30 µm of Cu and maintain unbridged filaments.

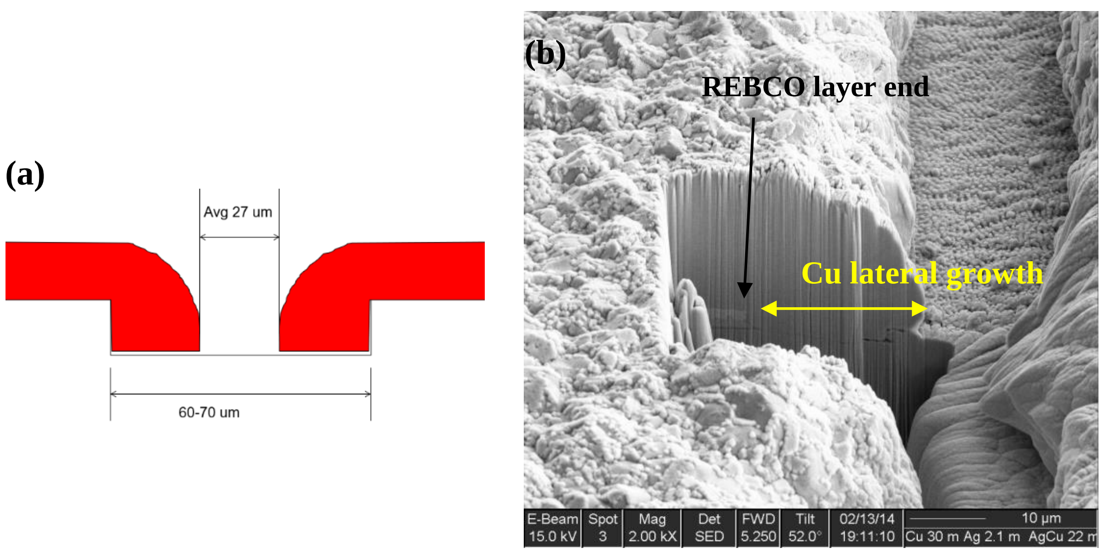

Figure 4-4 (a) A schematic of the groove morphology after depositing 22 µm of Cu. (b) An SEM/FIB image of the filament edge showing the Cu lateral growth inside the groove.

4.3.2. Pattern selection

Since the laser spot size is only 30 µm in diameter, to achieve a groove width in the 60 to 70 µm range, several laser marks are needed. A pattern of 4 lines, separated by 10 µm each, was chosen so there is enough overlap between the lines to obtain a smooth groove surface. The effect of the pattern order was checked for two configurations: cut the outer lines first then inner lines or do the opposite and start with the inner lines. The resulting groove morphology was then examined by a 3D laser scanning microscope from Keyence [150] which provides in addition to an optical image of the surface, high resolution profile and roughness measurements. The groove surface and lateral depth profile for the two configurations are shown in Figure 4-5. The inside-then-outside pattern yielded a flatter groove surface with less redeposited material in the groove's corners. Since there will be always some amount of redeposited material (during any laser ablation process), a groove depth in the range of 8 to 10 µm was opted, not only to ensure the cut through the REBCO layer but also to minimize the creation of any conductive paths by the redeposited material at the edge of the filament.

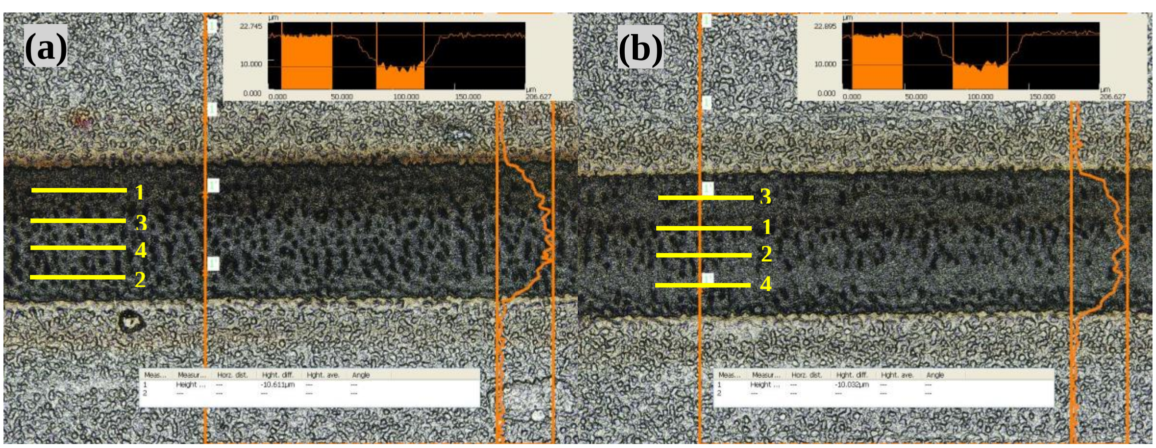

Figure 4-5 Optical microscope image and lateral groove depth profile when the 4 lines pattern is cut (a) outside then inside, (b) inside than outside.

4.3.3. Effect of laser parameters on the groove depth and uniformity

The laser used in this work offers several adjustable parameters such as the marking speed, the jump speed, the repetition rate and set output power. These parameters have to be chosen carefully in conjunction with the tape motion speed in order to obtain a continuous and uniform cut. First, considering the case of static ablation where the tape is fixed and only the laser mark moves, it is essential that there is enough spot overlap between pulses to obtain a continuous cut. A spot overlap percentage could be defined as

$$\text{spot overlap [\%]} = 100*\left(1 - \frac{\text{marker speed [mm/s]}}{\text{rep. rate [Hz] * spot size [mm]}}\right). \tag{4-1}$$

This parameter now links the marker speed and laser repetition rate for a given spot overlap ratio. For example, to achieve a 67% overlap between pulses it is possible to use a marker speed of 1 m/s and a repetition rate of a 100 kHz or increase the marker speed to 2 m/s and set the repetition rate to 200 kHz. To determine the appropriate set of parameters, two additional considerations have to be included. First, higher marking speeds are desirable since the marking speed along with the jump speed (the jump speed is the laser marker speed when it is moving from one mark to the other without outputting pulses) will determine the total mark time of a single pattern, which will in turn determine the tape moving speed during the reel-to-reel process. Second, since the laser maximum output power is fixed (in this case 4.1 W), the higher repetition rates will correspond to lower energies per pulses. However, the energy per pulse has to remain above the ablation threshold of the various layers of the tape in order for the plasma to form and effective ablation to occur. At 200 kHz, the maximum repetition rate for this laser, the energy per pulse is 20 μJ which would correspond to a fluence of 2.83 J/cm^2. The ablation threshold varies significantly from one layer to the other and the selected energy per pulse has to exceed the highest value. For femtosecond pulses, reported values for the ablation threshold are 1.5 J/cm^2 for the silver [151], 0.26 J/cm^2 for the Hastelloy [152] and 0.09 J/cm^2 for YBCO films on MgO substrates [153]. At 200 kHz, the laser fluence is well above the ablation threshold of all the layers.

Now, in order to determine the ablation rate, a static test with various number of passes (a pass refers to a full laser pattern of all the lines executed once) was performed. Figure 4-6 shows the groove morphology evolution with increasing number of passes and Figure 4-7 shows the corresponding average groove depth.

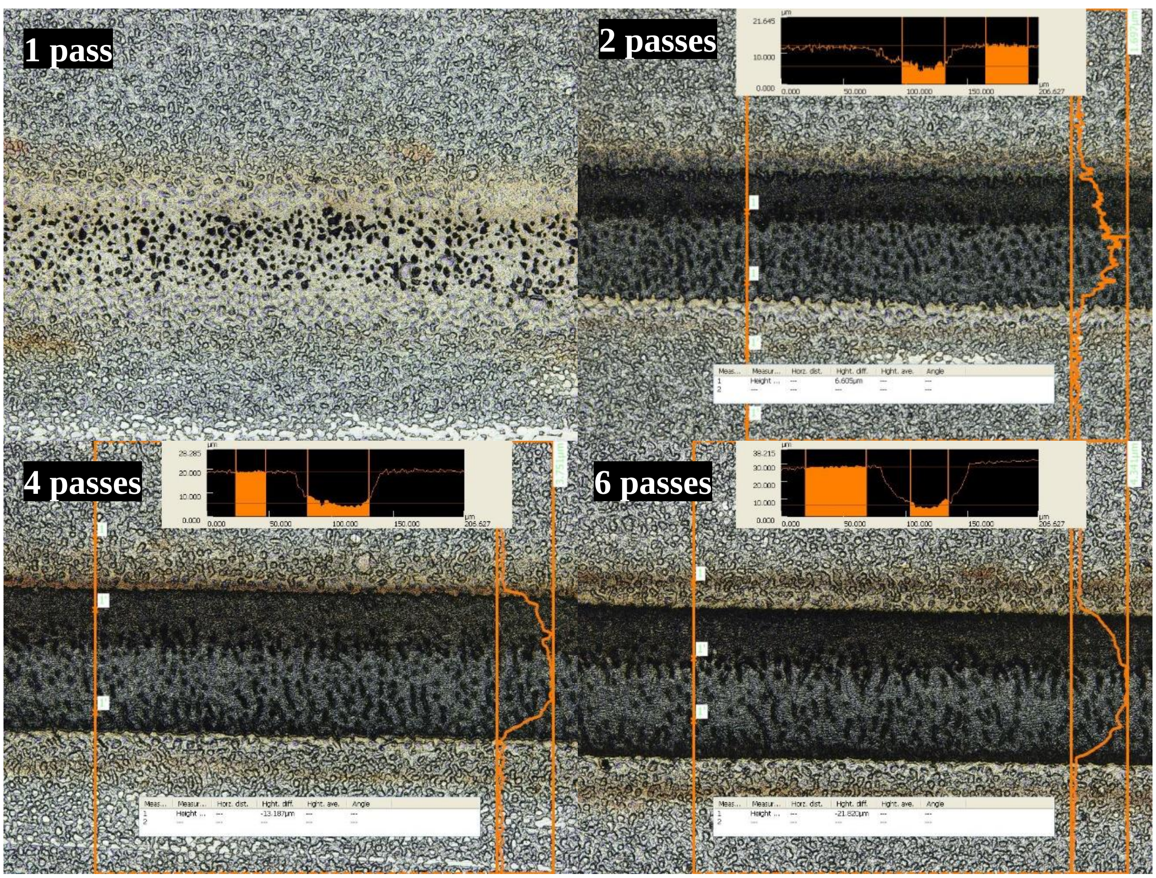

Figure 4-6 Optical images showing the groove shape for various number of passes.

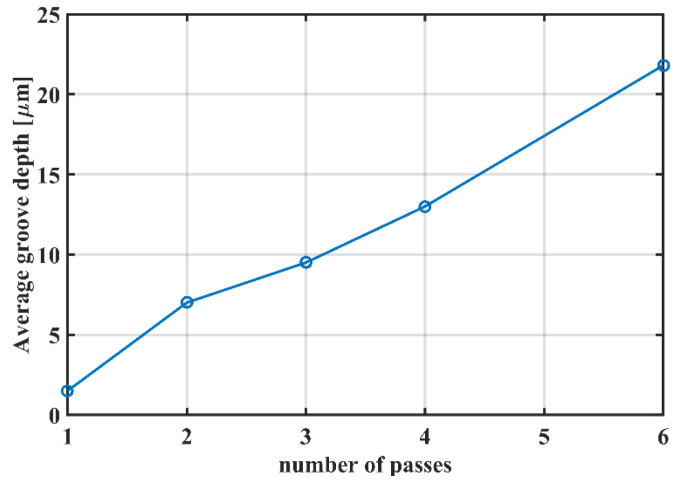

Figure 4-7 Average groove depth as a function of the number of passes

The test showed that while a single pass could not completely cut the silver layer which is less than 2 µm, the 2 passes reached a 7 µm depth. After that, the ablation rate was about 4.5 µm per additional pass. The low yield of the first pass is due to the high ablation threshold of the silver layer which is here in the same order of magnitude as the laser fluence, while for the REBCO and Hastelloy the laser fluence is an order of magnitude higher than the ablation threshold thus the high ablation rate [151, 152, 154].

4.3.4. Mark overlap and tape motion speed

The selection of the tape motion speed will depend on the mark length and desired overlap. The overlap could be expressed as

$$\text{Overlap [\%]} = 100 * \left(1 - \frac{\text{tape motion speed [mm/s]} * \text{single mark time [s]}}{\text{mark length [mm]}}\right). \qquad (4\text{-}2)$$

To achieve the desired depth, a minimum 67% overlap is needed (corresponding to a static cut with 3 passes). Although, a higher overlap ratio is desirable in term of uniformity, it comes at the expense of the process speed. A low overlap ratio will increase the requirement on the degree of alignment between the laser mark and tape motion direction. Figure 4-8 shows the effect of the bad alignment in the case of low overlap ratios. It will create kinks on the filament edges which will act as nucleation sites during the subsequent electroplating and could bridge the filaments. This will create unwanted coupling losses and reduce the effectiveness of the filamentization process. The final choice for the tape motion speed is a trade-off between groove quality and process speed. Striation speed up to 5 m/s were achieved for 12-filament samples. For higher number of filaments, the speed is inversely proportional to the number of grooves. Figure 4-9 shows the morphology of the final groove structure which was on average 9.5 μm deep and 67 μm wide.

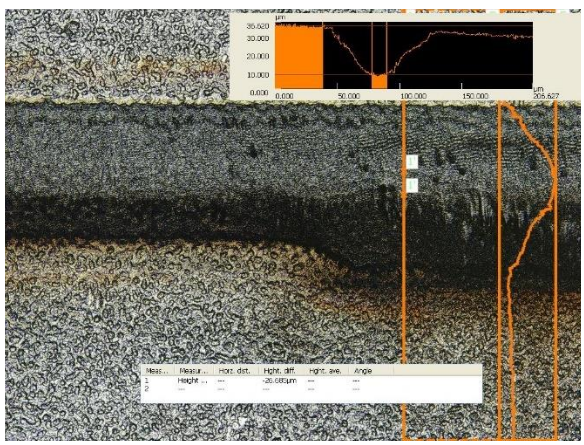

Figure 4-8 A test sample where the laser marks were misaligned with the tape motion.

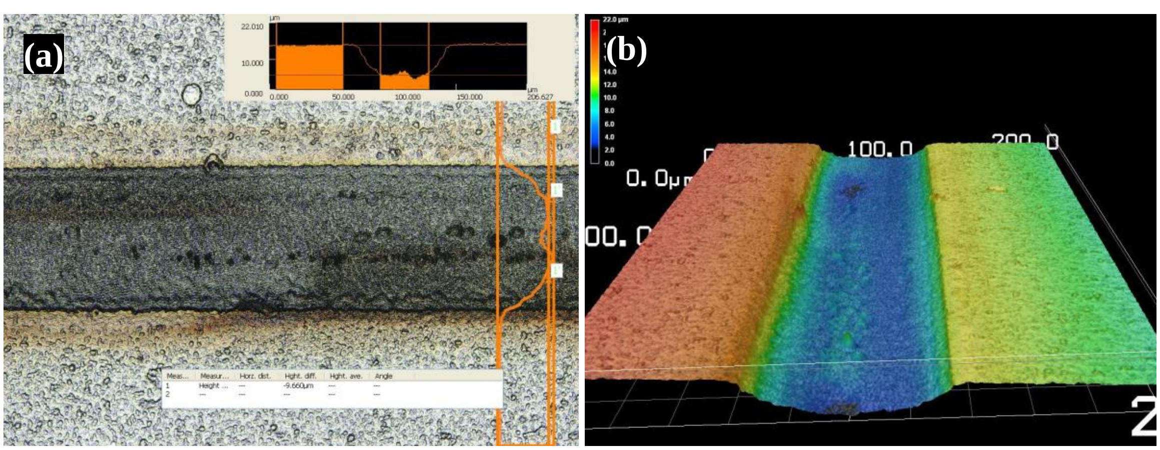

Figure 4-9 (a) Optical image of the final, reel-to-reel produced, groove and (b) its 3D surface morphology.

4.3.5. Effect on the tape critical current

Since the femtosecond laser ablation is a non-thermal process, the expected degradation in tape I_c should be caused only by the removed superconducting material volume. That percentage is determined by the groove's width and number of filaments. So, the width of the grooves has to be kept as small as possible to minimize the effect of the ablation on the tape's I_c. However, the measurements, summarized in Table 4-1, showed more degradation than the fraction of material removed. This additional degradation is more severe for the samples with 24 and 46 filaments, reaching about 8 and 5% respectively, while being less than 1% for the 12-filament samples. This is due to the fact that multifilamentary tapes are very sensitive to defects in the original tape. While defects in a wide superconducting tape do not constitute a major issue since the current can go around them, in a striated conductor these defects represent a more serious problem. Depending on the size of the filament, they could either reduce or block completely the current flow in that filament. This is consistent with the higher degradation observed on samples with narrower filaments. In addition, the samples measured after the ablation do not have a stabilizer layer to help carry the current around localized defects, and only a limited current redistribution between the filaments can happen through the highly resistive Hastelloy substrate.

Table 4-2 Effect of the laser ablation and oxygen annealing on samples with 12, 24 and 46 filaments. The original tape I_c was 430 A.

Number of filaments	**12**	**24**	**46**
I_c after laser ablation [A]	400	340	300
Degradation [%]	7	20.9	30.2
Material removed [%]	6.1	12.8	25.1
I_c after annealing/oxygenation [A]	360	310	270
Degradation [%]	16.2	27.9	37.2

Trapped field measurements by Scanning Hall Probe Microscopy (SHPM) [155] performed on 12 and 24-filament samples, shown in Figure 4-10, also confirms this explanation. The 12-filament sample showed multiple point defects in various locations while the 24-filament sample showed an entire region of lower critical current density at center of the tape extending over several filaments.

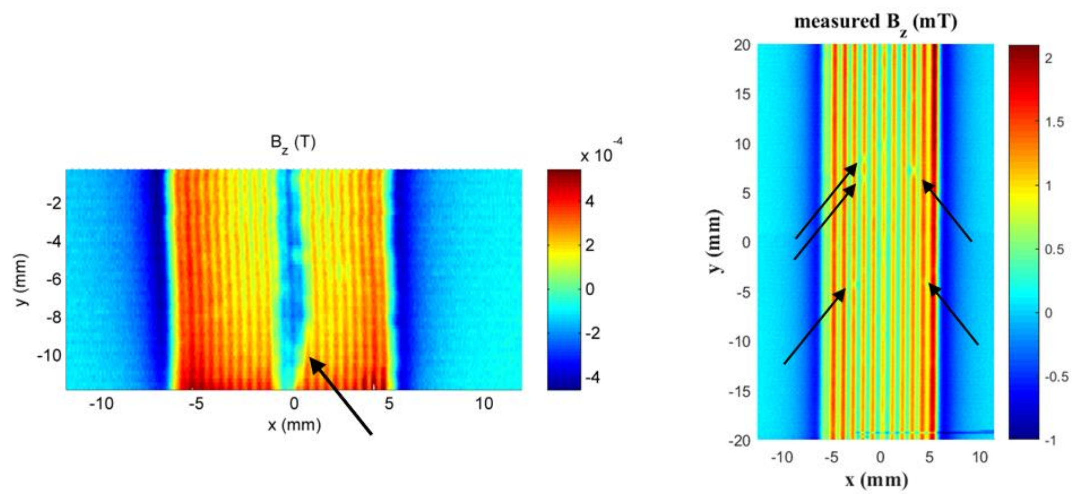

Figure 4-10 Trapped field measurement by SHPM on a 24-filament sample (left) and a 12-filament sample (right). Arrows point to defect regions with low critical current density.

4.4. Annealing / Oxygenation

In most applications, any superconducting material requires a certain amount of a high conductivity material for thermal and electrical stabilization [128, 156, 157]. However, if the resistance between the filaments is very low, for example due to the stabilizer layer connecting the filaments, this will create coupling losses which will reduce the effectiveness of the filamentization process. Coupling losses are generated by current flow between superconducting filaments through a resistive path [100, 106]. So, it would preferable if the stabilizer is deposited only on top of the filaments without covering the grooves. In order to achieve the selective (only on top of the filament) deposition of the stabilizer, the multifilamentary tapes were annealed at high temperature in oxygen flow.

This process referred to as oxidation was developed and studied earlier [86, 158] and it was found that the formation of an oxide layer at the bottom of the groove will prevent the copper (the stabilizer in this case) deposition inside the grooves during the electroplating process. While higher temperatures were found to produce a thicker oxide layer, the high temperature also tend to favor the diffusion of certain elements like Ni and Cr from the Hastelloy to the REBCO layer which degrades the tapes I_c significantly. Similar results, summarized in Table 4-3, were obtained on 12-filament samples annealed at various temperature. A 0.5 h annealing at 550 °C in O_2 flow was chosen since the oxide layer formed at that temperature was found to be enough to enable the following selective Cu electroplating. Even at 550 °C, depending on the number of filaments, this step of the process causes an additional degradation, shown in Table 4-2, of 7 to 9% in the tape's I_c.

Table 4-3 Critical current of 12-filament samples annealed in O_2 for 0.5 h at various temperatures. The original tape I_c was 430 A.

Annealing temperature [°C]	550	575	600
Critical current [A]	392	332	289

4.5. The selective electroplating process

As stated earlier, one of the main challenges in the filamentization process, in addition to cutting the REBCO layer without excessive damage, is the deposition of a relatively thick stabilizer layer only on top of the filaments to avoid creating additional coupling losses. Previously, several top-down approches were attempted where the striation is performed on an already copper-stablized tape. However, there are other challenges in these approches such as the excessive critical current (I_c) reduction with a limited number of filaments (up to 50% with 7 filaments) and AC losses reduction ratio of only 2 fold compared to the original tape [113]. The difficulties in making an effective laser striation on stabilized samples with a thick copper layer is due to the high energies required to cut through the thick copper, which results in significant melting and creates grooves with poorly defined edges. Also, significant redeposition of the copper inside the grooves happens in these processes hindering their effectiveness in reducing the AC losses [113, 159, 160]. In order to circumvent these issues, the selective electroplating approach was adopted in this work, where the laser striation is performed on the stablizer-free tape and then deposit the stablizer layer only on top of the filaments. This technique was developed earlier at the University of Houston [86], and the effects of the chemistry and some of electroplating parameters on the microstructure were previously studied [86, 161].

In the following subsections, results on short pieces of multifilamentary tapes electroplated in beaker using this technique are first reported. This will serve as a benchmark for the quality of the laser ablation process presented earlier. Optical and scanning electron microscopy were used to check the presence of copper inside the grooves and magnetization AC losses measurements were performed in order to estimate the level of loss reduction compared to the original non-striated tapes and evaluate the overall effectiveness of the filamentization process. In a second stage, the effort was focused on the reel-to-reel process and the production of long length multifilamentary tapes with the same levels of AC loss reduction obtained by stationary beaker electroplating.

4.5.1. Stationary electroplating: AC losses of 12,24 and 46-filament tapes

Non-striated, 12, 24 and 46-filament samples, each originally 14 cm long, were electroplated in beaker with an acid-free $Cu(NO_3)_2$ solution to deposit ~25 μm of Cu stabilizer. A standard four-probe method was used for I_c measurements with 1 μV/cm criterion. Then, a 3 cm piece was cut from the middle of each sample and its AC losses was measured. Magnetization AC loss measurements were performed using the pickup coil method at frequencies between 40 and 500 Hz at 77 K. Figure 4-11 shows photographs of a 12-filament sample after copper electroplating and 24- and 46-filament samples as striated (before copper electroplating).

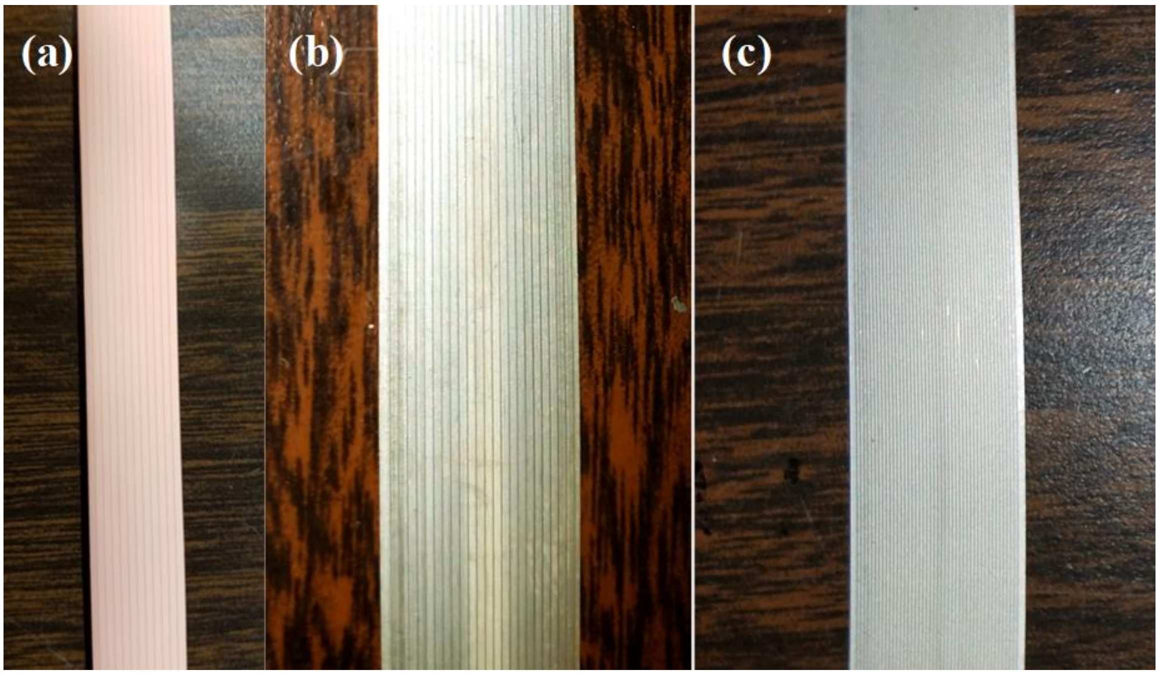

Figure 4-11 Photographs of (a) a 12-filament sample after copper electroplating, (b) a 24 and (c) a 46 filament-tape as striated.

Figure 4-12 shows the results of the magnetization AC losses measurements at a frequency of 40, 100, 300 and 500 Hz on 3 cm long pieces from the 12, 24 and 46-filament copper-stabilized tapes. Results from the non-striated original tape are also shown for comparison. Since these tapes have different I_c values, it is essential to normalize the measured loss values in order to make a meaningful comparison between the samples. The Brandt-Indenbom model [143] provides an expression for the hysteretic AC loss per cycle per unit length (P_h) for a superconducting strip in the presence of a perpendicular applied AC magnetic field of amplitude H_a as

$$P_h = \mu_0 w I_c H_a \left[\frac{2}{x} \ln(\cosh x) - \tanh x \right], \tag{4-3}$$

where μ_0 is the vacuum permeability, $x = (\pi H_a w) / I_c$ and w is the width of the tape in the non-striated case and the width of the filament for the filamentized tapes. Based on Equation (4-3), the hysteretic AC loss per cycle per unit length is expected to decrease by an order equal to the number of filaments. In addition, considering that the expression of the penetration field (from the virgin state) is given by

$$B_p = \mu_0 J_c w = \mu_0 I_c, \tag{4-4}$$

the expression of the AC loss per cycle per unit length can be re-written as a dimensionless normalized loss function as

$$g(x) = \frac{P_h}{\mu_0 I_c^2} = \frac{w H_a}{I_c} \left[\frac{2}{x} \ln(\cosh x) - \tanh x \right], \tag{4-5}$$

where $x = B_a / B_p = \pi H_a w / I_c$ and $B_a = \mu_0 H_a$. Now, to compare tapes with different I_c values, the normalized loss function should be used instead of the raw values of the measured loss per cycle for each tape. Besides, the expression established in Equation (4-5) allows us to estimate the pure hysteretic losses for each tape. Any deviation between the measurement and the calculated values (solid lines in Figure 4-12) will indicate the presence of mainly coupling losses, eddy current losses being negligible compared to hysteresis losses in the measurement range [162]. And since coupling losses are proportional to the squares of the amplitude and the frequency of the applied AC field, these losses will be more noticeable at higher frequencies or higher field amplitudes. The measured loss in the 46-filament tape was lower than the calculated loss at high field amplitudes. This is a measurement artefact, referred to as loss saturation, when at high field amplitudes the loss becomes so significant that it starts heating the sample. In this measurement, while the 46-filament sample has the lowest loss, it also has the smallest copper surface area to extract the heat generated by these losses. A better design of the sample holder, allowing for a better and more uniform cooling of the sample surface, should eliminate this issue of loss saturation at higher field amplitudes.

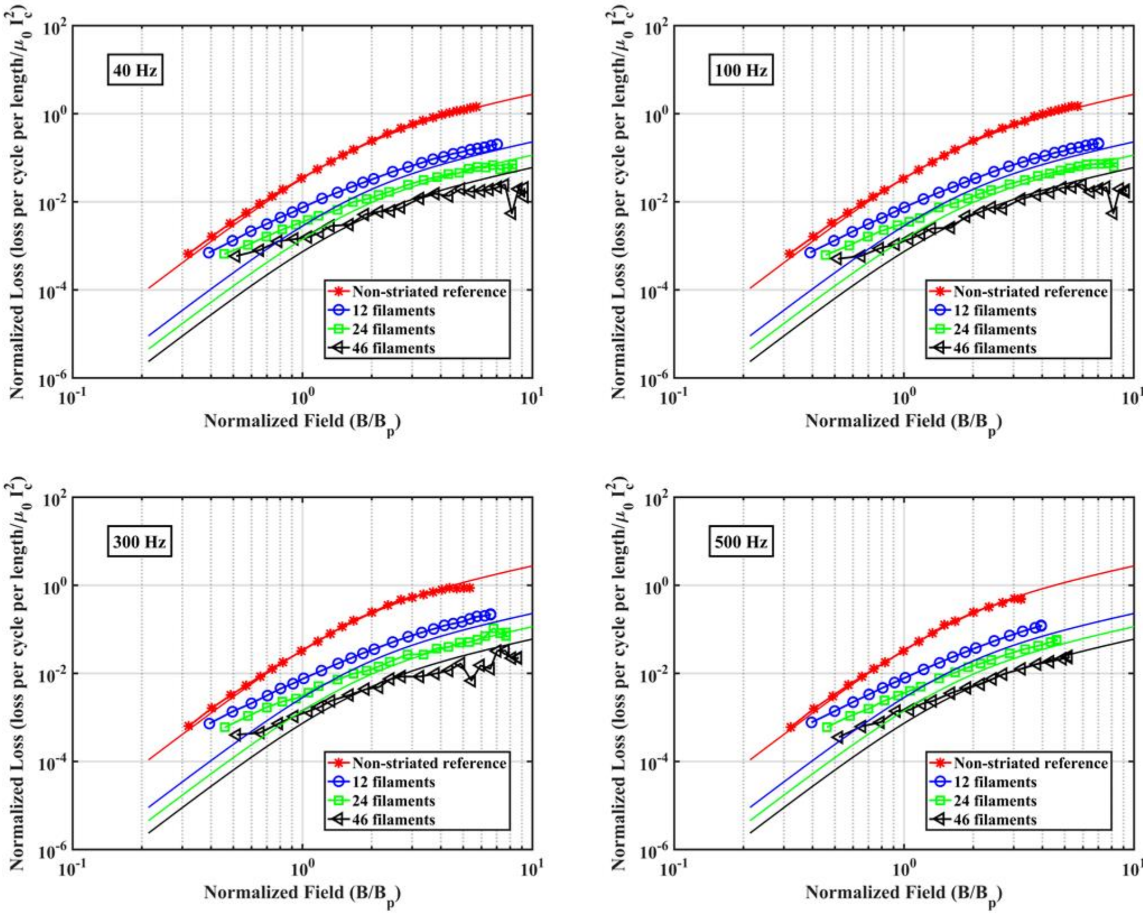

Figure 4-12 Normalized magnetization AC losses for non-striated, 12, 24 and 46-filament samples measured at 40, 100, 300 and 500 Hz. The solid lines represent the Brandt model for each configuration.

It can be seen that with increasing field, the AC loss behavior converges towards the Brandt model for each striated case. At lower fields, the behavior departs from the model and the losses become closer to that of a non-striated tape, indicating possible magnetic coupling at low fields [163]. The presence of a small frequency dependence in the AC loss, especially at higher fields, indicates also the presence of some electrical coupling between the filaments. Investigation of the groove's microstructure showed, occasionally, the presence of copper particles growing inside the groove (Figure 4-13(b)) that could have caused the additional coupling losses. This is due to the fact that any imperfection in the groove's bottom surface created during the laser ablation could act as favorable nucleation site for copper growth inside the groove. But overall the AC loss reduction levels were very close to the targeted values since the number of these particles was limited and the grooves were essentially copper free as shown in Figure 4-13(a).

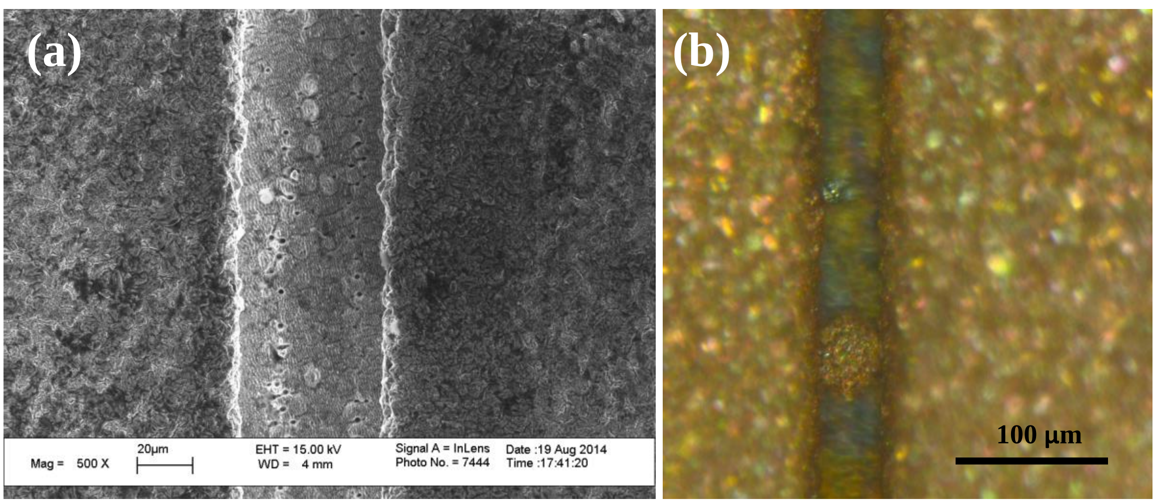

Figure 4-13 Microstructures of a groove between filaments of the beaker electroplated samples; (a) an SEM image of a clean groove and (b) an optical microscope image of a Cu particle growing inside a groove.

4.5.2. The reel-to-reel electroplating system

The reel-to-reel (R2R) electroplating (EP) system, shown in Figure 4-14, consists of a reel-to-reel motion system allowing to pass the tape through a 30 cm long electroplating cell (Figure 4-14(b)). The tape, used as a cathode, is connected to the DC power supply through metallic brushes contacting with both sides of the tape. The contact areas are continously rinsed with DI water to dissipate the heat generated at the contact area during the electroplating process. The anode of the plating cell consists of two titanium baskets filled with copper pellets, that are located on both sides of the tape and connected to the positive of the power supply. Table 4-4 shows the parameters of the electrolyte bath used in the reel-to-reel system. The chemistry and effect of the bath's various parameters were previously studied [161]. The plating cell is connected to a 100 L solution which is continuously pumped for filtering and agitation inside the plating cell. This also avoids local solution depletion during long plating runs. Following the electroplating cell, the tape passes through a DI rinse bath to remove the remants of the solution from its surface. Finally, it is dried with warm air before going into the collecting spool.

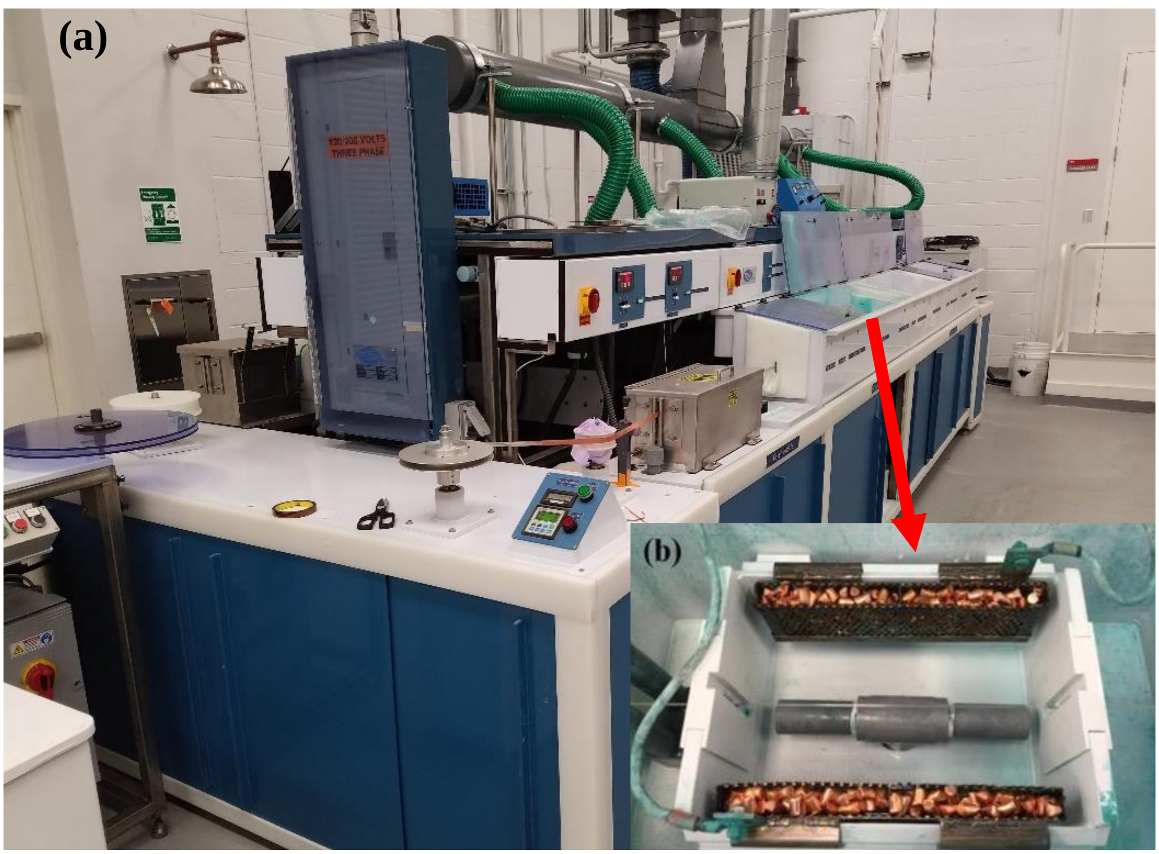

Figure 4-14 (a) The reel-to-reel electroplating system and (b) A close-up image of the 30 cm long electroplating cell.

Table 4-4 Parameters of the electrolyte bath used in the reel-to-reel copper electroplating process.

$CuSO_4 + 5H_2O$	1 M
H_2SO_4	5×10^{-4} M
pH	2.5
Temperature	40ºC

4.5.3. AC loss of early reel-to-reel electroplated tapes

The first test of the reel-to-reel electroplating of a long multifilamentary tape was performed on a 10-meter long 12-filament tape. After the electroplating, the tape was cut at two different positions, one near the start of the tape and the other near its end, and their AC losses measured. Figure 4-15 shows those results along with a non-striated reference and the expected losses based on Equation (4-5).

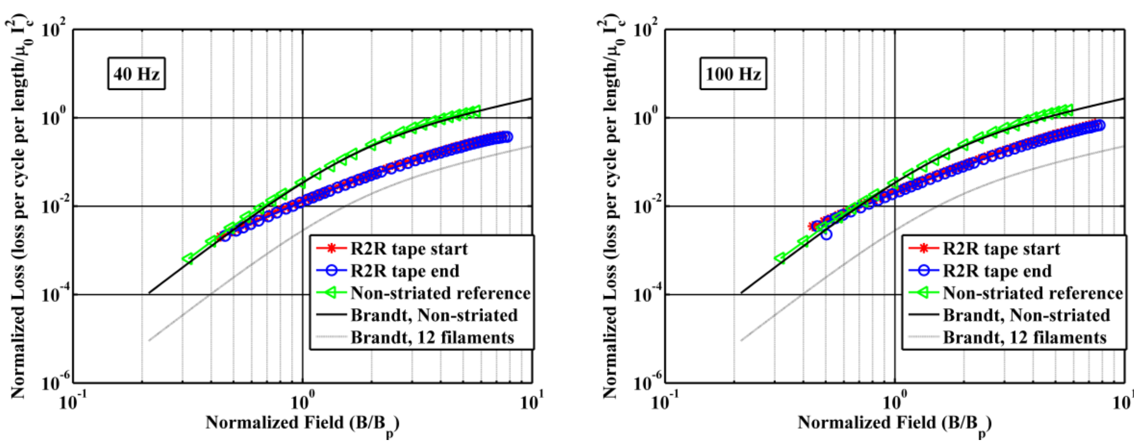

Figure 4-15 Normalized magnetization AC losses for a 12-filament tape produced using the reel-to-reel system measured at two different locations, near the tape start and end.

In the low-field region, a behavior similar to that of the beaker-plated samples is observed, where the magnetic coupling causes the losses in the striated tapes to be closer to those of a non-striated tape. At higher fields, a 5.2-fold reduction in the loss was obtained at a frequency of 40 Hz and a value of 3.2-fold reduction at 100 Hz. The frequency-dependent loss indicates that there is significant electric coupling between the filaments. The main reason for such behavior is that the original shield used in the R2R electroplating system, shown in Figure 4-16, was designed for copper deposition on both sides of the tape. That is not only an additional volume of copper (additional eddy current losses) but also the copper layer actually covers the edges of the tape thus creating a large coupling loop between the end filaments (1 and 12 in a 12-filament tape). Excessive Cu particle growth, shown in Figure 4-17, was observed in the groove that was electroplated near the lower side of the shield (Figure 4-16 orientation) due to its asymmetric design. It is therefore expected that by improving the shield design, both these issues could be solved and loss reduction values similar to that of the beaker-plated samples could be achieved.

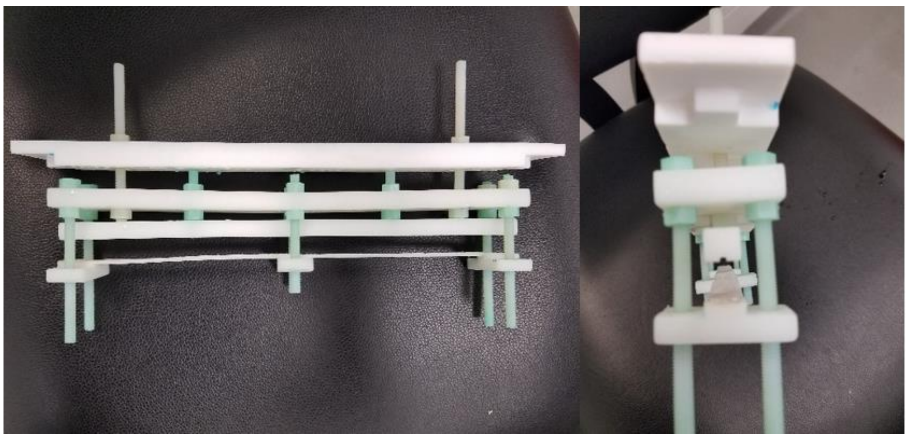

Figure 4-16 Original shield used in the R2R EP system.

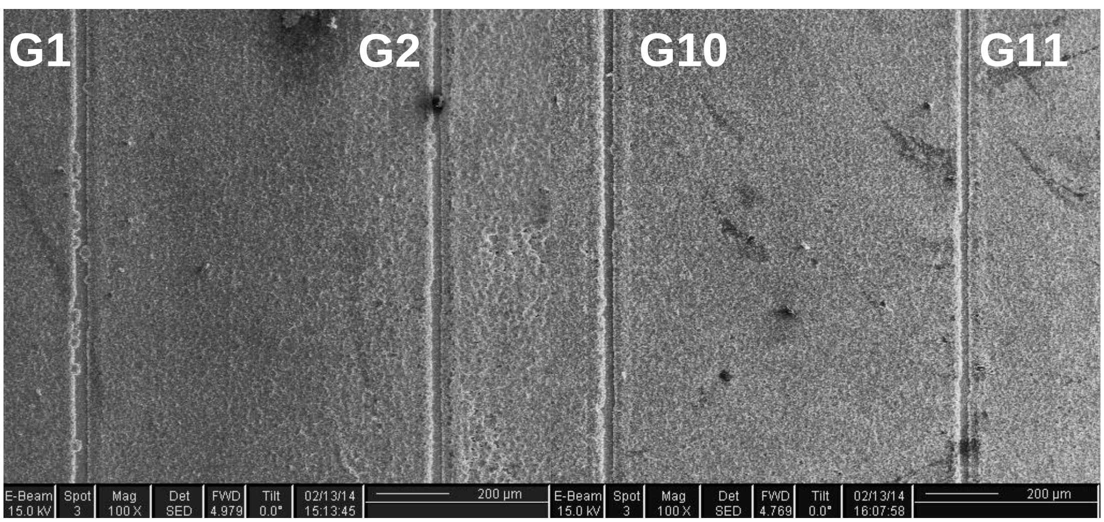

Figure 4-17 SEM images of the R2R electroplated tape. G1 refer to the bottom groove and G11 refer to the top groove (based on the shield orientation in Figure 4-16).

4.5.4. R2R electroplating with back side shielding

Following the previous observations, the shield was modified to prevent the copper growth on the back (substrate) side of the tape by blocking the solution flow to that side inside the electroplating bath. A more symmetric design, shown in Figure 4-18 was adopted to provide a more uniform copper growth along the width and avoid the excessive copper particle growth in the grooves near the lower side of the old shield. To test this new shield design, three samples, each 30 cm long, were electroplated with various Cu thickness by varying the applied current. The electroplating parameters for each sample are provided in Table 4-1.

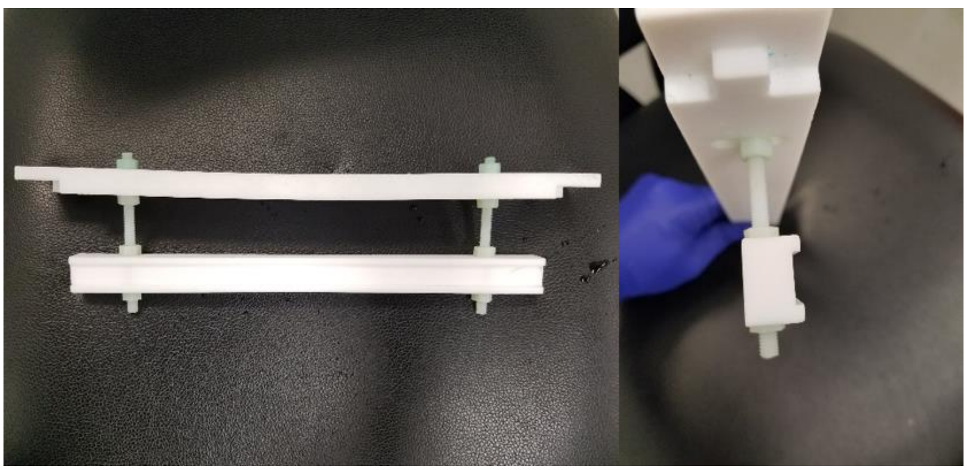

Figure 4-18 The modified shield.

Table 4-5 Electroplating parameters of the test samples using the new shield.

	S1	**S2**	**S3**
Tape speed (cm/min)	4	4	4
Current (A)	3	4	5
Temp (^{0}C)	40	40	40
Cu Thickness (µm)	15	20	25

The first observation on the electroplated samples, shown in Figure 4-19, is that the shield does not prevent completely the copper growth on the substrate side of the tape. A small amount of the solution slips behind the moving tape and enables the growth, on its back, of a thin layer of copper starting from the tape's edges and with increasing coverage at higher currents. A similar effect was observed when varying the tape speed; the slower the tape motion through the bath, the more copper is deposited on its back side.

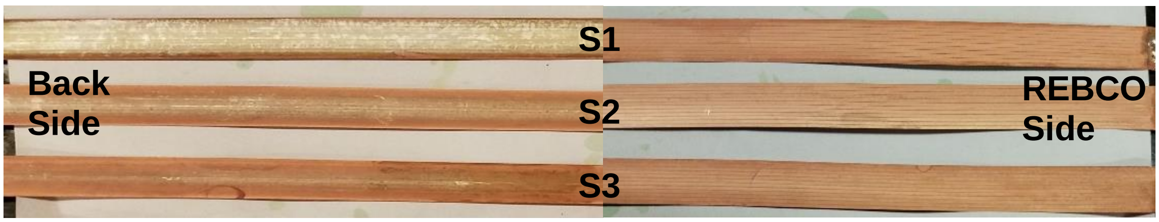

Figure 4-19 Picture of the samples electroplated using the new shield.

In term of AC losses, Sample S1, with the least amount of Cu, showed the highest AC losses reduction level, with near 12-fold reduction up to 300 Hz and 10-fold at 500 Hz. With increasing Cu thickness and back side Cu coverage, the amount of coupling losses increases gradually. But even for S3, with 25 µm on the REBCO side and a near complete coverage of the back side, a 6.6-fold reduction is achieved at 100 Hz, more than double the reduction achieved when the sample had a full 25 µm of Cu on the back side. It should be noted that this effect will be more pronounced for narrower tape, where the thin uniform copper coating in the back forms faster than in the case of a wider tape. An alternative solution to this problem was proposed [113] by cutting the tapes' edges after the electroplating, thus forcing the coupling currents flow through the more resistive substrate than only pure copper. However, this approach results not only in wasted tape width but tends also to weaken its mechanical properties.

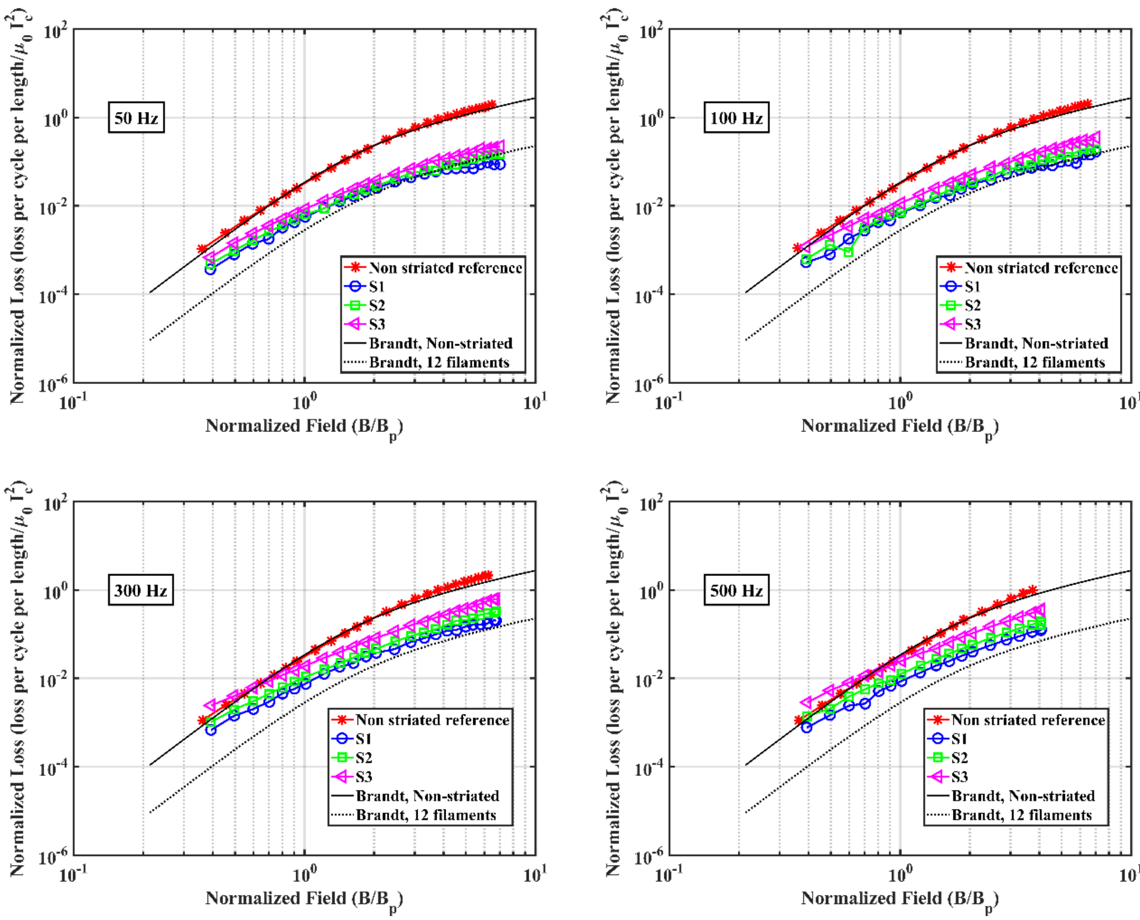

Figure 4-20 Normalized magnetization AC losses for the 12-filament tapes R2R electroplated using the new shield measured at frequencies of 50, 100, 300 and 500 Hz.

4.5.5. Long length striation with various number of filaments

Using the process described above, long lengths of multi-filamentary tape with various number of filaments were produced: 20 meters of a 12-filament tape, 10 meters of 24-filament tape and a one meter of 46-filament tape. Pictures of these tapes are shown in Figure 4-21. To evaluate the quality of the long length striation, five meters of the 12-filament tape were measured using a reel-to-reel SHPM system [164]. The magnetic field profile together with the calculated current distribution are shown in Figure 4-22. The measurement has 2 mm resolution along the tape length direction and 0.1 mm along its the width. This measurement allows not only to confirm the effective cut through the REBCO layer by observing the trapped field of the individual filaments but also to detect any defects or low I_c regions.

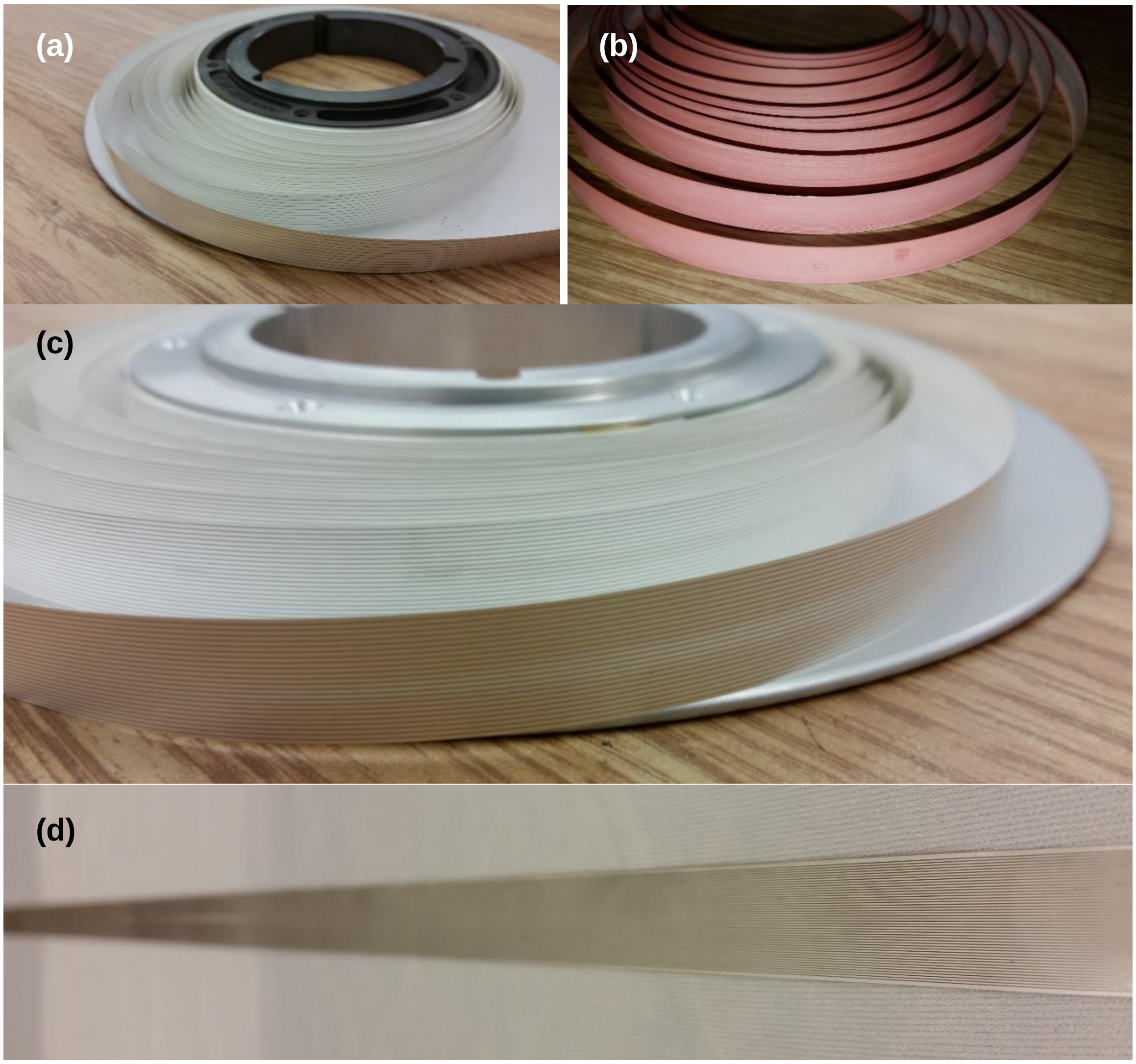

Figure 4-21 (a) 20 meters of a 12-filament tape (as striated), (b) 5 m of a 12-filament tape after Cu deposition, (c) 10 meters of a 24-filament tape and (d) a one meter of a 46-filament tape.

It can be clearly seen from the scan that the last filament (at y=-6 mm) has lower trapped field than the other filaments. This was actually due to the filament being narrower than the rest because of a small offset between the laser pattern and the tape's edge during the striation. The waviness seen in the plot is caused by a slight swing of the tape during the measurement. Measurement on the 24-filament tape were made also, however due to the lower signal from the narrower filaments and the noise level it not possible to distinguish the individual filaments on the reel-to-reel measurement.

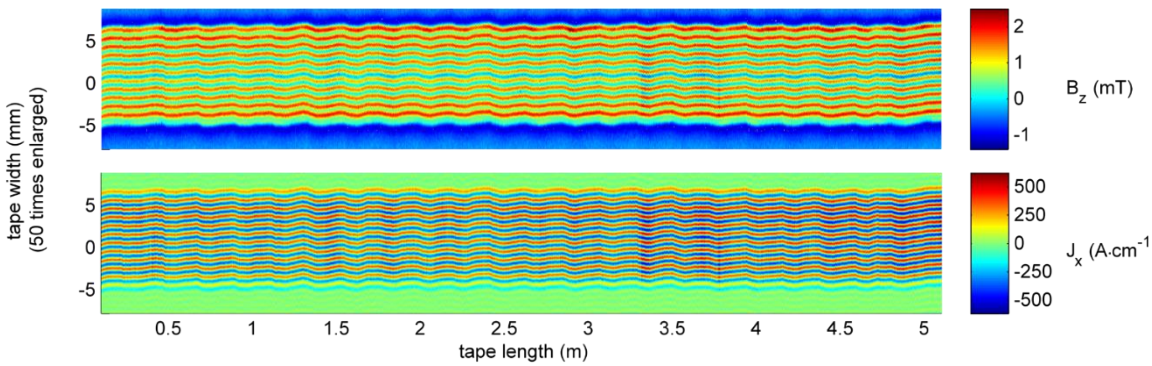

Figure 4-22 SHPM measurement of a 5 m section of a 12-filament tape. Both the measured field B_z and the calculated current density J_x (along the length of the tape width) are shown.

4.6. Filament-to-filament resistance

In order to characterize the striation quality and further investigate the possible coupling reasons, a measurement of the filament-to-to filament (F2F) transverse resistivity was carried on two 12-filament tapes; the first is a striated tape only oxidized and the second had an additional 25 μm of Cu electroplated on top. An example of the sample used in such measurement is shown in Figure 4-23. The average F2F resistance was 158.1 mΩ/cm for the Ag tape and 1.3 mΩ/cm for the Cu electroplated tape. The reason for such a big difference between the two tapes is that during the selective electroplating process, even though the center of the groove remains copper free, the copper grows also on the edge of the filaments (copper lateral growth shown in Figure 4-4) creating a second path for the current other than that through the buffer's oxides to reach the Hastelloy and then the next filament. Before electroplating, for the current to flow from one filament to another it has to pass from the superconductor through the buffer layers into the Hastelloy and then reach the other filament again through the buffer's oxides. For the Cu-electroplated samples, because of the copper lateral growth on the edge of the groove, there is a second path for the current to pass from one filament to the other, in parallel to the one through the buffer layers. The second path is from the superconducting layer to the silver, copper and then to the Hastelloy on the bottom of the groove. In fact, the groove that is initially 67 μm wide becomes only 20~25 μm wide after electroplating because of copper growth on the edges. This second current path explains such a drop in the F2F resistance after Cu-electroplating. It should be noted that for both paths, while the oxide layers have a very high resistivity (whether it is the buffer layers or the oxide layer at the bottom of the groove), their effective resistivity, considering the layers layout, is reduced by a factor t/w where t is the oxide layer thickness and w is the width of the contact area.

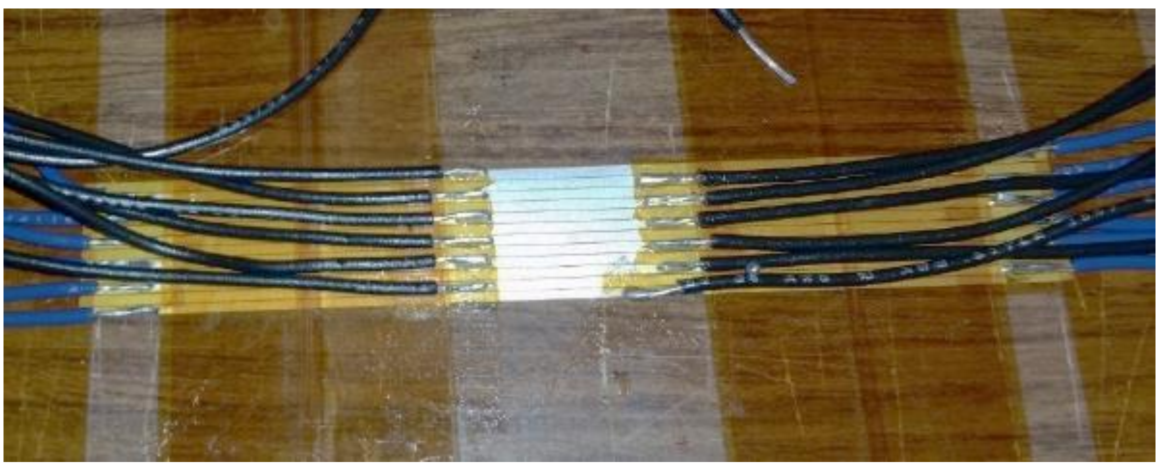

Figure 4-23 Example of F2F resistance measurement performed on a 12-filament sample, blue wires were used as current leads and black wires were used to monitor the voltage.

Figure 4-24 shows the results of the F2F resistance measurement for the two tapes. It shows that the values of the F2F resistance spreads over almost two orders of magnitude even for the tape before electroplating. This indicates that during the laser ablation some of the removed material is redeposited on the edges of the grooves. While the deep grooves guarantee a complete cut through the superconducting layer, the round smooth edges of these grooves create a less resistive path more favorable to coupling. This was further confirmed by EDX analysis of the groove across its width and the discovery of silver up to 15% at the edge of the grooves.

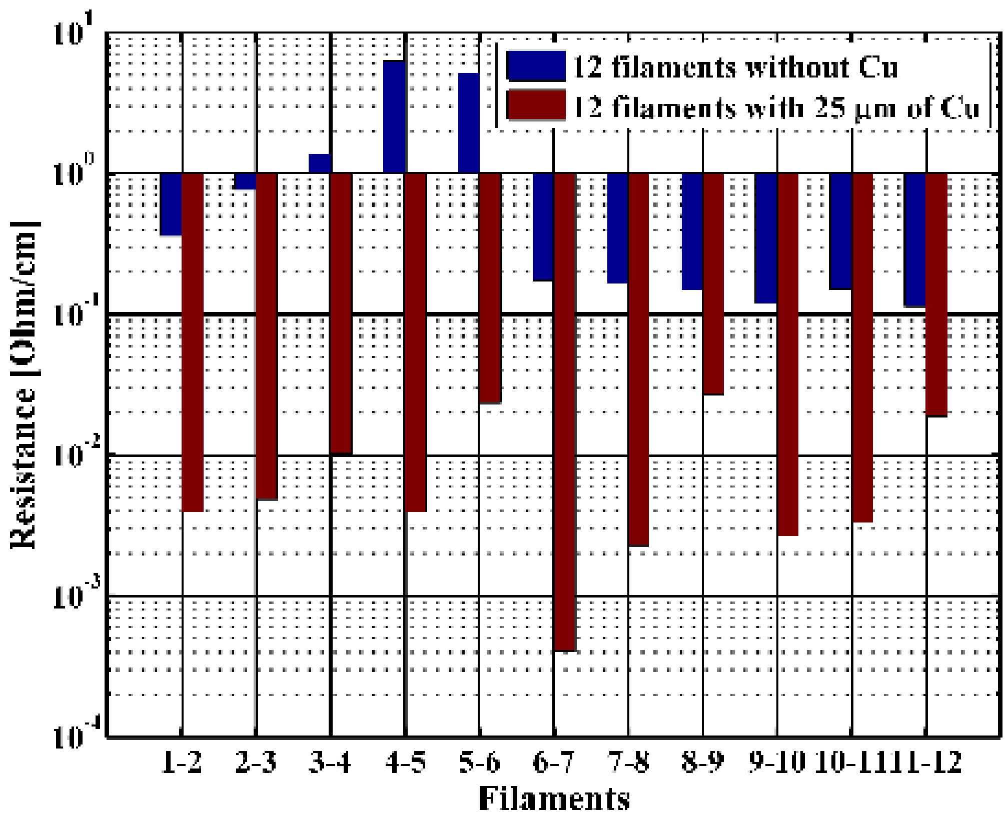

Figure 4-24 Filament-to-filament resistance for 12-filament tapes with and without copper stabilizer.

4.7. Filament transposition

Although expected AC losses reduction levels have been shown over short segments of multifilamentary tapes, the filament-to-filament resistance remains a finite value, and over long lengths, coupling losses will arise. And they need to be suppressed by transposing the filaments in order for this technique to remain effective in reducing AC losses over long lengths [101]. Some solutions based on tape cabling techniques [113, 165, 166] have been proposed to solve the coupling issue where the tape is bent and/or twisted to achieve the transposed configuration (A similar approach integrating the above presented striation process into helically wound REBCO STAR wires will be presented at the end of the chapter). Other solutions, based on a zig-zag pattern [167], have been proposed but this configuration imposes a reduction of the critical current just by geometrical considerations.

4.7.1. Concept and implementation

The pattern used to achieve the transposition is illustrated in Figure 4-25(a). Each single tape is made of four 3 mm wide filaments, comprised of a straight section from 5 to 10 cm long and a 5 cm area containing a transposition pattern consisting of “L-shaped” grooves. These tapes are set face-to-face and joined only at their edge filaments. The current flow in such a configuration is described in Figure 4-25(b).

In order to achieve this structure, the unconnected region of the transposition area is first coated with an Y_2O_3 insulating layer. A mask made with Kapton tapes covers the rest of the sample while overlap area is dip coated into a solution of YAc_3 in methanol and diethanolamine. The deposited layer is then cured at 400 ºC for 0.5 h in O_2 flow. Additionally, a thin silver layer is deposited on the connecting regions at the edge of the tape to compensate for the thickness difference. Silver-to-silver diffusion bonding was used to join the samples without the use of any soldering material. The tapes were held face to face with a pressure of ~ 15 MPa, heated and held at 500 ºC for 2 h in O_2 flow. The joint resistance for these samples was measured to be around 0.6 $\mu\Omega.cm^2$. The joint area is then reinforced with Kapton tape. Finally, the resulting joint was electroplated with copper in a beaker using a $Cu(NO_3)_2$ methanol-based solution.

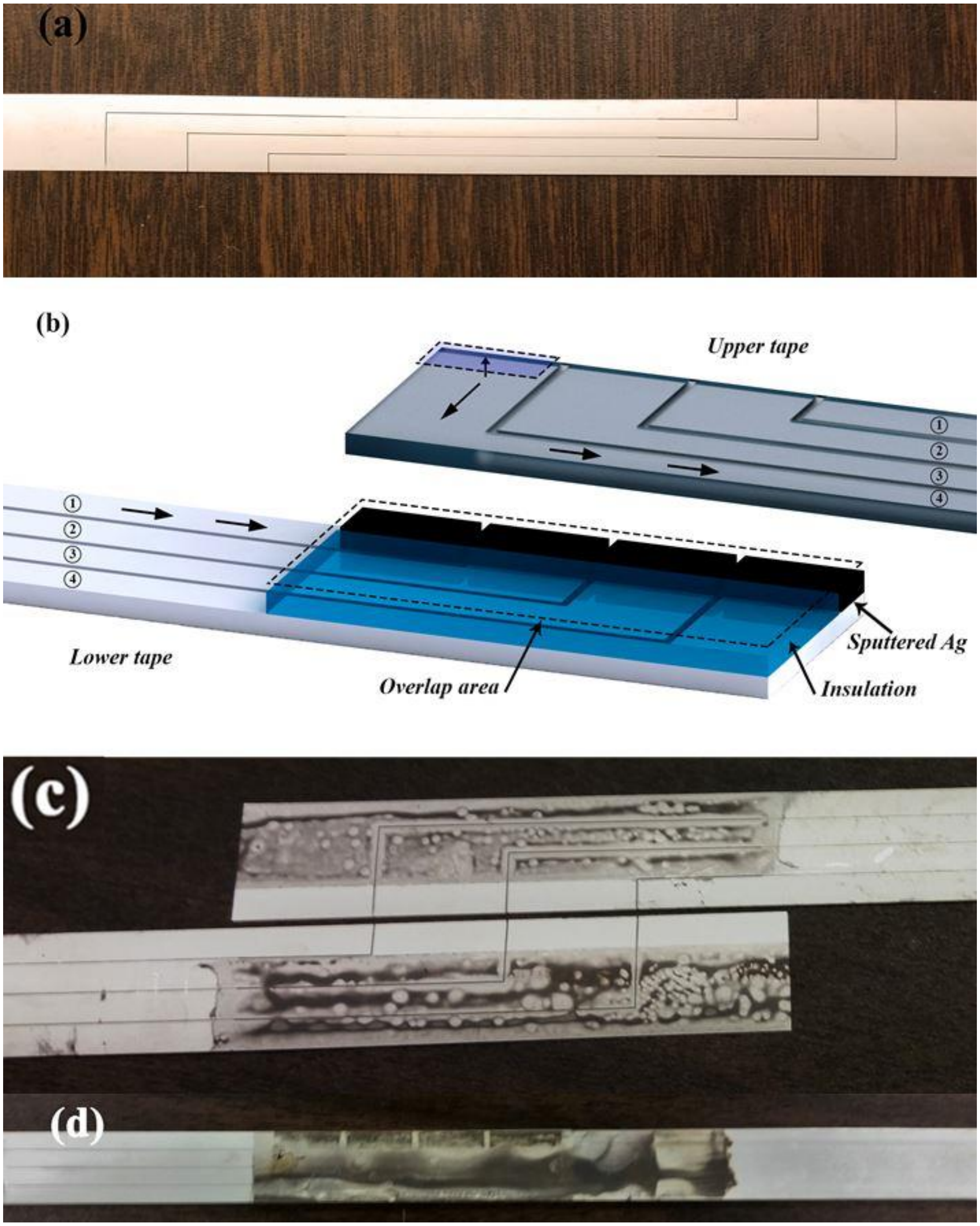

Figure 4-25 (a) Photograph of the tape used in the transposed configuration (b) Representation of the transposed multifilament tapes. (c) Photograph of the tapes before joining. (d) Photograph of the transposed tapes after joining.

4.7.2. AC losses of transposed samples

Transposed samples were made in this work using two 4-filament tapes each 10.5 cm long. The two tapes consisted of a 5 cm long area with the transposition pattern (shown in Figure 4-25) continued with 4 straight filaments on the remaining 5.5 cm resulting in a 16 cm sample with one transposition at its center. Two transposed samples were measured, T1 as described above and T2 coupled over 3 cm at both ends with 25 μm of copper. This was achieved by first sputtering a thin layer of silver on the ends to enable electroplating of copper. Sample T2 was made in such way to exclude the possibility that over the available sample measurement length, the F2F resistance could be high enough to prevent electrical coupling by itself alone, without the need for transposition. Additionally, two straight 4-filament samples were measured; S1 is a 4-filament sample coupled at both ends with copper similar to T2 and S2 is without any copper.

Figure 4-26 shows the results of the magnetization AC losses for these four samples. It can be seen that S1 behaves as fully coupled and its losses are similar to that of a non-striated tape. Sample S2, however, is in fully decoupled configuration showing a 4-fold reduction of AC losses at 50 and 100 Hz compared to a normal tape and exhibits the same behavior of the multifilament tapes discussed in the previous sections.

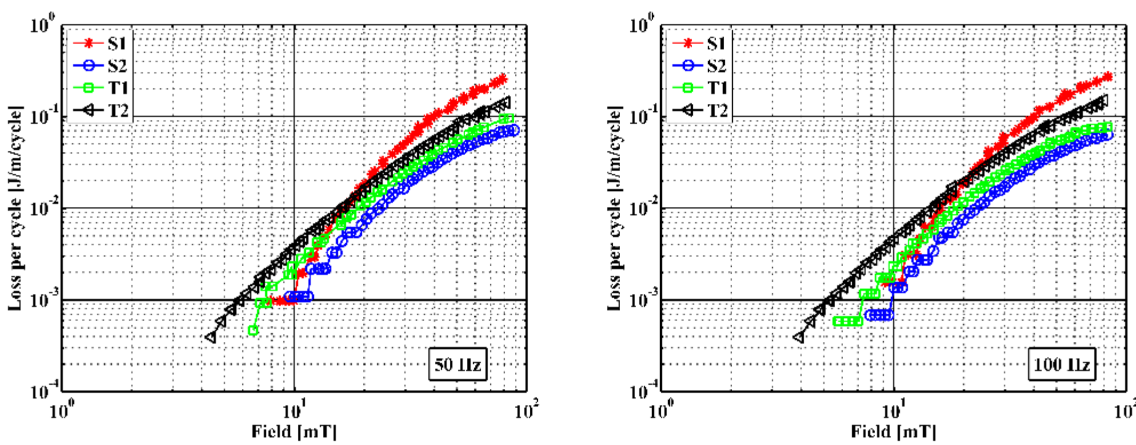

Figure 4-26 Magnetization ac losses vs applied field. S1 is a straight 4-filament tape with copper on both ends, S2 is a straight 4-filament tape without copper, T1 is a transposed sample without copper and T2 is transposed sample with copper on both ends.

Sample T1 shows ~25% higher loss than S2. This is due to the additional superconductor volume present in the overlap area. Besides, the frequency-independent behavior suggest that the sample is fully decoupled and the slight loss reduction at higher fields at 100 Hz is due to sample heating because the sample was not coated with copper. Sample T2, which was selectively electroplated with 25 μm of copper except for the both ends where the grooves were completely covered with copper (similar to S1) ensuring that the only mechanism allowing the decoupling of the filaments is the transposition. The measured loss is half of that of S1 but slightly higher than that of T1 with a frequency-dependent component. The possible reason for this is that the 3 cm area used to couple the filaments is longer than necessary, resulting in part of the sample behaving as a normal tape and generating significant additional losses.

It should be noted also that the results for samples T1 and T2 are in a qualitative agreement with AC losses of CORC cables wound using a single tape 12 mm wide and wound using three 4 mm tapes [166]. For low fields, the AC losses increase proportionally to the third power of the magnetic field amplitude followed by a linear dependence at higher fields. The observed crossover in the AC losses has been attributed to better screening abilities of the non-striated tape (in this case the fully coupled 4-filament tape behaving as a non-striated tape) in the low-field region.

4.8. Nano second laser striation

As mentioned in the beginning of this chapter, the main reason behind the choice of a femtosecond laser for the ablation was the absence of thermal heat conduction during the ablation process. This not only ensures that there no degradation in the REBCO layer properties, but also enables precision micromachining, which is crucial in achieving a good groove structure that will enable the selective electroplating process later on. In femtosecond ablation processes, the laser's pulses interact only with the electrons and thermal heat conduction is negligible (the lattice is heated on a picosecond time scale). So, the ablation process is essentially a direct solid-vapor (or solid-plasma) transition. However, in case of long laser pulses, the thermal wave to propagate into the target which can lead to melting and vaporization in the case of low intensity pulses [154, 168, 169] and to ionization, vaporization and shockwaves if the laser fluence is high enough [145, 147]. Although a detailed study of nanosecond ablation processes is beyond the scope of this dissertation, a brief discussion of some of the key process parameters will be presented along with the ablation strategy that will be used to achieve the same results previously obtained with the femtosecond laser. The main motivation behind this work is to reduce the striation process cost. While over the last few years high-power femtosecond lasers became more readily available and less expensive, they still represent a large investment and are the single component that makes the striation process quite expensive.

The first challenge in this process is the thermal effect on the REBCO layer. Oxygen out-diffusion causes the degradation of the REBCO layer superconducting properties way before melting can occur [136, 137]. So, the heat accumulation needs to be minimized to avoid the degradation of the tape's critical current. Once that condition is satisfied, the second challenge would lay in finding the right set of laser parameters (output power, repetition rate, marker speed, mark overlap and number of passes) that will result in the proper groove morphology, so that the selective electroplating part of the process remains possible. This is particularly difficult to control in nanosecond ablation not only because of the melting but also because of the melt ejection that happens during phase explosion [145-147].

The laser used in this work is capable of producing laser pulses ranging from 4 ns to 200 ns with a repetition rate ranging from 1.6 to 1000 kHz. The laser maximum output power is 20 W. Similar to the femtosecond laser, it is equipped with a scanning system allowing to cover a marking area of 10 by 10 cm. Also, a reel-to-reel motion system was installed along with the previously used vacuum stage and a vacuum suction to remove the fumes and particles resulting from the ablation process. A picture of the setup is shown in Figure 4-27.

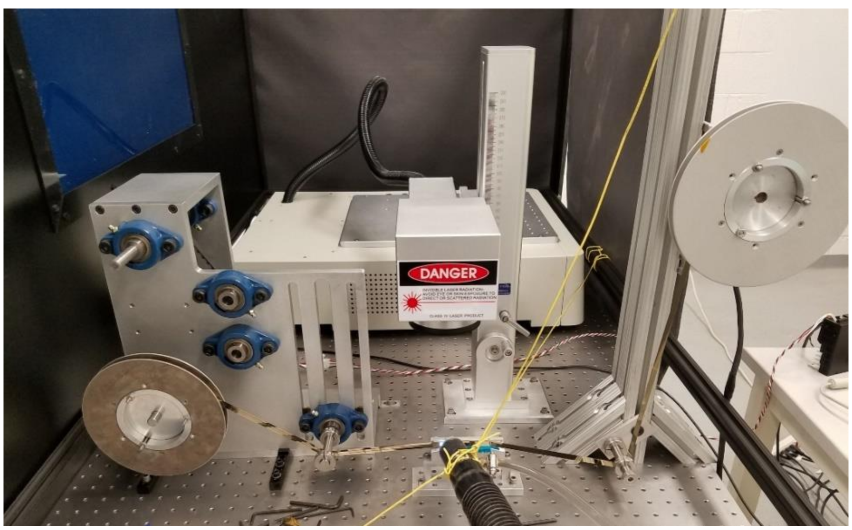

Figure 4-27 The reel-to-reel nanosecond laser striation setup.

The spot diameter for this laser is 50 µm (compared to the 30 µm of the previous laser). Based on Equation (4-1), the maximum laser marking speed can be determined by the desired spot overlap and the chosen repetition rate. Figure 4-28 shows the maximum laser marking speed to achieve a minimum of 70% spot overlap. While the laser scanner is rated by the manufacturer up to 7000 mm/s, during the tests, when the speed exceeded 3000 mm/s, the marking became inconsistent.

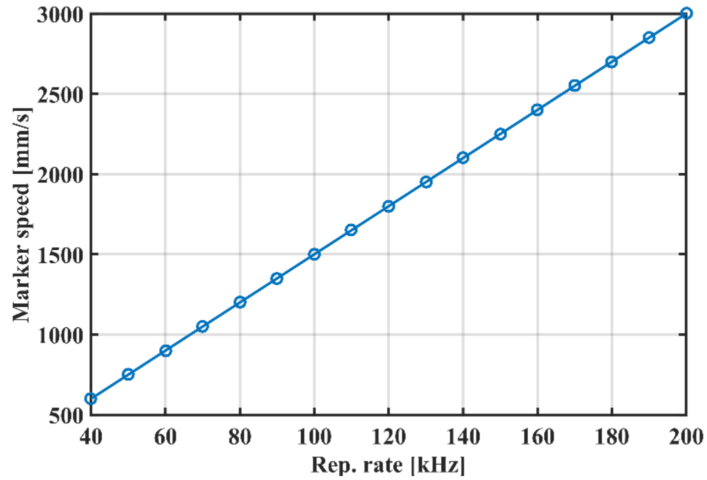

Figure 4-28 Maximum laser marking speed to achieve 70% spot overlap.

For the choice of the laser mode (the pulse width), the first observation about this particular laser is that the shortest pulse mode corresponds to the highest peak power density: 0.5 GW/cm^2 for 4 ns pulses and 0.127 GW/cm^2 for 200 ns pulses. The higher peak power is desirable for the plasma formation besides the shorter pulses should minimize the interaction between the plasma and the laser pulse [168]. The shortest pulses combined with a low repetition rate will reduce the duty cycle (percentage of time the target is subject to the laser pulses) thus reducing the heat accumulation. But, since the marker speed decreases in turn with the repetition rate, that is effectively equivalent to a lower average power (since to maintain the desired overlap, each unit area will have to experience a certain number of pulses). Furthermore, the output energies for each pulse width are given at the maximum repetition rate above which the energy per pulse will decrease gradually. Based on the above, the cutting strategy would be to use the shortest pulses and the maximum marker speed (since later on that will determine the speed of the reel-to-reel process) and reduce the output power gradually if there is any degradation to the REBCO layer properties. Preliminary tests showed that at maximum output power and a laser marking speed of 1 m/s or higher, there was no degradation in the tape's critical current and marking speeds less than 0.5 m/s at 90% output power caused I_c degradation from 8 to 36%. This suggests that the degradation of the REBCO is determined essentially by the output power and the marking speed. In a very simplified way, the heat accumulation in this particular process, could be viewed as the ratio of the average power to the marker speed (in units of J/cm). It is essential to keep in mind that the REBCO can sustain temperatures up to ~180 °C without I_c degradation by oxygen out diffusion. Even if the temperature exceeds that threshold, if it is only locally at the edge of the groove, confined within few micrometers, that effect on the tape's I_c will be very small. It could be compensated for by making a groove few micrometers narrower. To summarize, in order to use this nanosecond laser for the ablation process, the thermal effects were not eliminated but simply minimized so their effect on the REBCO layer properties is either negligible or acceptable from a practical point of view (as a compromise for using a much inexpensive laser than the femtosecond one).

Once the criteria to mitigate the thermal effect on the tape's I_c is established, the final choice of parameters will be based on the groove's morphology. The two main criteria remain the same as earlier with the femtosecond laser: sharp groove edges and a bottom surface as clean and flat as possible to avoid copper nucleation inside the grooves. Since it is possible to use any of the laser pulse width without lowering the tape's I_c, a test of the effect of the different pulse widths on the groove shape was conducted. 24 passes of a 3 mm long pattern (the same 4 lines, inside than outside, pattern as in section 4.3.2) were cut with each pulse width. Figure 4-29 shows optical images of the obtained grooves using 4, 8, 14 and 20 ns pulses.

With increasing pulse width, the redeposited material at the edge increases significantly. This is also visible from the depth profile scans shown in Figure 4-30. With increasing pulse width, there is an increasing amount of melt redeposition at the edge of the grooves. Besides, the higher energies of the longer pulses resulted in more spread of the ejected melt outside the grooves due to the stronger shock wave produced [147]. Also, it can be seen from Figure 4-30 that there is significant amount of material redeposited inside the grooves, making it very difficult to control the groove structure using the longer pulses at these energy levels. If the longer pulses had to be used, the output energy will have to be reduced to control the shape of the groove. Only the 4 ns pulse were “gentle enough” to produce a groove close to the desired U-shape.

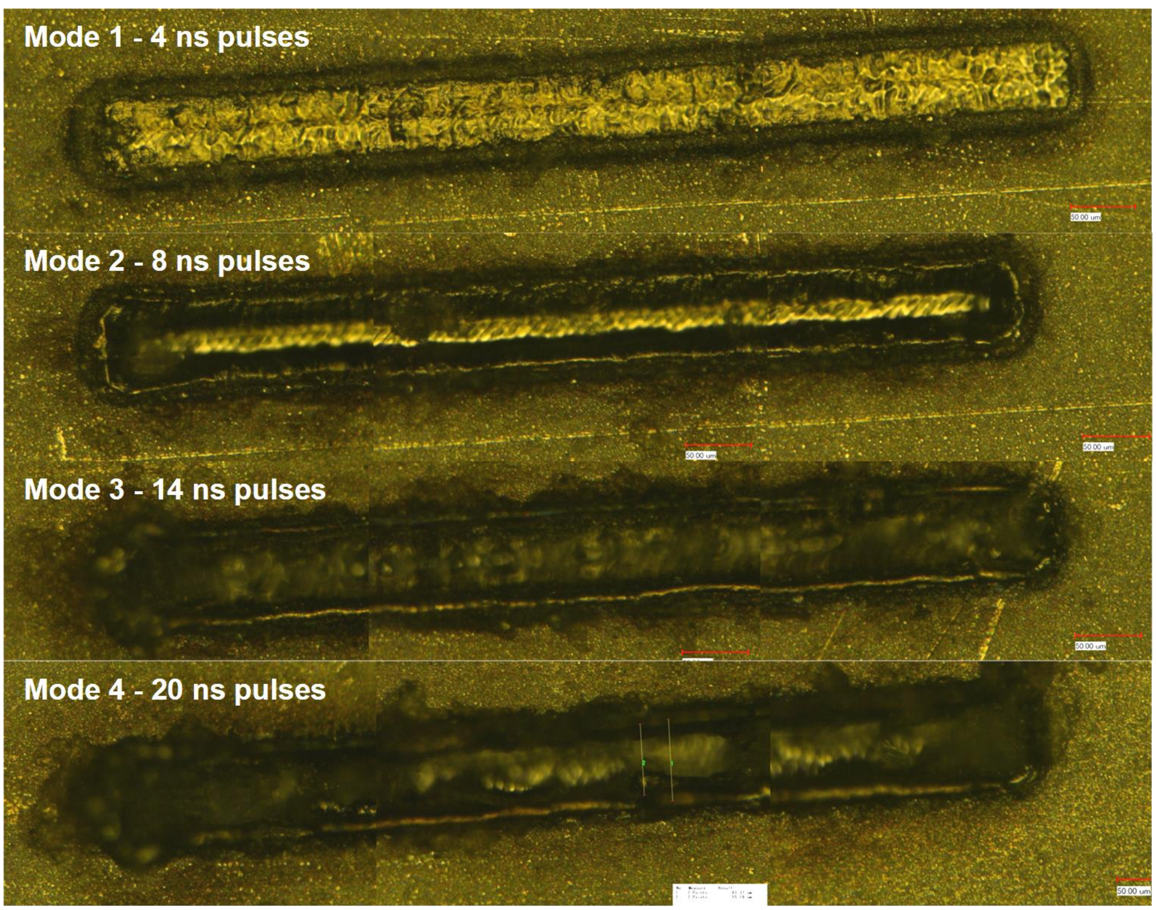

Figure 4-29 Optical images of grooves obtained using different pulse widths.

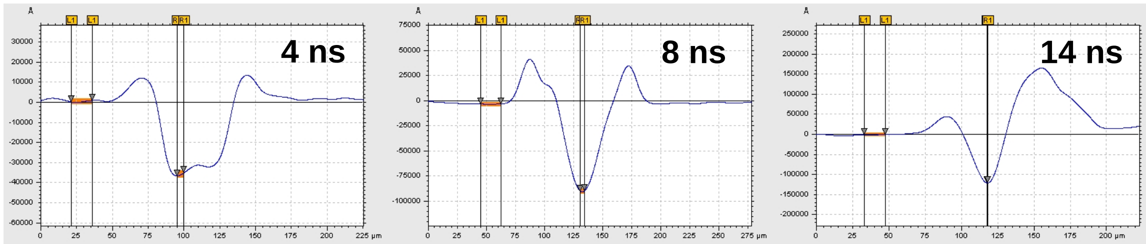

Figure 4-30 Depth profile along the groove's width.

Based on the previous results, mode 1, with 4 ns pulses, was selected and the ablation rate was determined as a function of the number of passes in a static test. Then, the average groove depth was determined by depth profile scans. The corresponding tape speed for reel-to-reel striation can be calculated from Equation (4-2). Table 4-1 summarizes the results of the test. The given tape speed corresponds to a single groove pattern. The tape speed for multiple grooves can be calculated as

$$\text{Speed} = \frac{\text{mark time of the single groove pattern}}{\text{mark time of the multiple grooves pattern}} * \text{Tape speed of the single groove.} \qquad (4\text{-}6)$$

Table 4-6 Ablation rate as function of the number of passes and corresponding tape speed for R2R striation.

Laser setting	Number of passes	Tape speed (mm/s)	Average depth (μm)
Mode 1, 200 kHz, 100% output power 2 m/s mark speed	12	10	3.56
	24	5	5.05
	36	3.33	5.8
	48	2.5	7.33
	72	1.67	9.27
	144	0.83	13.93

It should be noted that the ablation rate is much lower than earlier result with femtosecond laser. With the femtosecond laser, only 3 passes were enough to achieve 9.33 μm deep grooves while here it takes 72 passes. This is simply due to the fact that the ablation rate was reduced in favor of the more control of the final on the groove's shape. Figure 4-31 shows the depth profile of the nanosecond laser grooves in comparison with the femtosecond ones with similar depth. While the bottom surface of grooves is comparable, there is still a small amount of redeposited melted material at the edge of the groove about 1~2 µm thick.

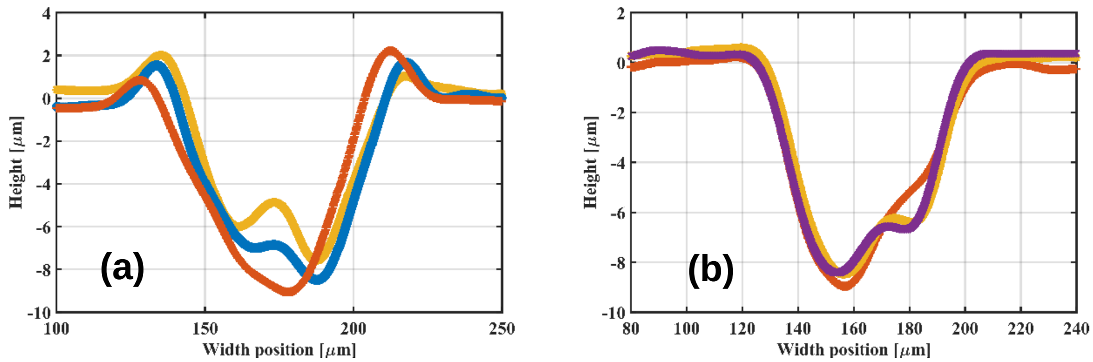

Figure 4-31 Depth profile of grooves made with (a) nanosecond laser and (b) femtosecond laser.

To compare the quality of this reel-to-reel process with the results obtained earlier using the femtosecond laser, five meters of 12-filament tape were striated using the nanosecond laser, annealed and electroplated with 25 µm of Cu (with back side shielding). The microstructure of the groove was examined by both optical microscope and SEM, shown in Figure 4-32. In term of selective electroplating, the obtained grooves were remarkably copper free, even more than previously. This can be explained by two features of the nanosecond ablation, both related to the presence of a melt layer. First, the bump present at the edge of the groove (Figure 4-31(a)) acts a preferred nucleation site for Cu (E-field concentration caused by the bump) causing an accelerated ion depletion inside the grooves, thus reducing the chances of Cu particles nucleating inside the grooves. The second feature which is visible in Figure 4-32 (c) and (d) is related to the smoothness of the groove's bottom surface. The fine ripple features observed in section 4.3, typical of femtosecond pulses ablation [146], are completely erased in the case of nanosecond pulses. And this smoothed groove surface seems to be less prone to Cu nucleation at the bottom of the groove. It should be noted that occasionally Cu particles were found inside the grooves, but even then, they seemed to nucleate on the copper at the edge of the filament and not in the bottom of the groove.

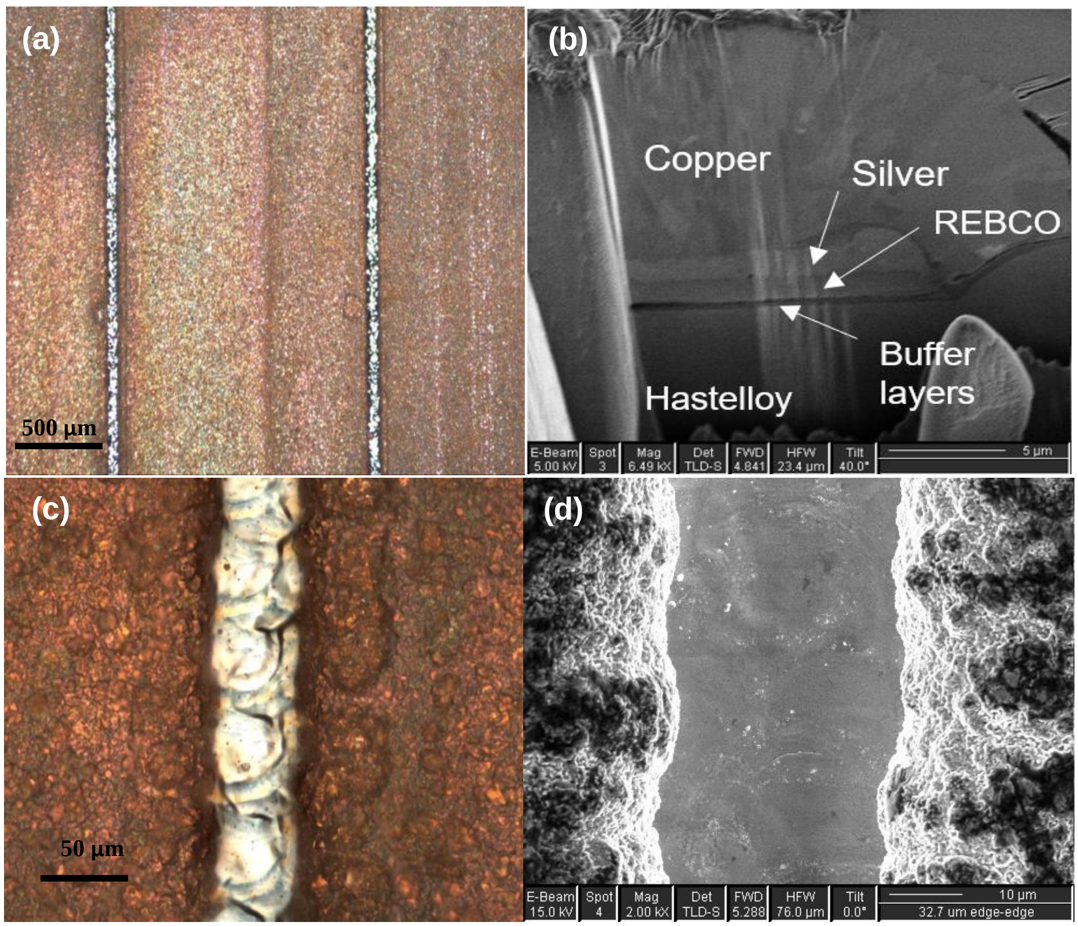

Figure 4-32 (a) Optical microscope image of the nanosecond laser striation after Cu EP, (b) FIB/SEM cross section of the edge of the groove, (c) optical image at higher magnification of the groove and (d) similar higher magnification using SEM.

To evaluate the effect of the process of the tape critical current, SHPM measurement was performed on the 5 m tape. Figure 4-33 shows the 2D maps of the measured trapped field and corresponding current density. The calculated I_c from the SHPM data is shown in Figure 4-34. The data was calibrated by performing transport critical current measurement on pieces from the start and the end of the tape. The original tape I_c was 380 A, and the I_c after the striation was not lower than 340 A. The degradation level of ~10.5% is not much more than what was previously obtained with the femtosecond laser.

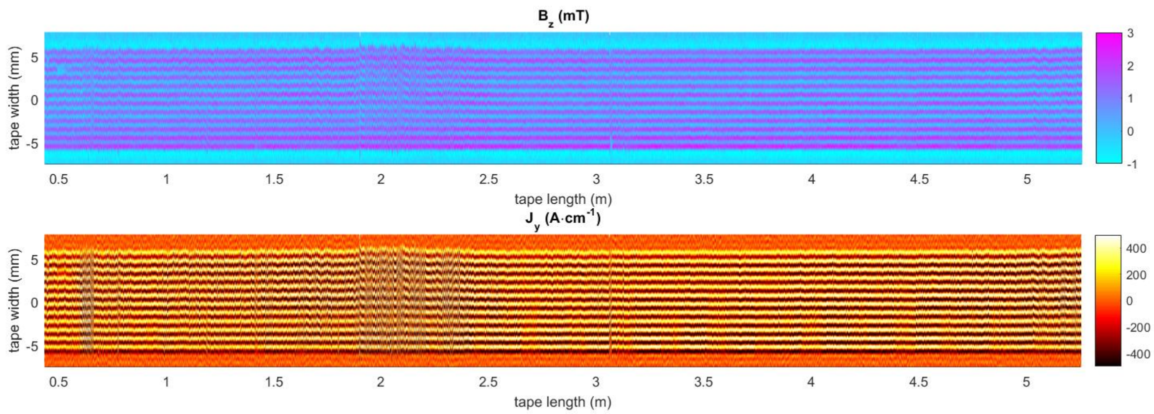

Figure 4-33 SHPM measurement on a 5 m section of a 12-filament tape made using the nanosecond laser.

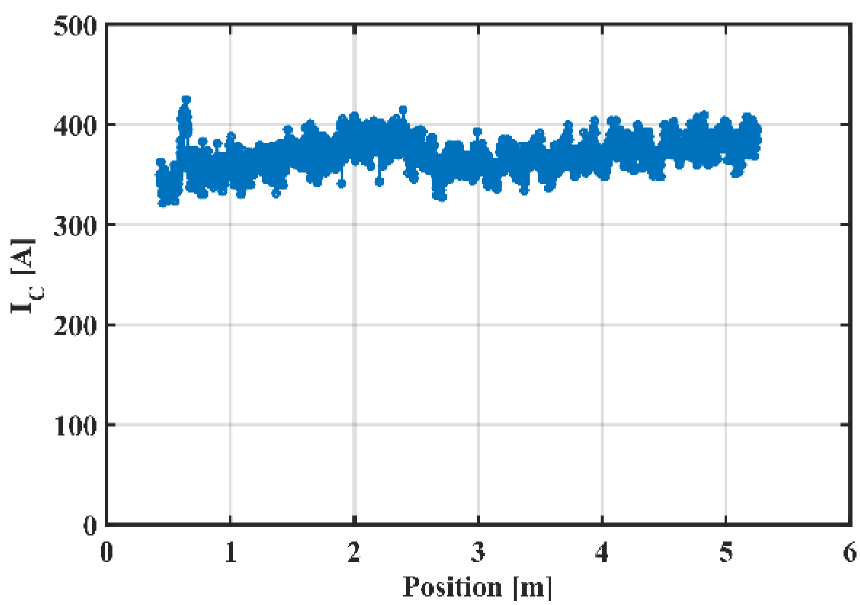

Figure 4-34 Calculated tape I_c from the SHPM data.

Finally, the AC losses were measured on pieces from both ends and compared to the tape before the striation. The obtained loss reduction ratios are similar to those of the femtosecond laser striation process (obtained in Section 4.5.4). A small frequency dependence is also present but to a lesser extent than previously. That is most likely due to the better selective electroplating obtained in this case because of the smoother grooves.

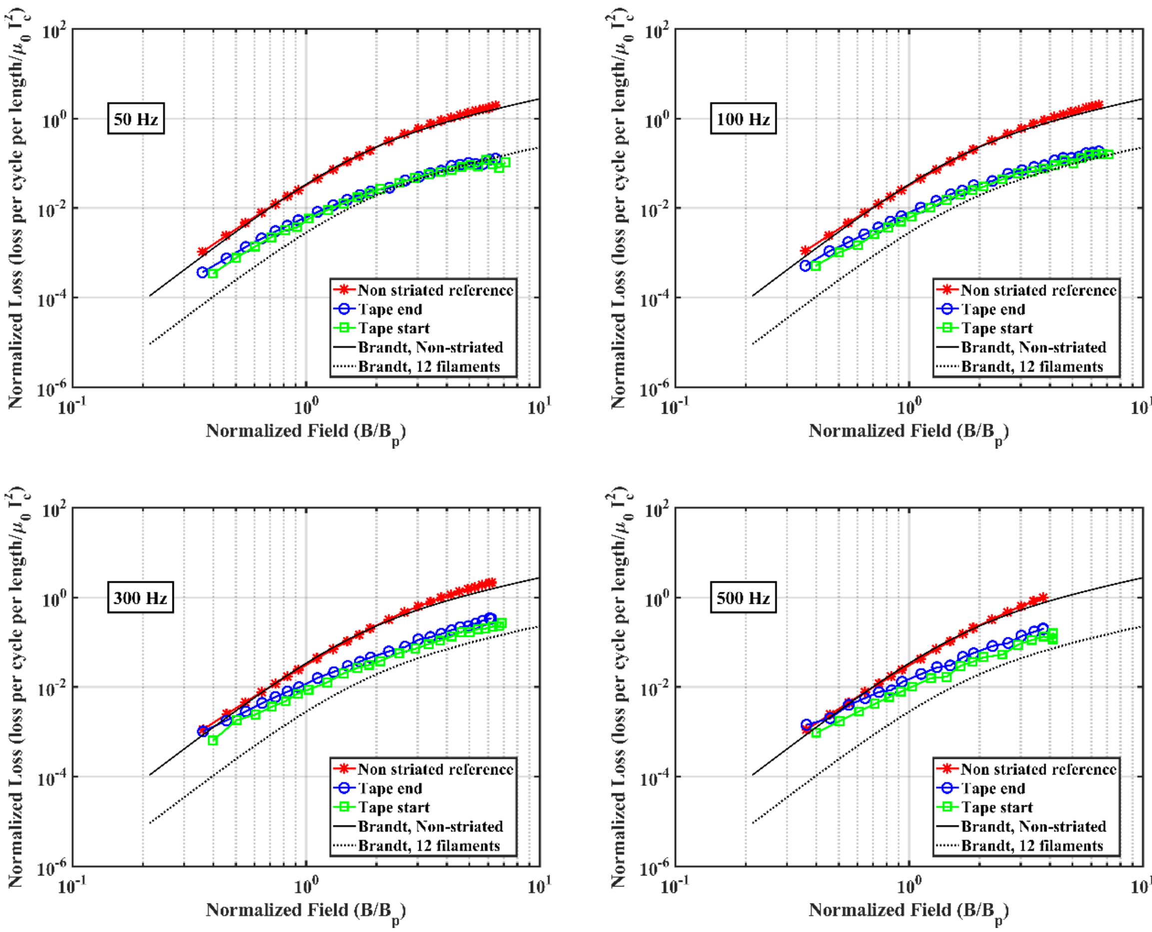

Figure 4-35 Normalized magnetization ac losses for the 12-filament tape (made using the nanosecond laser) after copper electroplating measured at frequencies of 50, 100, 300 and 500 Hz.

To summarize, in this section an approach to striate REBCO tapes using a nanosecond laser has been presented. Once the thermal effects on the REBCO layer were mitigated, the laser parameters were adjusted to achieve the desired groove structure. The process speed (ablation rate) was sacrificed in favor of more control on the groove microstructure. The presence of a melt layer in nanosecond laser ablation had a beneficial side effect. The grooves surface was smoother resulting in less copper particles growing inside the grooves during the selective electroplating, which resulted in AC loss reduction levels not only equal but slightly better than that obtained with the femtosecond laser (albeit with a much slower process).

4.9. AC losses reduction in multifilamentary REBCO STAR wires

The transposition pattern proposed in Section 4.7 shows the necessity and the effectiveness of filament transposition in AC loss reduction. However, its implementation in a larger scale is rather challenging, since it involves multiple heat treatments and processes such as diffusion bonding which are hard to scale for a reel-to-reel production. Another way to address coupling losses over long length is to use tape cabling techniques to achieves the transposition. Aside from AC losses, multistrand cables are used for high field, low inductance magnets. Most of the cabling scheme aim at: first making a high current cable, then addressing other practical issue such as the conductor's anisotropy or the high aspect ratio of coated conductors. However, there are certain practical limits on the strand size usually based on the cable type and the cabling process, resulting generally in a strand size in the range of 2 to 4 mm. If the filamentization process is incorporated in these cabling concepts, the benefits of the striation will be maximized since all of them offer strand transposition by design. The filamentization will allow to overcome the practical strand size limit imposed by cabling processes and further decrease the AC losses in such cables.

A particular geometry of interest is that of helically-wound REBCO wires such as the STAR wire, where the extremely short twist pitches of the various layers in these wires will be very effective in preventing the filaments coupling over a wide range of frequencies and AC fields. However, this particular type of wire (or cable) comes with an additional challenge - maintaining a high enough I_c retention at small bend diameters. The high I_c retention of the tapes used in the STAR wire is based on the use of thin substrate tapes combined with a single-sided optimal stabilizer thickness on REBCO side only.

The effect of the filamentization on the tape bending properties was first investigated. Then, the grooves structure was optimized in order to maximize the I_c retention at small bend diameter. Finally, ultra-small diameter REBCO STAR wires with 2 and 4 filaments per tape were made and their AC losses measured.

4.9.1. Bending performance of multifilamentary thin tapes

The striation in the following was performed on 2 mm wide, 18 μm thick substrate tapes using the nanosecond laser. The striation was done reel-to-reel using the same process parameters presented in Table 4-6 except for the output power which was lowered to 50%. The reason behind that is the tendency of the 18 μm substrate tape to curl along its width after making a single groove at 100% output power because of the thermal effects present during nanosecond laser ablation. The output power has to be lower to maintain the flatness of the tape. In fact, this effect is always present in the nanosecond striation but its intensity depends on the substrate thickness and the filament width. Earlier, on a 50 μm substrate and with 1 mm wide filaments, the effect is negligible. On the 18 μm substrate tape, even with 50% output power, the curl along the width becomes significant if the filament size is smaller 0.5 mm. Figure 4-36 shows the result of the laser ablation on such tapes when the filament size is reduced down to 0.125 mm. The curvature that’s created with higher number of filaments makes 2 mm wide tapes with more than 4 filaments not suitable for use in the STAR wire. While it might be possible to further reduce the output power to maintain the tape's flatness with the smaller filaments, this work was limited to 0.5 mm and 1 mm wide filaments corresponding to 4 and 2 filaments per 2 mm tape.

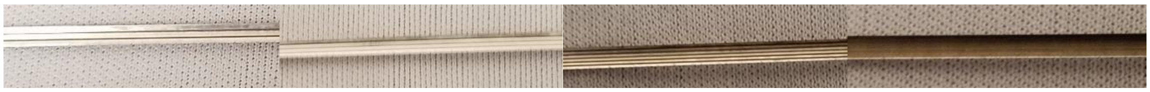

Figure 4-36 18 µm substrate tape with various number of filaments. From left to right 3, 4, 6 and 16 filaments on a 2 mm wide tape.

The I_c dependence on the bend diameter was measured on a 2 mm wide, 2-filament tape (with the REBCO layer being in compression). The result, shown in Figure 4-37, is for an 18 µm substrate tape selectively electroplated with 25 µm of copper on the REBCO side only. The result shows a different behavior from what was reported earlier in Chapter 3. First, the results obtained earlier showed that for the single sided Cu electroplated tapes, the I_c retention remained constant around 95% of the flat I_c and once the degradation starts there is a rapid and sharp drop in the I_c retention. However, in the case of the multifilamentary tape there a slow and gradual drop of the I_c with reduced bend diameter, from 88% at 3.2 mm bend diameter to 33% at 0.5 mm bend diameter with a near linear trend. Besides, an 18 µm substrate tape electroplated with 25 µm of copper on the REBCO side should, based on the results from Chapter 3, have ~75% Ic retention at 1.1 mm bend diameter. This different behavior is most likely due to the laser ablation exposing the REBCO layer at the edge of the filaments and since the copper grows only on top of the filament, this makes the REBCO layer more prone to delamination and cracks. Thus, the poor bending performance at small diameter and the discrepancy with calculations (delamination invalidates the first assumptions of the model which is the continuity of the strain throughout the tape's cross section).

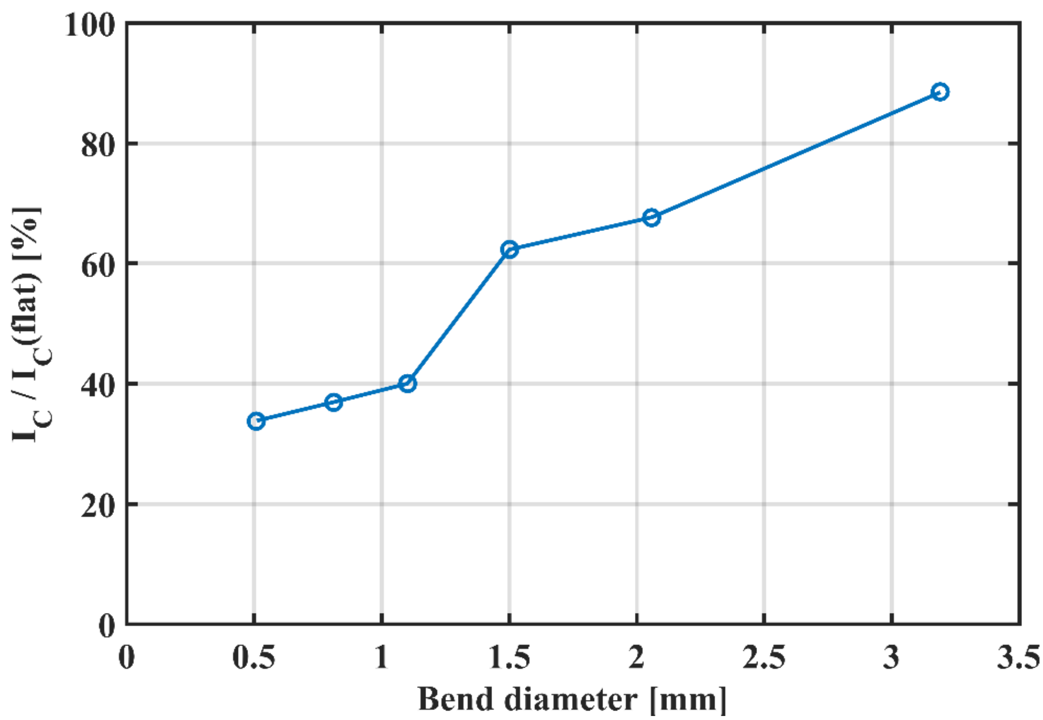

Figure 4-37 I_c retention as a function of the bend diameter for a 2 mm wide, 2 filaments (18 µm substrate) tape made with selective EP

To address this issue and improve the I_c retention of the multifilamentary tapes at small bend diameters, it is possible to cover the edge of the filaments with some material to prevent the delamination. A natural choice would be to use silver for various reasons: first it is already used to cover the outer edges of the entire tape and second it has a good adhesion strength with the electroplated copper. Covering the grooves with high conductivity materials like silver and copper might seem contradictory with all work presented to make the low AC loss, selectively electroplated, tapes. But, in the case of the STAR wires, the short twist pitch of the helical winding, shown in Figure 4-38, will minimize the coupling losses over a much broader range of fields and frequencies compared to a straight untwisted tape where without selective electroplating coupling losses will erase any AC losses reduction achieved by the striation.

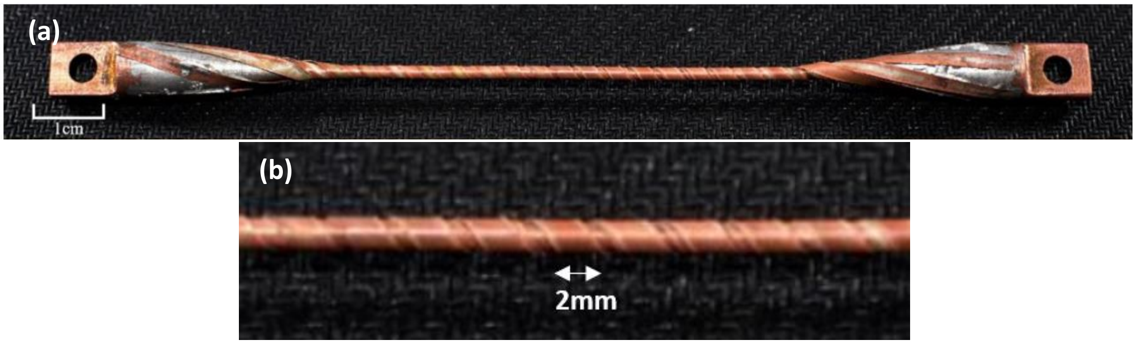

Figure 4-38 (a) A picture of a 6-layer STAR wire wound on 0.8 mm Cu former, (b) a magnified image showing the short twist pitch.

The coupling power loss per unit volume for a multifilamentary tape is given by [101]

$$P_c = \frac{1}{4\rho_{\perp}}(fLB_a)^2, \tag{4-7}$$

where f is applied field frequency, B_a is the peak magnetic field intensity, L the twist pitch and

$$\rho_{\perp} = \rho_b\left[\frac{(n-1)w_{gr}}{(n-1)w_{gr} + nw_f}\right], \tag{4-8}$$

where n is the number of filaments, w_{gr} is the width of the groove, w_f is the width of the filament and ρ_b is the inter-filament resistivity barrier.

Equation (4-7) shows two possible ways to decrease the coupling losses: increase the inter-filament resistance barrier or decrease the twist pitch. In fact, the twist pitch has bigger effect on the coupling since the coupling losses are proportional to the square of the twist pitch while only linearly proportional to the inter-filament resistance. So, it is possible, if the twist pitch is small enough, to achieve the desired AC loss reduction and maintain the benefit of the striation even though the grooves are covered with silver and copper. Besides, reducing AC losses should not be at the expense of critical current. A compromise between I_c retention and AC loss reduction need to be determined. The final evaluation of the benefit of the striation will strongly depend on a specific application frequency and field amplitudes.

When the applied external field amplitude B_a is much larger than B_p (B_p is the penetration field), the hysteretic loss per unit volume can be given by [101]

$$P_h = \frac{2}{\pi} f w_f J_c B_a. \tag{4-9}$$

So, as long as the additional coupling losses remain small compared to the hysteretic losses (which is proportional to the I_c) or at a maximum become equal, the benefit of the striation can be maintained. Figure 4-39 shows an example of the dependence of the calculated hysteretic and coupling losses on the inter-filament resistance value, based on Equations (4-7) and (4-9), for a 2 mm wide tape with 2 filaments with a critical current density of 2 MA/cm^2 and a twist pitch of 2.5 mm. Although, these calculations are based on the filaments being instantly twisted and does not account for the special variation of the between the field and the tape caused by the helical winding, they represent the extreme case (highest loss) where the tape is always subject to a perpendicular field. The actual losses in the wire should be less.

To determine the I_c retention of multifilamentary tapes stabilized without selective electroplating, a series of 18 μm thick, 2 mm wide substrate tapes, was striated into two filaments with variable groove depths. The average groove depth of the samples was 4.2

µm for S1, 6.1 µm for S2, 6.9 µm for S3, 9 µm for S4 and 13 µm for S5. The samples were then sputtered with ~2 µm Ag, annealed in O_2 flow for 0.5 h at 500 °C, then electroplated with 25 µm of copper on the REBCO side

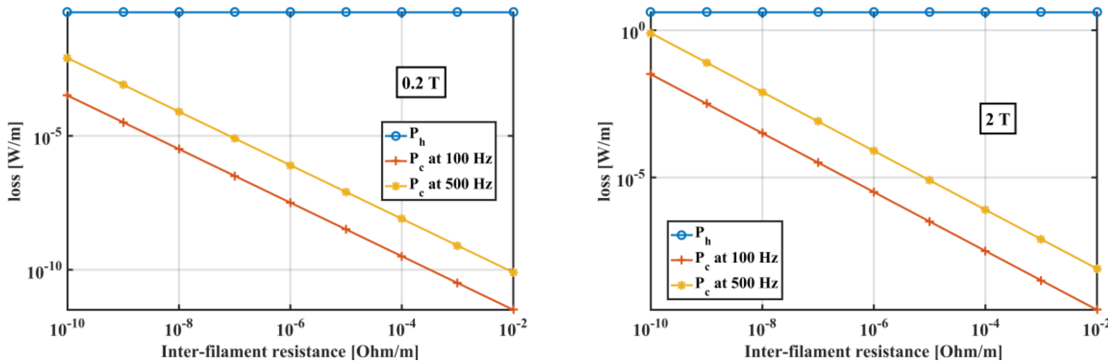

Figure 4-39 Hysteretic and coupling losses calculated for a 2 mm 2 filament tape assuming a twist pitch of 2.5 mm at various peak fields and frequencies.

To evaluate the bending performance of these structures, the I_c dependence on the bend diameter was measured by helically winding a single turn on cylindrical formers ranging from 12.5 to 0.8 mm in diameter. Results in Figure 4-40 shows indeed a significant improvement of the I_c retention with above 80% retention up to 1.1 mm bend diameter. Besides, the typical dependence of the I_c retention on the bend diameter of REBCO CC described earlier and observed also in Chapter 3 is seen here. The sputtered silver after the striation creates a layer first covering the filaments' edges and the grooves uniformly and then allowing the electroplated copper to adhere properly to the entire tape surface.The dependence of the I_c retention of the groove depth showed the best values for S4 corresponding to a groove depth of 9 µm. That is the same value selected earlier for the striation with selective electroplating.

To further investigate the effectiveness of this approach in maintaining a good I_c retention at small bend diameter with smaller filament size, similar samples (2 mm wide, 18 μm substrate tapes with 25 μm Cu) were prepared with 2, 3 and 4 filaments. The bending results, shown in Figure 4-41, do not show a clear trend with decreasing filament size. All the samples showed a high I_c retention (more than 80% of the flat I_c) up to 1.1 mm bend diameter and then a sharp drop. However, the samples with finer filaments retained higher I_c after the drop with I_c retention around 60% for the 3- and 4-filament samples compared to the 30% of the 2-filament sample.

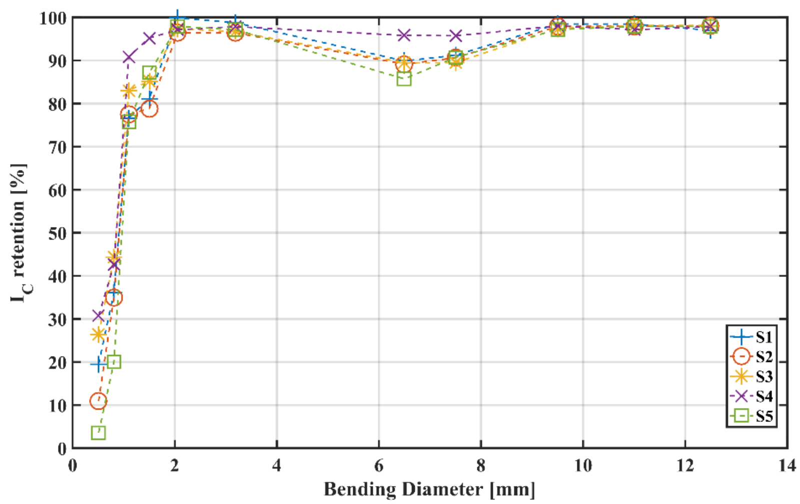

Figure 4-40 I_c retention as a function of the bend diameter for a 2 mm wide, 2-filament (18 μm substrate) tapes made without selective EP with various groove depths.

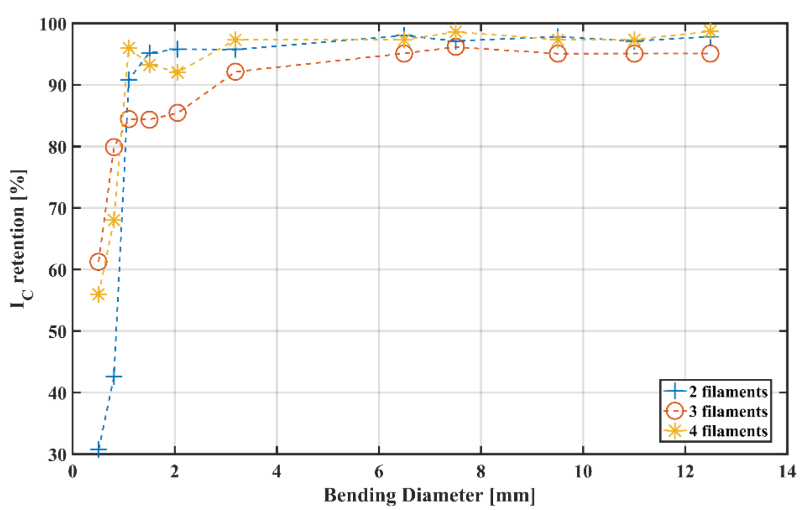

Figure 4-41 I_c retention as a function of the bend diameter for a 2 mm wide (18 μm thick substrate) tape with 2, 3 and 4 filaments made without selective EP.

4.9.2. STAR wires AC losses measurements

Using the results obtained in the last section, three STAR wires were prepared. Each was made of 6 layers of 2 mm wide tapes: the first with non-striated tapes, the second with tapes having two filaments and the third with 4 filaments. The Cu former used had a diameter of 0.8 mm. The critical current was measured to be 189, 179 and 172 A respectively for the wires made of non-striated, 2 and 4-filament tapes. The wires were all reinforced with shrink tubes so that after the critical current measurement, the central part could be cut and used for AC loss measurements without the layers unwinding. The magnetization AC losses were measured using the pick-up method on 3 cm long pieces.

The measured magnetization AC losses for the three wires are shown in Figure 4-42, along with the loss measured for a 12 mm wide non-striated tape and one with 12 filaments. The STAR wires showed up to 30X lower AC losses than a normal tape with 1 mm wide filaments and up to 55X lower losses with 0.5 mm wide filaments. These levels of AC losses reduction suggest that the filaments are indeed fully decoupled in our measurement range. This is in agreement with what was discussed earlier based on Equations (4-7) and (4-9). The results in Figure 4-42 represent the loss per cycle in J/m/cycle. Unlike the previous results where the loss was normalized by the I_c, the results here cannot be normalized in the same way. The previous results on losses in a flat tape were based on the expression of pure hysteretic losses in a perpendicular magnetic field while the tape in the STAR wires experience all field orientations within a single twist pitch length. The AC losses of the 12 mm tape both non-striated and with 12 filaments are presented to serve as a baseline for the order-of-magnitude of losses for the same total tape width.

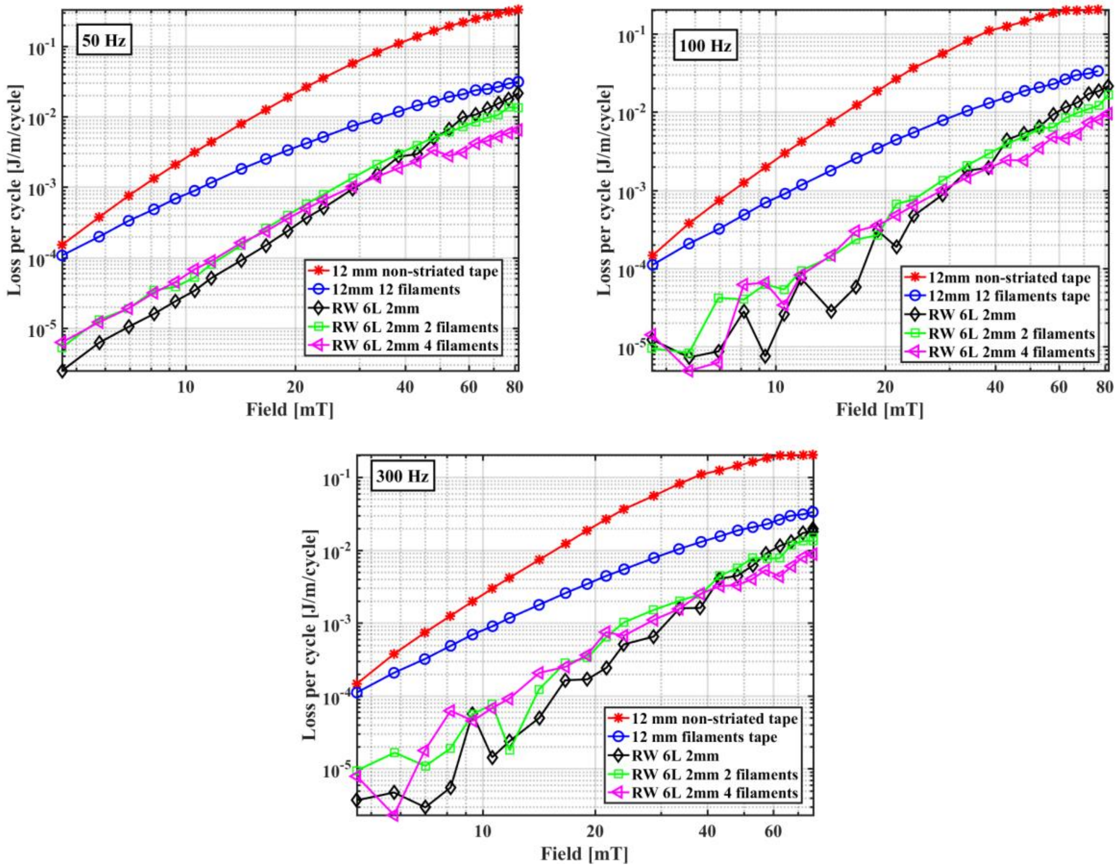

Figure 4-42 Magnetization AC losses of the 6-layer STAR wires with various number of filaments compared with losses of non-striated and 12-filament flat tapes

The three wires exhibit two distinct behavior at the low and the high-field regions. At low fields, the wire made with the larger filaments had low losses. That's due to the fact that the wider tapes have better screening capabilities at low fields. In the high field region, the behavior is reversed. Besides, the linear dependence of the loss, for three wires, on the applied field, suggest that tapes are fully penetrated [84]. The loss of the wire made with 2-filament tapes was 1.8 times lower than that made with non-striated tapes and that of the wire made with 4-filament tapes was 3.7 times lower.

4.10. Conclusion

In this chapter, a laser striation method followed by selective electroplating of copper have been used to fabricate long lengths of fully-stabilized multifilamentary REBCO tapes with various number of filaments. The striation was achieved using two different lasers: a femtosecond and a nanosecond one. The AC losses of reel-to-reel-produced multifilamentary tapes were significantly reduced by adjusting the copper electroplating shield to prevent Cu growth on the back side of the tape.

To address the coupling losses overlong length, a transposition pattern was proposed and implemented. Finally, the striation process was adjusted to allow the integration of the multifilamentary tapes into the ultra-small diameter, helically-wound, STAR wires. STAR wires with various number of filaments per tape were fabricated and their AC losses characterized.

CHAPTER 5. Conclusions

In this dissertation, REBCO CC flexibility and AC losses problems were studied and methods to address those challenges were developed with the ultimate goal of producing highly flexible, low AC losses REBCO tapes and wires. To achieve such result, initially, an analytical model based on beam theory was developed to assess the bending behavior of REBCO CC. The model accounts for the progressive plastic deformations occurring in the various layers during the bending. The calculation results showed that by using an optimized Cu thickness on the REBCO side only, significant reduction in the strains in the REBCO layer could be achieved at small bend diameter. Such reduction is due to the shift of the neutral axis position closer to the REBCO layer. The validity of the calculation results was confirmed by measuring the I_c retention for a series of 50 and 30 μm substrate tapes with various Cu thicknesses. The scaling of the critical current retention as a function of the strain in the REBCO layer confirmed that difference in bending performance is due to the differences in neutral axis location between the various configurations. The validity of the model predictions was also evaluated against the experimentally-determined optimal Cu thickness corresponding to ~75% I_c retention on thinner substrate tapes and the results were found to be in good agreement. Finally, the model predictions were used to provide an optimized design aiming at maximizing the J_e of helically wound ultra-small diameter STAR wires. The calculations showed that a better layout could be achieved if the copper thickness is decreased gradually with increasing layer.

In a second stage, an alternative tape architecture allowing to build highly flexible REBCO wires with high J_e was proposed and investigated. Following the same principle of placing the REBCO layer in a more mechanically favorable location closer to the neutral axis, but instead of tuning the stabilizer thickness to achieve such result, the alternate architecture is based on two tapes joined face-to-face thus placing the two REBCO layers of the resulting structure closer to the neutral axis. Initial calculation results showed that in such a symmetric structure, the improvement of bending properties is independent of the substrate thickness of the original tapes and depends only on the thickness of the interlayer separating the REBCO layers from the interface and on their strain limits. In the case where the REBCO layer has different tensile and compressive strain limits, an offset between the two substrate thicknesses allows the shift of the neutral axis of the structure toward the tape with the lower strain limit. During the bending, both layers will reach their maximum allowable strain at the same bend diameter, thus, maximizing the bending performance of these structures. Finally, two methods to make such structures were implemented and tested: diffusion bonding and soldering. The obtained results showed the potential of such tape structure in enhancing the mechanical properties of REBCO CC regardless of the substrate thickness, given enough control on the thickness and homogeneity of the interlayer between the two tapes.

To address the AC losses in REBCO CC, a laser striation method followed by selective electroplating of copper has been used to fabricate long lengths of fully-stabilized multifilamentary REBCO tapes with various number of filaments. The striation was achieved using two different lasers: a femtosecond and a nanosecond one. While the absence of thermal effects during femtosecond ablation allowed to achieve high striation speeds, minimizing their effects during nanosecond ablation was the limiting factor for the process speed. Using optimal parameters, striation using both lasers did not cause I_c

degradation beyond what is expected from the removed superconducting volume. Investigation of the striated tapes by SHPM techniques showed that defects and non-uniformities in the original tape critical current density were the causes of additional I_c degradation, if any. Besides, regardless of the type of laser used, a certain groove shape was found to be crucial to enable the subsequent selective electroplating. The investigation of the filament-to-filament resistance showed that the most significant coupling was caused by Cu layer on the back side of the tape. AC losses of reel-to-reel produced multifilamentary tapes were significantly reduced by adjusting the copper electroplating shield to prevent Cu growth on the back side of the tape. To address coupling losses overlong length, a new transposition pattern was developed and implemented, allowing to transpose the filaments and thus significantly reducing the AC losses. Finally, the striation process was modified to allow the integration of the multifilamentary tapes into the ultra-small diameter, helically-wound, STAR wires. STAR wires with various number of filaments per tape were fabricated and their AC losses characterized. The STAR wires showed up to 30X lower AC losses than an equivalent non-striated tape with 1 mm wide filaments and up to 55X lower losses with 0.5 mm wide filaments.

5.1. Future studies

Following the results obtained in this dissertation, there remains several venues for investigation and possible improvement. A list of possible future studies is given in the following:

- Based on the developed model, scaling of the critical current retention as a function of the calculated strain in the REBCO layer was good up to about 1.4% compressive strain. At higher strain values, there was some scatter in the results.

The model could be adjusted to account for the large deformations occurring under those conditions.

- A method to further reduce or completely eliminate the voids at the interface of the two-tape structure made by soldering has yet to be developed to achieve the full potential of that concept.
- The motivation behind using a soldering approach in making the two-tapes structure is its potential to be applied to a reel-to-reel process. A setup to test the concept of the R2R tape soldering process is under development. If enough control could be achieved on the thickness and voids in the solder layer, it could enable the production of long lengths of highly flexible REBCO tapes.
- Further reduction in AC losses could be achieved by making finer filaments. The striation process should be optimized for the production of finer filaments. However, the optimal filament size will be based on the targeted application requirement as tradeoff between the tape critical current reduction (by material removal) and the AC loss targeted values.
- The benefit of this striation method needs to be demonstrated in coil applications also. Two prototype coils, shown in Figure 5-1, were built using non striated and 12-filament tapes. Their AC losses need to be investigated at various different operating conditions especially under a combination of an AC field with an AC transport current. The development of long length multifilamentary REBCO tapes was addressed in this work but further study of the electro-mechanical behavior these tapes is needed to further understand and optimize this product to

meet application requirement and enable the use of REBCO CC in future applications.

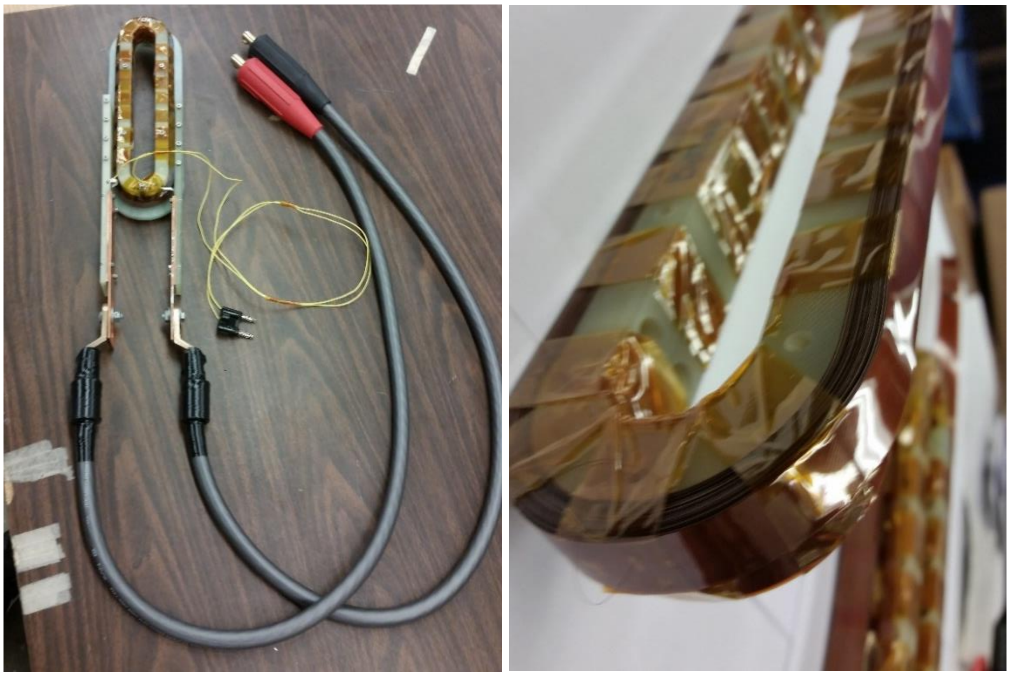

Figure 5-1 Pictures of the racetrack coil made with 10 meters of a 12-filament tape.

References

[1] H. Kamerlingh Onnes, "The resistance of pure mercury at helium temperatures," *Commun. Phys. Lab. Univ. Leiden, b,* vol. 120, 1911.

[2] D. J. Quinn, and W. B. Ittner, "Resistance in a Superconductor," *Journal of Applied Physics,* vol. 33, no. 2, pp. 748-&, 1962.

[3] W. Meissner, and R. Ochsenfeld, "Ein neuer effekt bei eintritt der supraleitfähigkeit," *Naturwissenschaften,* vol. 21, no. 44, pp. 787-788, 1933.

[4] J. R. Gavaler, "Superconductivity in Nb-Ge Films above 22 K," *Applied Physics Letters,* vol. 23, no. 8, pp. 480-482, 1973.

[5] J. Bardeen, L. N. Cooper, and J. R. Schrieffer, "Theory of Superconductivity," *Physical Review,* vol. 108, no. 5, pp. 1175-1204, 1957.

[6] J. G. Bednorz, and K. A. Muller, "Possible High-Tc Superconductivity in the Ba-La-Cu-O System," *Zeitschrift Fur Physik B-Condensed Matter,* vol. 64, no. 2, pp. 189-193, 1986.

[7] M. K. Wu, J. R. Ashburn, C. J. Torng, P. H. Hor, R. L. Meng, L. Gao, Z. J. Huang, Y. Q. Wang, and C. W. Chu, "Superconductivity at 93-K in a New Mixed-Phase Y-Ba-Cu-O Compound System at Ambient Pressure," *Physical Review Letters,* vol. 58, no. 9, pp. 908-910, Mar 2, 1987.

[8] A. Schilling, M. Cantoni, J. D. Guo, and H. R. Ott, "Superconductivity above 130-K in the Hg-Ba-Ca-Cu-O System," *Nature,* vol. 363, no. 6424, pp. 56-58, May 6, 1993.

[9] L. Gao, Y. Y. Xue, F. Chen, Q. Xiong, R. L. Meng, D. Ramirez, C. W. Chu, J. H. Eggert, and H. K. Mao, "Superconductivity up to 164-K in Hgba2cam-

1cumo2m+2+Delta (M=1,2, and 3) under Quasi-Hydrostatic Pressures," *Physical Review B,* vol. 50, no. 6, pp. 4260-4263, Aug 1, 1994.

[10] T. C. Ozawa, and S. M. Kauzlarich, "Chemistry of layered d-metal pnictide oxides and their potential as candidates for new superconductors," *Science and Technology of Advanced Materials,* vol. 9, no. 3, Sep, 2008.

[11] G. Wu, Y. L. Xie, H. Chen, M. Zhong, R. H. Liu, B. C. Shi, Q. J. Li, X. F. Wang, T. Wu, Y. J. Yan, J. J. Ying, and X. H. Chen, "Superconductivity at 56 K in samarium-doped SrFeAsF," *Journal of Physics-Condensed Matter,* vol. 21, no. 14, Apr 8, 2009.

[12] J. Nagamatsu, N. Nakagawa, T. Muranaka, Y. Zenitani, and J. Akimitsu, "Superconductivity at 39 K in magnesium diboride," *Nature,* vol. 410, no. 6824, pp. 63-64, Mar 1, 2001.

[13] R. Pia Jensen, "Master's thesis: Structural investigation of La(2-x)Sr(x)CuO(4+y) - Following staging as a function of temperature," 2016.

[14] D. Larbalestier, A. Gurevich, D. M. Feldmann, and A. Polyanskii, "High-T-c superconducting materials for electric power applications," *Nature,* vol. 414, no. 6861, pp. 368-377, Nov 15, 2001.

[15] N. Bay, and M. S. Nielsen, "Mechanical processing of Ag/BSCCO high temperature superconductor tape," *Journal of materials processing technology,* vol. 151, no. 1-3, pp. 18-26, 2004.

[16] K. Heine, J. Tenbrink, and M. Thoner, "High-Field Critical Current Densities in Bi2sr2ca1cu2o8+X/Ag Wires," *Applied Physics Letters,* vol. 55, no. 23, pp. 2441-2443, Dec 4, 1989.

[17] D. C. Larbalestier, J. Jiang, U. P. Trociewitz, F. Kametani, C. Scheuerlein, M. Dalban-Canassy, M. Matras, P. Chen, N. C. Craig, P. J. Lee, and E. E. Hellstrom, "Isotropic round-wire multifilament cuprate superconductor for generation of magnetic fields above 30 T," *Nature Materials,* vol. 13, no. 4, pp. 375-381, Apr, 2014.

[18] E. Barzi, V. Lombardo, D. Turrioni, F. J. Baca, and T. G. Holesinger, "BSCCO-2212 Wire and Cable Studies," *Ieee Transactions on Applied Superconductivity*, vol. 21, no. 3, pp. 2335-2339, Jun, 2011.

[19] P. Vanderbemden, A. D. Bradley, R. A. Doyle, W. Lo, D. M. Astill, D. A. Cardwell, and A. M. Campbell, "Superconducting properties of natural and artificial grain boundaries in bulk melt-textured YBCO," *Physica C,* vol. 302, no. 4, pp. 257-270, Jul 1, 1998.

[20] P. Vanderbemden, S. Dorbolo, N. Hari-Babu, A. Ntatsis, D. A. Cardwell, and A. M. Campbell, "Behavior of bulk melt-textured YBCO single domains subjected to crossed magnetic fields," *Ieee Transactions on Applied Superconductivity,* vol. 13, no. 2, pp. 3746-3749, Jun, 2003.

[21] D. Dimos, P. Chaudhari, and J. Mannhart, "Superconducting Transport-Properties of Grain-Boundaries in Yba2cu3o7 Bicrystals," *Physical Review B,* vol. 41, no. 7, pp. 4038-4049, Mar 1, 1990.

[22] A. Goyal, D. F. Lee, F. A. List, E. D. Specht, R. Feenstra, M. Paranthaman, X. Cui, S. W. Lu, P. M. Martin, D. M. Kroeger, D. K. Christen, B. W. Kang, D. P. Norton, C. Park, D. T. Verebelyi, J. R. Thompson, R. K. Williams, T. Aytug, and C.

Cantoni, “Recent progress in the fabrication of high-J(c) tapes by epitaxial deposition of YBCO on RABiTS,” *Physica C,* vol. 357, pp. 903-913, Aug, 2001.

[23] Y. Iijima, K. Kakimoto, M. Kimura, K. Takeda, and T. Saitoh, “Reel to reel continuous formation of Y-123 coated conductors by IBAD and PLD method,” *Ieee Transactions on Applied Superconductivity,* vol. 11, no. 1, pp. 2816-2821, Mar, 2001.

[24] C. L. H. Thieme, S. Fleshler, D. M. Buczek, M. Jowett, L. G. Fritzemeier, P. N. Arendt, S. R. Foltyn, J. Y. Coulter, and J. O. Willis, “Axial strain dependence at 77K of the critical current of thick YBaCuO films on Ni-alloy substrates with IBAD buffer layers,” *Ieee Transactions on Applied Superconductivity,* vol. 9, no. 2, pp. 1494-1497, Jun, 1999.

[25] W. Prusseit, G. Sigl, R. Nemetschek, C. Hoffmann, J. Handke, A. Lumkemann, and H. Kinder, “Commercial coated conductor fabrication based on inclined substrate deposition,” *Ieee Transactions on Applied Superconductivity,* vol. 15, no. 2, pp. 2608-2610, Jun, 2005.

[26] P. N. Arendt, S. R. Foltyn, J. R. Groves, R. F. DePaula, P. C. Dowden, J. M. Roper, and J. Y. Coulter, “YBCO/YSZ coated conductors on flexible Ni alloy substrates,” *Applied Superconductivity,* vol. 4, no. 10-11, pp. 429-434, Oct-Nov, 1996.

[27] A. Bailey, S. L. Town, G. Alvarez, G. J. Russell, and K. N. R. Taylor, “High Critical Current-Density Thick-Films of Ybco on Ysz,” *Physica C*, vol. 161, no. 3, pp. 347-350, Nov 15, 1989.

[28] C. P. Wang, K. B. Do, M. R. Beasley, T. H. Geballe, and R. H. Hammond, “Deposition of in-plane textured MgO on amorphous Si3N4 substrates by ion-

beam-assisted deposition and comparisons with ion-beam-assisted deposited yttria-stabilized-zirconia," *Applied Physics Letters*, vol. 71, no. 20, pp. 2955-2957, Nov 17, 1997.

[29] J. R. Groves, P. N. Arendt, S. R. Foltyn, Q. X. Jia, T. G. Holesinger, L. A. Emmert, R. F. DePaula, P. C. Dowden, and L. Stan, "Improvement of IBAD MgO template layers on metallic substrates for YBCO HTS deposition," *Ieee Transactions on Applied Superconductivity*, vol. 13, no. 2, pp. 2651-2654, Jun, 2003.

[30] SuperPower. "Configuration of SuperPower® 2G HTS Wire," http://www.superpower-inc.com/content/2g-hts-wire#Attributes%20of%20SuperPower%C3%82%C2%AE%202G%20HTS%20Wire.

[31] F. E. Ltd. "Fujikura 2G High Temperature Superconductor," https://www.fujikura.co.uk/products/energy-and-environment/2g-ybco-high-tempurature-superconductors/#!prettyPhoto.

[32] V. Selvamanickam, M. H. Gharahcheshmeh, A. Xu, E. Galstyan, L. Delgado, and C. Cantoni, "High critical currents in heavily doped (Gd,Y)Ba2Cu3Ox superconductor tapes," *Applied Physics Letters*, vol. 106, no. 3, Jan 19, 2015.

[33] V. Selvamanickam, A. Guevara, Y. Zhang, I. Kesgin, Y. Xie, G. Carota, Y. Chen, J. Dackow, Y. Zhang, Y. Zuev, C. Cantoni, A. Goyal, J. Coulter, and L. Civale, "Enhanced and uniform in-field performance in long (Gd, Y)-Ba-Cu-O tapes with zirconium doping fabricated by metal-organic chemical vapor deposition," *Superconductor Science & Technology*, vol. 23, no. 1, Jan, 2010.

[34] A. Xu, Y. Zhang, M. H. Gharahcheshmeh, Y. Yao, E. Galstyan, D. Abraimov, F. Kametani, A. Polyanskii, J. Jaroszynski, V. Griffin, G. Majkic, D. C. Larbalestier, and V. Selvamanickam, “J(e)(4.2 K, 31.2 T) beyond 1 kA/mm(2) of a similar to 3.2 mu m thick, 20 mol% Zr-added MOCVD REBCO coated conductor,” *Scientific Reports*, vol. 7, Jul 31, 2017.

[35] F. E. Ltd., “Industrial and scientific applications for superconductors.”

[36] T. N. H. M. F. Laboratory. "Engineering Critical Current Density vs. Applied Field for Superconductors Available in Long Lengths," https://nationalmaglab.org/magnet-development/applied-superconductivity-center/plots.

[37] G. Y. Jiang, J. M. Zhu, Z. H. Gao, Y. C. Chen, Y. Zhao, and Y. Yamada, “High-Speed Deposition of High-Performance REBCO Films by Using a Radiation Assisted Conductive Heating PLD System,” *Ieee Transactions on Applied Superconductivity*, vol. 29, no. 5, Aug, 2019.

[38] V. Chepikov, N. Mineev, P. Degtyarenko, S. Lee, V. Petrykin, A. Ovcharov, A. Vasiliev, A. Kaul, V. Amelichev, A. Kamenev, A. Molodyk, and S. Samoilenkov, “Introduction of BaSnO3 and BaZrO3 artificial pinning centres into 2G HTS wires based on PLD-GdBCO films. Phase I of the industrial R&D programme at SuperOx,” *Superconductor Science & Technology*, vol. 30, no. 12, Dec, 2017.

[39] G. Majkic, R. Pratap, A. X. Xu, E. Galstyan, and V. Selvamanickam, “Over 15 MA/cm(2) of critical current density in 4.8 mu m thick, Zr-doped (Gd,Y)Ba2Cu3Ox superconductor at 30 K, 3T,” *Scientific Reports*, vol. 8, May 3, 2018.

[40] Y. Park, M. Lee, H. Ann, Y. H. Choi, and H. Lee, "A superconducting joint for GdBa2Cu3O7 (-delta)-coated conductors," *Npg Asia Materials*, vol. 6, May, 2014.

[41] Y. J. Park, M. W. Lee, Y. K. Oh, and H. G. Lee, "Laser drilling: enhancing superconducting joint of GdBa2Cu3O7-delta coated conductors," *Superconductor Science & Technology*, vol. 27, no. 8, Aug, 2014.

[42] X. Z. Jin, Y. Yanagisawa, H. Maeda, and Y. Takano, "Development of a superconducting joint between a GdBa2Cu3O7-delta-coated conductor and YBa2Cu3O7-delta bulk: towards a superconducting joint between RE (Rare Earth) Ba2Cu3O7-delta coated conductors," *Superconductor Science & Technology*, vol. 28, no. 7, Jul, 2015.

[43] K. Ohki, T. Nagaishi, T. Kato, D. Yokoe, T. Hirayama, Y. Ikuhara, T. Ueno, K. Yamagishi, T. Takao, R. Piao, H. Maeda, and Y. Yanagisawa, "Fabrication, microstructure and persistent current measurement of an intermediate grown superconducting (iGS) joint between REBCO-coated conductors," *Superconductor Science & Technology*, vol. 30, no. 11, Nov, 2017.

[44] N. Cheggour, J. W. Ekin, C. C. Clickner, D. T. Verebelyi, C. L. H. Thieme, R. Feenstra, and A. Goyal, "Reversible axial-strain effect and extended strain limits in Y-Ba-Cu-O coatings on deformation-textured substrates," *Applied Physics Letters*, vol. 83, no. 20, pp. 4223-4225, Nov 17, 2003.

[45] N. Cheggour, J. W. Ekin, C. L. H. Thieme, Y. Y. Xie, V. Selvamanickam, and R. Feenstra, "Reversible axial-strain effect in Y-Ba-Cu-O coated conductors," *Superconductor Science & Technology*, vol. 18, no. 12, pp. S319-S324, Dec, 2005.

[46] S. Otten, A. Kario, A. Kling, and W. Goldacker, "Bending properties of different REBCO coated conductor tapes and Roebel cables at T=77 K," *Superconductor Science & Technology,* vol. 29, no. 12, Dec, 2016.

[47] K. L. Hwu, and B. Derby, "Fracture of metal/ceramic laminates - II. Crack growth resistance and toughness," *Acta Materialia,* vol. 47, no. 2, pp. 545-563, Jan 15, 1999.

[48] S. Lee, W. S. Kim, S. H. Park, J. K. Lee, C. Park, J. H. Bae, K. C. Seong, H. Lee, J. H. Lee, K. Choi, and S. Hahn, "Design of HTS Modular Magnets for a 2.5 MJ Toroidal SMES: ReBCO vs. BSCCO," *Ieee Transactions on Applied Superconductivity,* vol. 20, no. 3, pp. 1320-1324, Jun, 2010.

[49] A. Badel, A. Ballarino, C. Barth, L. Bottura, M. M. J. Dhalle, J. Fleiter, W. Goldacker, J. Himbele, A. Kario, L. Rossi, A. Rutt, C. Scheuerlein, C. Senatore, P. Tixador, A. Usoskin, and Y. Yang, "Advances in the Development of a 10-kA Class REBCO Cable for the EuCARD2 Demonstrator Magnet," *Ieee Transactions on Applied Superconductivity,* vol. 26, no. 3, Apr, 2016.

[50] N. Bykovsky, D. Uglietti, R. Wesche, and P. Bruzzone, "Design Optimization of Round Strands Made by Twisted Stacks of HTS Tapes," *Ieee Transactions on Applied Superconductivity,* vol. 26, no. 2, Mar, 2016.

[51] A. Koski, and S. L. Wipf, "Computational design study for an accelerator dipole in the range of 15-20 T," *Ieee Transactions on Magnetics,* vol. 32, no. 4, pp. 2159-2162, Jul, 1996.

[52] R. Gupta, M. Anerella, A. Ghosh, S. L. Lalitha, W. Sampson, J. Schmalzle, J. Kolonko, R. Scanlan, R. Weggel, E. Willen, and K. Nakao, "Hybrid High-Field

Cosine-Theta Accelerator Magnet R&D With Second-Generation HTS," *Ieee Transactions on Applied Superconductivity,* vol. 25, no. 3, Jun, 2015.

[53] J. van Nugteren, G. Kirby, J. Murtomaki, G. DeRijk, L. Rossi, and A. Stenvall, "Toward REBCO 20 T+ Dipoles for Accelerators," *Ieee Transactions on Applied Superconductivity,* vol. 28, no. 4, Jun, 2018.

[54] R. Gupta, M. Anerella, J. Cozzolino, J. Escallier, G. Ganetis, A. Harrison, and P. Wanderer, "Next generation IR magnets for hadron colliders," *Ieee Transactions on Applied Superconductivity,* vol. 13, no. 2, pp. 1351-1354, Jun, 2003.

[55] S. Caspi, F. Borgnolutti, L. Brouwer, D. Cheng, D. Dietderich, H. Felice, A. Godeke, R. Hafalia, M. Martchevskii, and S. Prestemon, "Canted–Cosine–Theta magnet (CCT)—A concept for high field accelerator magnets," *IEEE Transactions on Applied Superconductivity,* vol. 24, no. 3, pp. 1-4, 2014.

[56] C. Lorin, M. Segreti, A. Ballarino, L. Bottura, M. Durante, P. Fazilleau, J. Fleiter, G. Kirby, J. van Nugteren, and C. Pes, "Cos-$\theta $ design of dipole inserts made of ReBCO-Roebel or BSCCO-Rutherford cables," *IEEE Transactions on Applied Superconductivity,* vol. 25, no. 3, pp. 1-5, 2015.

[57] W. Wan, L. Brouwer, S. Caspi, S. Prestemon, A. Gerbershagen, J. M. Schippers, and D. Robin, "Alternating-gradient canted cosine theta superconducting magnets for future compact proton gantries," *Physical Review Special Topics-Accelerators Beams,* vol. 18, no. 10, pp. 103501, 2015.

[58] "New life for an old technology: canted cosine theta magnets," https://home.cern/news/news/engineering/new-life-old-technology-canted-cosine-theta-magnets.

[59] V. Selvamanickam, Y. Chen, J. Xie, Y. Zhang, A. Guevara, I. Kesgin, G. Majkic, and M. Martchevsky, “Influence of Zr and Ce doping on electromagnetic properties of (Gd,Y)-Ba-Cu-O superconducting tapes fabricated by metal organic chemical vapor deposition,” *Physica C-Superconductivity and Its Applications,* vol. 469, no. 23-24, pp. 2037-2043, Dec 1, 2009.

[60] D. W. Hazelton, H. Fukushima, A. Knoll, A. Sundaram, and Y. Zhang, “Improved current density in 2G HTS conductors using thin Hastelloy® C276 substrates,” *Applied Superconductivity Conference*, 2014.

[61] A. Sundaram, Y. Zhang, A. R. Knoll, D. Abraimov, P. Brownsey, M. Kasahara, G. M. Carota, R. Nakasaki, J. B. Cameron, G. Schwab, L. V. Hope, R. M. Schmidt, H. Kuraseko, T. Fukushima, and D. W. Hazelton, “2G HTS wires made on 30 mu m thick Hastelloy substrate,” *Superconductor Science & Technology,* vol. 29, no. 10, Oct, 2016.

[62] W. Luo, “FABRICATION AND ELECTROMECHANICAL STUDY OF SYMMETRIC TAPE ROUND (STAR) REBCO WIRES,” 2019.

[63] W. L. Soumen Kar, Jithin sai Sandra, Goran Majkic, Venkat Selvamanickam, “Symmetric Tape Round (STAR) REBCO Wires with Superior Mechanical Properties for Accelerator Magnets,” 2019.

[64] S. Kar, W. B. Luo, and V. Selvamanickam, “Ultra-Small Diameter Round REBCO Wire With Robust Mechanical Properties,” *Ieee Transactions on Applied Superconductivity,* vol. 27, no. 4, Jun, 2017.

[65] W. B. Luo, S. Kar, A. X. Xu, X. F. Li, A. Ben Yahia, and V. Selvamanickam, “Fabrication and Electromagnetic Characterization of Ultrasmall Diameter

REBCO Wires," *Ieee Transactions on Applied Superconductivity*, vol. 27, no. 4, Jun, 2017.

[66] L. Roebel, "Electrical conductor," U.S. Patent No. 1,144,252, 1915.

[67] D. S. Beard, W. Klose, S. Shimamoto, and G. Vecsey, "The Iea Large Coil Task - Development of Superconducting Toroidal Field Magnets for Fusion Power," *Fusion Engineering and Design*, vol. 7, no. 1-2, pp. 1-&, Sep, 1988.

[68] G. A. Kirby, J. van Nugteren, H. Bajas, V. Benda, A. Ballarino, M. Bajko, L. Bottura, K. Broekens, M. Canale, A. Chiuchiolo, L. Gentini, N. Peray, J. C. Perez, G. de Rijk, A. Rijllart, L. Rossi, J. Murtomaeki, J. Mazet, F. O. Pincot, G. Volpini, M. Durante, P. Fazilleau, C. Lorin, A. Stenvall, W. Goldacker, A. Kario, and A. Usoskin, "First Cold Powering Test of REBCO Roebel Wound Coil for the EuCARD2 Future Magnet Development Project," *Ieee Transactions on Applied Superconductivity*, vol. 27, no. 4, Jun, 2017.

[69] CERN. "Prototype Roebel cable to be used to wind a HTS accelerator demonstration dipole," https://cds.cern.ch/record/1744900.

[70] M. Takayasu, L. Chiesa, L. Bromberg, and J. V. Minervini, "HTS twisted stacked-tape cable conductor," *Superconductor Science & Technology*, vol. 25, no. 1, Jan, 2012.

[71] M. Takayasu, L. Chiesa, L. Bromberg, and J. V. Minervini, "Electrical and Mechanical Characteristics of HTS Twisted Stacked-Tape Cable Conductor," *Ieee Transactions on Applied Superconductivity*, vol. 27, no. 4, Jun, 2017.

[72] M. Takayasu, L. Chiesa, P. D. Noyes, and J. V. Minervini, "Investigation of HTS Twisted Stacked-Tape Cable (TSTC) Conductor for High-Field, High-Current

Fusion Magnets," *Ieee Transactions on Applied Superconductivity,* vol. 27, no. 4, Jun, 2017.

[73] M. Takayasu, F. J. Mangiarotti, J. V. Minervini, L. Bromberg, L. Chiesa, N. Allen, W. Nachtrab, M. K. Rudziak, and T. Wong, "Development of REBCO twisted stacked-tape cables for magnet application," *Proc. 1st Workshop Accel. Magn. HTS,* pp. 1-27, 2014.

[74] D. Uglietti, R. Wesche, and P. Bruzzone, "Design and Strand Tests of a Fusion Cable Composed of Coated Conductor Tapes," *Ieee Transactions on Applied Superconductivity,* vol. 24, no. 3, Jun, 2014.

[75] V. Selvamanickam, and Y. Xie, "Superconductor components," U.S. Patent No. 7,417,192, 2005.

[76] D. C. van der Laan, "YBa2Cu3O7-delta coated conductor cabling for low ac-loss and high-field magnet applications," *Superconductor Science & Technology,* vol. 22, no. 6, Jun, 2009.

[77] J. D. Weiss, T. Mulder, H. J. ten Kate, and D. C. van der Laan, "Introduction of CORC (R) wires: highly flexible, round high-temperature superconducting wires for magnet and power transmission applications," *Superconductor Science & Technology,* vol. 30, no. 1, Jan, 2017.

[78] X. R. Wang, S. Caspi, D. R. Dietderich, W. B. Ghiorso, S. A. Gourlay, H. C. Higley, A. Lin, S. O. Prestemon, D. van der Laan, and J. D. Weiss, "A viable dipole magnet concept with REBCO CORC (R) wires and further development needs for high-field magnet applications," *Superconductor Science & Technology,* vol. 31, no. 4, Apr, 2018.

[79] D. Verebelyi, E. Harley, J. Scudiere, A. Otto, U. Schoop, C. Thieme, M. Rupich, and A. Malozemoff, "Practical neutral-axis conductor geometries for coated conductor composite wire," *Superconductor Science & Technology,* vol. 16, no. 10, pp. 1158-1161, Oct, 2003.

[80] M. Sugano, S. Machiya, M. Sato, T. Koganezawa, K. Shikimachi, N. Hirano, and S. Nagaya, "Bending strain analysis considering a shift of the neutral axis for YBCO coated conductors with and without a Cu stabilizing layer," *Superconductor Science & Technology,* vol. 24, no. 7, Jul, 2011.

[81] S. Kar, W. B. Luo, A. Ben Yahia, X. F. Li, G. Majkic, and V. Selvamanickam, "Symmetric tape round REBCO wire with J(e) (4.2K, 15T) beyond 450Amm(-2) at 15mm bend radius: a viable candidate for future compact accelerator magnet applications (vol 31, 04LT01, 2018)," *Superconductor Science & Technology,* vol. 31, no. 4, Apr, 2018.

[82] W. B. Luo, S. Kar, X. F. Li, E. Galstyan, M. Kochat, J. S. Sandra, J. Jaroszynski, D. Abraimov, and V. Selvamanickam, "Superior critical current of Symmetric Tape Round (STAR) REBCO wires in ultra-high background fields up to 31.2T," *Superconductor Science & Technology,* vol. 31, no. 12, Dec, 2018.

[83] M. D. Sumption, E. W. Collings, and P. N. Barnes, "AC loss in striped (filamentary) YBCO coated conductors leading to designs for high frequencies and field-sweep amplitudes," *Superconductor Science & Technology,* vol. 18, no. 1, pp. 122-134, Jan, 2005.

[84] W. J. Carr, *AC loss and macroscopic theory of superconductors,* New York: Gordon and Breach, 1983.

[85] W. T. Norris, “Calculation of Hysteresis Losses in Hard Superconductors Carrying Ac - Isolated Conductors and Edges of Thin Sheets,” *Journal of Physics D-Applied Physics,* vol. 3, no. 4, pp. 489-&, 1970.

[86] I. Kesgin, “Processing and Electromagnetic Properties of Low AC Loss, Multifilamentary Rare Earth-barium-copper-oxide Superconductor Tapes,” 2013.

[87] M. N. Wilson, “Superconducting magnets,” 1983.

[88] M. P. Oomen, “AC loss in superconducting tapes and cables,” University of Twente, 2000.

[89] M. D. Sumption, “AC Loss of Superconducting Materials for Very High Density Motors and Generators of Hybrid-Electric Aircraft,” *AIAA/IEEE Electric Aircraft Technologies Symposium (EATS)*, pp. 1-6, 2018.

[90] P. N. Barnes, M. D. Sumption, and G. L. Rhoads, “Review of high power density superconducting generators: Present state and prospects for incorporating YBCO windings,” *Cryogenics,* vol. 45, no. 10-11, pp. 670-686, Oct-Nov, 2005.

[91] K. S. Haran, S. Kalsi, T. Arndt, H. Karmaker, R. Badcock, B. Buckley, T. Haugan, M. Izumi, D. Loder, J. W. Bray, P. Masson, and E. W. Stautner, “High power density superconducting rotating machines-development status and technology roadmap,” *Superconductor Science & Technology*, vol. 30, no. 12, Dec, 2017.

[92] J. L. Felder, G. V. Brown, H. DaeKim, and J. Chu, “Turboelectric distributed propulsion in a hybrid wing body aircraft,” *Proc. 20th Int. Society for Airbreathing Engines*, 2011.

[93] L. Sumitomo Electric Industries. "3 cores High Tc Superconducting Cable," https://global-sei.com/super/cable_e/ingridj.html.

[94] T. Takahashi, H. Suzuki, M. Ichikawa, T. Okamoto, S. Akita, S. Mukoyama, N. Ishii, A. Kimura, and K. Yasuda, "Demonstration and verification tests of 500 m long HTS power cable," *Ieee Transactions on Applied Superconductivity,* vol. 15, no. 2, pp. 1823-1826, Jun, 2005.

[95] H. Yumura, Y. Ashibe, H. Itoh, M. Ohya, M. Watanabe, T. Masuda, and C. S. Weber, "Phase II of the Albany HTS Cable Project," *Ieee Transactions on Applied Superconductivity,* vol. 19, no. 3, pp. 1698-1701, Jun, 2009.

[96] J. H. Lim, S. H. Sohn, H. S. Ryoo, H. O. Choi, H. S. Yang, D. L. Kim, Y. H. Ma, K. Ryu, and S. D. Hwang, "Performance Test of 100 m HTS Power Cable System," *Ieee Transactions on Applied Superconductivity,* vol. 19, no. 3, pp. 1710-1713, Jun, 2009.

[97] V. E. Sytnikov, K. A. Shutov, N. V. Polyakova, S. S. Fetisov, A. A. Nosov, and V. S. Vysotsky, "The AC Loss Analysis in the 5 m HTS Power Cables," *Ieee Transactions on Applied Superconductivity,* vol. 19, no. 3, pp. 1706-1709, Jun, 2009.

[98] N. Amemiya, Z. Jiang, M. Nakahata, M. Yagi, S. Mukoyama, N. Kashima, S. Nagaya, and Y. Shiohara, "AC loss reduction of superconducting power transmission cables composed of coated conductors," *Ieee Transactions on Applied Superconductivity,* vol. 17, no. 2, pp. 1712-1717, Jun, 2007.

[99] T. YAMAGUCHI, Y. SHINGAI, M. KONISHI, M. OHYA, Y. ASHIBE, and H. YUMURA, "Large Current and Low AC Loss High Temperature Superconducting Power Cable Using REBCO Wires," *SEI TECHNICAL REVIEW,* vol. 78, pp. 79-85, 2014.

[100] W. J. Carr, and C. E. Oberly, “Filamentary YBCO conductors for AC applications,” *Ieee Transactions on Applied Superconductivity*, vol. 9, no. 2, pp. 1475-1478, Jun, 1999.

[101] C. Oberly, G. Rhoads, P. Barnes, L. Long, D. Scott, and W. Carr Jr, "The importance of interfilamentary barrier resistance in YBCO coated conductor to minimize ac losses." pp. 621-630.

[102] C. B. Cobb, P. N. Barnes, T. J. Haugan, J. Tolliver, E. Lee, M. Sumption, E. Collings, and C. E. Oberly, “Hysteretic loss reduction in striated YBCO,” *Physica C-Superconductivity and Its Applications*, vol. 382, no. 1, pp. 52-56, Oct 15, 2002.

[103] G. Majkic, I. Kesgin, Y. Zhang, Y. F. Qiao, R. Schmidt, and V. Selvamanickam, “AC Loss Filamentization of 2G HTS Tapes by Buffer Stack Removal,” *Ieee Transactions on Applied Superconductivity*, vol. 21, no. 3, pp. 3297-3300, Jun, 2011.

[104] X. W. Cai, I. Kesgin, R. Schmidt, Y. M. Chen, and V. Selvamanickam, “Completely Etch-Free Fabrication of Multifilamentary Coated Conductor Using Inkjet Printing and Electrodeposition,” *Ieee Transactions on Applied Superconductivity*, vol. 23, no. 3, Jun, 2013.

[105] R. C. Duckworth, M. P. Paranthaman, M. S. Bhuiyan, F. A. List, and M. J. Gouge, “AC losses in YBCO coated conductor with inkjet filaments,” *Ieee Transactions on Applied Superconductivity*, vol. 17, no. 2, pp. 3159-3162, Jun, 2007.

[106] G. A. Levin, P. N. Barnes, J. W. Kell, N. Amemiya, Z. Jiang, K. Yoda, and F. Kimura, “Multifilament YBa2Cu3O6+x-coated conductors with minimized coupling losses,” *Applied Physics Letters*, vol. 89, no. 1, Jul 3, 2006.

[107] H. Okamoto, H. Hayashi, A. Tomioka, M. Konno, M. Owa, A. Kawagoe, F. Sumiyoshi, M. Iwakuma, K. Suzuki, T. Izumi, Y. Yamada, and Y. Shiohara, "AC loss properties in YBCO model coils for loss reduction," *Physica C-Superconductivity and Its Applications*, vol. 468, no. 15-20, pp. 1731-1733, Sep 15, 2008.

[108] A. C. Wulff, M. Solovyov, F. Gomory, A. B. Abrahamsen, O. V. Mishin, A. Usoskin, A. Rutt, J. H. Lundeman, K. Thyden, J. B. Hansen, and J. C. Grivel, "Two level undercut-profile substrate for filamentary YBa2Cu3O7 coated conductors," *Superconductor Science & Technology*, vol. 28, no. 7, Jul, 2015.

[109] J. C. Prestigiacomo, R. C. Y. Auyeung, and M. S. Osofsky, "Process for scalable fabrication of low AC loss HTS conductors," *Superconductor Science & Technology*, vol. 31, no. 11, Nov, 2018.

[110] I. Kesgin, G. A. Levin, T. J. Haugan, and V. Selvamanickam, "Multifilament, copper-stabilized superconductor tapes with low alternating current loss," *Applied Physics Letters*, vol. 103, no. 25, Dec 16, 2013.

[111] A. Ben Yahia, X. F. Li, M. Majoros, M. D. Sumption, and V. Selvamanickam, "AC Loss Reduction in Multifilamentary Coated Conductors With Transposed Filaments," *Ieee Transactions on Applied Superconductivity*, vol. 27, no. 4, Jun, 2017.

[112] X. W. Cai, I. Kesgin, and V. Selvamanickam, "Reel-to-Reel Selective Electroplating of Cu Stabilizer for Multifilamentary Coated Conductors," *Ieee Transactions on Applied Superconductivity*, vol. 25, no. 3, Jun, 2015.

[113] M. Vojenčiak, A. Kario, B. Ringsdorf, R. Nast, D. van der Laan, J. Scheiter, A. Jung, B. Runtsch, F. Gömöry, W. J. S. S. Goldacker, and Technology, “Magnetization ac loss reduction in HTS CORC® cables made of striated coated conductors,” vol. 28, no. 10, pp. 104006, 2015.

[114] N. Amemiya, N. Tominaga, R. Toyomoto, T. Nishimoto, Y. Sogabe, S. Yamano, and H. Sakamoto, “Coupling time constants of striated and copper-plated coated conductors and the potential of striation to reduce shielding-current-induced fields in pancake coils,” *Superconductor Science & Technology*, vol. 31, no. 2, Feb, 2018.

[115] D. C. van der Laan, and J. W. Ekin, “Dependence of the critical current of YBa2Cu3O7-delta coated conductors on in-plane bending,” *Superconductor Science & Technology*, vol. 21, no. 11, Nov, 2008.

[116] K. Gramoll. "MECHANICS - THEORY - Bending Strain and Stress," http://www.ecourses.ou.edu/cgi-bin/ebook.cgi?topic=me&chap_sec=06.1&page=theory.

[117] Y. Zhang, D. W. Hazelton, R. Kelley, M. Kasahara, R. Nakasaki, H. Sakamoto, and A. Polyanskii, “Stress-Strain Relationship, Critical Strain (Stress) and Irreversible Strain (Stress) of IBAD-MOCVD-Based 2G HTS Wires Under Uniaxial Tension,” *Ieee Transactions on Applied Superconductivity*, vol. 26, no. 4, Jun, 2016.

[118] W. Ramberg, and W. R. Osgood, “Description of stress-strain curves by three parameters,” 1943.

[119] T. H. Courtney, *Mechanical Behavior of Materials*, p.^pp. 59, Boston: McGraw Hill, 2000.

[120] J. J. Roa, X. G. Capdevila, M. Martinez, F. Espiell, and M. Segarra, "Nanohardness and Young's modulus of YBCO samples textured by the Bridgman technique," *Nanotechnology*, vol. 18, no. 38, Sep 26, 2007.

[121] T. Randle, *A few mathematical notes on constant perimeter layers in coil windings*, 1974.

[122] X. R. Wang, D. Arbelaez, S. Caspi, S. O. Prestemon, G. Sabbi, and T. M. Shen, "Strain Distribution in REBCO-Coated Conductors Bent With the Constant-Perimeter Geometry," *Ieee Transactions on Applied Superconductivity*, vol. 27, no. 8, Dec, 2017.

[123] E. Kreyszig, *Differential geometry*, New York: Dover Publications, 1991.

[124] H. W. Weijers, W. D. Markiewicz, A. J. Voran, S. R. Gundlach, W. R. Sheppard, B. Jarvis, Z. L. Johnson, P. D. Noyes, J. Lu, H. Kandel, H. Bai, A. V. Gavrilin, Y. L. Viouchkov, D. C. Larbalestier, and D. V. Abraimov, "Progress in the Development of a Superconducting 32 T Magnet With REBCO High Field Coils," *Ieee Transactions on Applied Superconductivity*, vol. 24, no. 3, Jun, 2014.

[125] S. Ito, Y. Seino, N. Yanagi, Y. Terazaki, A. Sagara, H. J. P. Hashizume, and F. Research, "Bridge-type mechanical lap joint of a 100 kA-class HTS conductor having stacks of GdBCO tapes," vol. 9, pp. 3405086-3405086, 2014.

[126] N. Bagrets, A. Augieri, G. Celentano, G. Tomassetti, K. P. Weiss, and A. della Corte, "Investigation of ReBCO Conductor Tape Joints for Superconducting Applications," *Ieee Transactions on Applied Superconductivity*, vol. 25, no. 3, Jun, 2015.

[127] H. S. Shin, J. R. C. Dizon, S. S. Oh, and R. F. Bonifacio, “Bending Strain Characteristics of the Transport Property in Lap-Jointed Coated Conductor Tapes,” *Ieee Transactions on Applied Superconductivity,* vol. 19, no. 3, pp. 2991-2994, Jun, 2009.

[128] C. Cantoni, T. Aytug, D. T. Verebelyi, M. Paranthaman, E. D. Specht, D. P. Norton, and D. K. Christen, “Conductive buffer layers and overlayers for the thermal stability of coated conductors,” *Ieee Transactions on Applied Superconductivity,* vol. 11, no. 1, pp. 3309-3312, Mar, 2001.

[129] S. A. Harrington, J. L. MacManus-Driscoll, and J. H. Durrell, “Practical vortex diodes from pinning enhanced YBa2Cu3O7-delta,” *Applied Physics Letters,* vol. 95, no. 2, Jul 13, 2009.

[130] E. Pardo, M. Vojenciak, F. Gomory, and J. Souc, “Low-magnetic-field dependence and anisotropy of the critical current density in coated conductors,” *Superconductor Science & Technology,* vol. 24, no. 6, Jun, 2011.

[131] B. Maiorov, B. J. Gibbons, S. Kreiskott, V. Matias, T. G. Holesinger, and L. Civale, “Effect of the misalignment between the applied and internal magnetic fields on the critical currents of "tilted coated conductors",” *Applied Physics Letters,* vol. 86, no. 13, Mar 28, 2005.

[132] N. J. Long, “Model for the angular dependence of critical currents in technical superconductors,” *Superconductor Science & Technology,* vol. 21, no. 2, Feb, 2008.

[133] C. Barth, G. Mondonico, and C. Senatore, "Electro-mechanical properties of REBCO coated conductors from various industrial manufacturers at 77K, self-field and 4.2K, 19T," *Superconductor Science & Technology,* vol. 28, no. 4, Apr, 2015.

[134] H. S. Shin, and M. J. Dedicatoria, "Intrinsic strain effect on critical current in Cu-stabilized GdBCO coated conductor tapes with different substrates," *Superconductor Science & Technology*, vol. 26, no. 5, May, 2013.

[135] J. Y. Kato, N. Sakai, S. Tajima, S. Miyata, M. Konishi, Y. Yamada, N. Chikumoto, K. Nakao, T. Izumi, and Y. Shiohara, "Diffusion joint of YBCO coated conductors using stabilizing silver layers," *Physica C-Superconductivity and Its Applications,* vol. 445, pp. 686-688, Oct 1, 2006.

[136] R. J. Cava, A. W. Hewat, E. A. Hewat, B. Batlogg, M. Marezio, K. M. Rabe, J. J. Krajewski, W. F. Peck, and L. W. Rupp, "Structural Anomalies, Oxygen Ordering and Superconductivity in Oxygen Deficient Ba2ycu3ox," *Physica C,* vol. 165, no. 5-6, pp. 419-433, Feb 15, 1990.

[137] A. Preuss, W. H. Fietz, F. Immel, S. Kauffmann-Weiss, and M. J. Wolf, "Critical Current Degradation of Coated Conductors Under Soldering Conditions," *Ieee Transactions on Applied Superconductivity,* vol. 28, no. 4, Jun, 2018.

[138] T. Maebatake, Y. Ichinose, K. Yamada, N. Mori, R. Teranishi, M. Inoue, T. Kiss, M. Yoshizumi, T. Izumi, K. Kaneko, S. Munetoh, and M. Mukaida, "Joint properties of REBCO coated conductors," *Physica C-Superconductivity and Its Applications,* vol. 471, no. 21-22, pp. 987-989, Nov, 2011.

[139] G. Garmong, N. E. Paton, and A. S. Argon, “Attainment of Full Interfacial Contact during Diffusion Bonding,” *Metallurgical Transactions a-Physical Metallurgy and Materials Science,* vol. 6, no. 6, pp. 1269-1279, 1975.

[140] R. Aspandiar, "Voids in solder joints."

[141] M. Yunus, K. Srihari, J. M. Pitarresi, and A. Primavera, “Effect of voids on the reliability of BGA/CSP solder joints,” *Microelectronics Reliability,* vol. 43, no. 12, pp. 2077-2086, Dec, 2003.

[142] G. P. Tandon, and G. J. Weng, “Stress-Distribution in and around Spheroidal Inclusions and Voids at Finite Concentration,” *Journal of Applied Mechanics-Transactions of the Asme,* vol. 53, no. 3, pp. 511-518, Sep, 1986.

[143] E. H. Brandt, and M. Indenbom, “Type-Ii-Superconductor Strip with Current in a Perpendicular Magnetic-Field,” *Physical Review B,* vol. 48, no. 17, pp. 12893-12906, Nov 1, 1993.

[144] E. G. Gamaly, A. V. Rode, B. Luther-Davies, and V. T. J. P. o. p. Tikhonchuk, “Ablation of solids by femtosecond lasers: Ablation mechanism and ablation thresholds for metals and dielectrics,” vol. 9, no. 3, pp. 949-957, 2002.

[145] Y. Cao, “Ablation and plasma effects during nanosecond laser matter interaction in air and water,” 2015.

[146] F. Poitrasson, X. L. Mao, S. S. Mao, R. Freydier, and R. E. Russo, “Comparison of ultraviolet femtosecond and nanosecond laser ablation inductively coupled plasma mass spectrometry analysis in glass, monazite, and zircon,” *Analytical Chemistry,* vol. 75, no. 22, pp. 6184-6190, Nov 15, 2003.

[147] S. S. Mao, “Laser ablation. Fundamentals and applications,” *University of California, Berkeley*, vol. 39, 2005.

[148] S. Hashmi, *Comprehensive materials processing*: Newnes, 2014.

[149] "Fumex Inc.," https://fumexinc.com/.

[150] "Keyence 3D laser scanning microscope," https://www.keyence.com/.

[151] J. Byskov-Nielsen, J.-M. Savolainen, M. S. Christensen, and P. J. A. P. A. Balling, “Ultra-short pulse laser ablation of metals: threshold fluence, incubation coefficient and ablation rates,” vol. 101, no. 1, pp. 97-101, 2010.

[152] N. Semaltianos, W. Perrie, P. French, M. Sharp, G. Dearden, S. Logothetidis, and K. Watkins, “Femtosecond laser ablation characteristics of nickel-based superalloy C263,” *J Applied Physics A*, vol. 94, no. 4, pp. 999, 2009.

[153] S. Proyer, E. Stangl, P. Schwab, D. Bäuerle, P. Simon, and C. J. A. P. A. Jordan, “Patterning of YBCO films by excimer-laser ablation,” vol. 58, no. 5, pp. 471-474, 1994.

[154] S. Nolte, C. Momma, H. Jacobs, A. Tünnermann, B. N. Chichkov, B. Wellegehausen, and H. J. J. B. Welling, “Ablation of metals by ultrashort laser pulses,” vol. 14, no. 10, pp. 2716-2722, 1997.

[155] X. F. Li, A. Ben Yahia, G. Majkic, and V. Selvamanickam, “Scanning Hall Probe Microscopy on Laser Striated Multifilament Coated Conductor,” *Ieee Transactions on Applied Superconductivity*, vol. 25, no. 3, Jun, 2015.

[156] F. Juster, J. Lottin, L. Boldi, R. De Lorenzi, P. Fabbricatore, R. Musenich, D. Baynham, and P. J. I. t. o. a. s. Sampson, “Stability of Al-stabilized conductors for LHC detector magnets,” vol. 5, no. 2, pp. 377-380, 1995.

[157] E. Martinez, L. Angurel, J. Pelegrin, Y. Xie, V. J. S. S. Selvamanickam, and Technology, “Thermal stability analysis of YBCO-coated conductors subject to over-currents,” vol. 23, no. 2, pp. 025011, 2009.

[158] K. Suzuki, J. Matsuda, M. Yoshizumi, T. Izumi, Y. Shiohara, M. Iwakuma, A. Ibi, S. Miyata, Y. J. S. S. Yamada, and Technology, “Development of a laser scribing process of coated conductors for the reduction of AC losses,” vol. 20, no. 8, pp. 822, 2007.

[159] G. Levin, J. Murphy, T. Haugan, J. Šouc, J. Kováč, and P. J. I. T. o. A. S. Kováč, “AC losses of copper stabilized multifilament YBCO coated conductors,” vol. 23, no. 3, pp. 6600604-6600604, 2013.

[160] E. Demenčík, F. Grilli, A. Kario, R. Nast, A. Jung, M. Vojenčiak, J. Scheiter, and W. J. I. T. o. A. S. Goldacker, “AC magnetization loss and transverse resistivity of striated YBCO coated conductors,” vol. 25, no. 3, pp. 1-5, 2015.

[161] X. Cai, “Solution Fabrication for Multifilamentary tapes of the Second Generation High-Temperature Superconductor,” 2016.

[162] K.-H. J. P. C. S. Müller, “AC power losses in flexible thick-film superconducting tapes,” vol. 281, no. 1, pp. 1-10, 1997.

[163] M. Marchevsky, E. Zhang, Y. Y. Xie, V. Selvamanickam, and P. G. Ganesan, “AC Losses and Magnetic Coupling in Multifilamentary 2G HTS Conductors and Tape Arrays,” *Ieee Transactions on Applied Superconductivity*, vol. 19, no. 3, pp. 3094-3097, Jun, 2009.

[164] X. F. Li, A. Ben Yahia, G. Majkic, M. Kochat, S. Kar, and V. Selvamanickam, “Reel-To-Reel Critical Current Measurement of REBCO Coated Conductors,” *Ieee Transactions on Applied Superconductivity,* vol. 27, no. 4, Jun, 2017.

[165] J. Šouc, F. Gömöry, J. Kováč, R. Nast, A. Jung, M. Vojenčiak, F. Grilli, W. J. S. S. Goldacker, and Technology, “Low AC loss cable produced from transposed striated CC tapes,” vol. 26, no. 7, pp. 075020, 2013.

[166] M. Majoros, M. D. Sumption, E. W. Collings, and D. C. van der Laan, “Magnetization losses in superconducting YBCO conductor-on-round-core (CORC) cables,” *Superconductor Science & Technology,* vol. 27, no. 12, Dec, 2014.

[167] D. Abraimov, A. Gurevich, A. Polyanskii, X. Cai, A. Xu, S. Pamidi, D. Larbalestier, C. J. S. S. Thieme, and Technology, “Significant reduction of AC losses in YBCO patterned coated conductors with transposed filaments,” vol. 21, no. 8, pp. 082004, 2008.

[168] A. H. Hamad, "Effects of different laser pulse regimes (nanosecond, picosecond and femtosecond) on the ablation of materials for production of nanoparticles in liquid solution," *High Energy and Short Pulse Lasers*: InTech, 2016.

[169] B. N. Chichkov, C. Momma, S. Nolte, F. vonAlvensleben, and A. Tunnermann, “Femtosecond, picosecond and nanosecond laser ablation of solids,” *Applied Physics a-Materials Science & Processing,* vol. 63, no. 2, pp. 109-115, Aug, 1996.